# Latest LHAASO Results, with Emphasis on Cosmic-Ray Anisotropy

Yi Zhang （张毅）
on behalf of LHAASO collaboration
Purple Mountain Observatory (PMO), Chinese Academy of Science (CAS)

# LHAASO Collaboration

Currently, **334** members from **39** institutions.







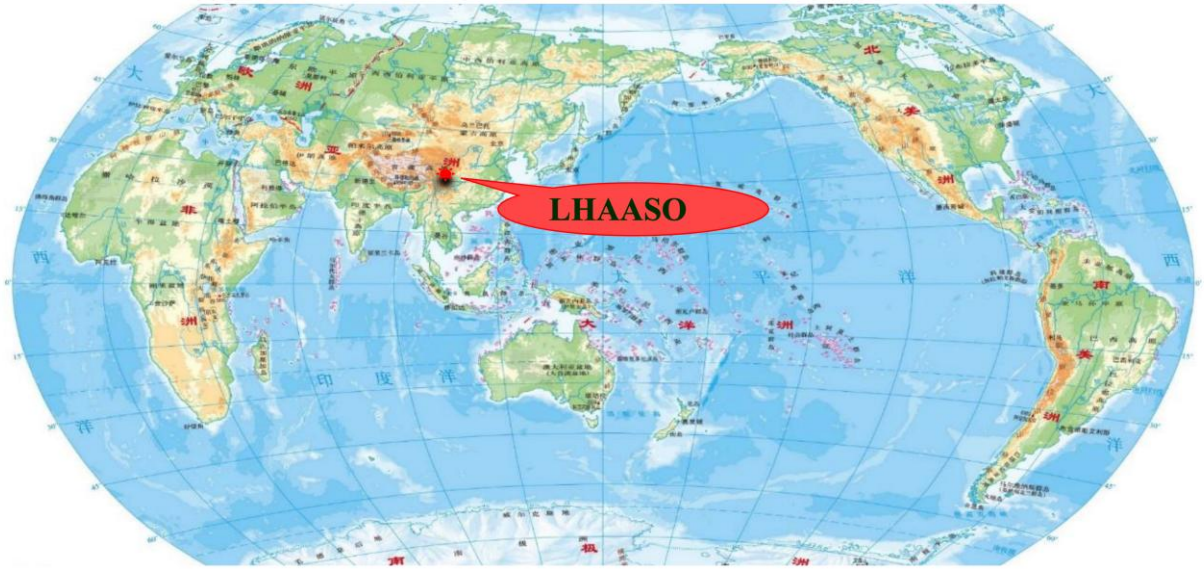

Zhen Cao[1,2,3], F. Aharonian[3,4,5,6], Y.X. Bai[1,3], Y.W. Bao[7], D. Bastieri[8], X.J. Bi[1,2,3], Y.J. Bi[1,3], W. Bian[7], J. Blunier[9], A.V. Bukevich[10], C.M. Cai[11], W.Y. Cao[12], Zhe Cao[13,4], J. Chang[14], J.F. Chang[1,3,13], E.S. Chen[1,3], G.H. Chen[8], H.K. Chen[15], L.F. Chen[15], Liang Chen[16], Long Chen[11], M.J. Chen[1,3], M.L. Chen[1,3,13], Q.H. Chen[11], S. Chen[17], S.H. Chen[1,2,3], S.Z. Chen[1,3], T.L. Chen[18], X.B. Chen[19], X.J. Chen[11], X.P. Chen[14], Y. Chen[19], N. Cheng[1,3], Q.Y. Cheng[1,2,3], Y.D. Cheng[1,2,3], M.Y. Cui[14], S.W. Cui[15], X.H. Cui[20], Y.D. Cui[21], B.Z. Dai[17], H.L. Dai[1,3,13], L.X. Dai[22], Z.G. Dai[4], Danzengluobu[18], Y.X. Diao[11], A.J. Dong[23], X.D. Duan[24], J.H. Fan[8], Y.Z. Fan[14], J. Fang[17], J.H. Fang[25], K. Fang[1,3], C.F. Feng[26], H. Feng[1], L. Feng[14], S.H. Feng[1,3], X.T. Feng[26], Y. Feng[25], Y.L. Feng[18], S. Gabici[9], B. Gao[1,3], Q. Gao[18], W. Gao[1,3], C. Ge[27], M.M. Ge[17], T.T. Ge[21], L.S. Geng[1,3], G. Giacinti[9], G.H. Gong[28], Q.B. Gou[1,3], M.H. Gu[1,3,13], W.M. Gu[27], F.L. Guo[16], J. Guo[28], K.J. Guo[11], X.L. Guo[11], Y.Q. Guo[1,3], R.P. Han[1,2,3], O.A. Hannuksela[12], M. Hasan[1,2,3], H.H. He[1,2,3], H.N. He[14], J.Y. He[14], X.Y. He[14], Y. He[11], S. Hernández-Cadena[7], C. Hou[1,3], X. Hou[29], H.B. Hu[1,2,3], S.C. Hu[1,3,30], D.H. Huang[11], F. Huang[27], J.J. Huang[1,2,3], X.L. Huang[23], X.T. Huang[26], X.Y. Huang[14], Y. Huang[1,3,30], Z.J. Huang[1,2,3], A. Inventar[9], X.L. Ji[1,3,13], H.Y. Jia[11], K. Jia[26], H.B. Jiang[1,3], K. Jiang[13,4], X.W. Jiang[1,3], Z.J. Jiang[17], M. Jin[11], S. Kaci[7], M.M. Kang[31], I. Karpikov[10], D. Khangulyan[1,3] D. Kuleshov[10], K. Kurinov[10], W.H. Lei[32], Cheng Li[13,4], Cong Li[1,3], D. Li[1,2,3], F. Li[1,3,13], H.B. Li[1,2,3], H.C. Li[1,3], Jian Li[4], Jie Li[1,3,13], K. Li[1,3], L. Li[33], R.L. Li[14], T.Y. Li[7], W.L. Li[7], X.R. Li[1,3], X.Y. Li[4,14], Y. Li[7], Zhe Li[1,3], Zhuo Li[34], E.W. Liang[35], Y.F. Liang[35], S.J. Lin[21], B. Liu[14], C. Liu[1,3], D. Liu[26], D.B. Liu[7], H. Liu[11], J. Liu[1,3], J.L. Liu[1,3], J.R. Liu[11], M.Y. Liu[18], Q. Liu[15], R.Y. Liu[19], S.M. Liu[11], T. Liu[27], W. Liu[1,3], Y. Liu[8], Y. Liu[11], Y.N. Liu[28], Y.Q. Lou[28], Q. Luo[21], Y. Luo[7], H.K. Lv[1,3], B.Q. Ma[34], L.L. Ma[1,3], X.H. Ma[1,3], I.O. Maliy[10], J.R. Mao[29], Z. Min[1,3], W. Mitthumsiri[36], Y. Mizuno[7], G.B. Mou[37], A. Neronov[9], C.-Y. Ng[22], K.C.Y. Ng[12], M.Y. Ni[14], L. Nie[11], L.J. Ou[8], Z.W. Ou[7], P. Pattarakijwanich[36], Z.Y. Pei[8], D.Y. Peng[15], J.C. Qi[1,2,3], M.Y. Qi[1,3], J.J. Qin[4], H. Qu[7], A. Raza[26], C.Y. Ren[14], M.Q. Ruan[1,3], D. Ruffolo[36], A. Sáiz[36], D. Savchenko[9], D. Semikoz[9], L. Shao[15], O. Shchegolev[10,38], Y.Z. Shen[19], X.D. Sheng[1,3], F.W. Shu[33], H.C. Song[34], Yu.V. Stenkin[10,38], Y. Su[14], C.Y. Sun[32], D.X. Sun[4,14], H. Sun[26], J.X. Sun[19], M. Sun[27], Q.N. Sun[1,3], X.N. Sun[35], Z.B. Sun[39], N.H. Tabasam[26], J. Takata[32], P.H.T. Tam[21], H.B. Tan[19], Q.W. Tang[33], R. Tang[7], Z.B. Tang[13,4], W.W. Tian[2,20], C.N. Tong[19], L.H. Wan[21], C. Wang[39], D.H. Wang[23], G.W. Wang[4], H.G. Wang[8], J.C. Wang[29], J.F. Wang[27], J.S. Wang[7], K. Wang[34], Kai Wang[19], Kai Wang[32], L.P. Wang[1,2,3], L.Y. Wang[1,3], W. Wang[21], X.G. Wang[35], X.J. Wang[11], X.Y. Wang[19], Y. Wang[11], Y.D. Wang[1,3], Z.H. Wang[31], Z.X. Wang[17], Zheng Wang[1,3,13], D.M. Wei[14], J.J. Wei[14], Y.J. Wei[1,2,3], T. Wen[1,3], S.S. Weng[37], C.Y. Wu[1,3], H.R. Wu[1,3], Q.W. Wu[32], S. Wu[1,3], X.F. Wu[14], Y.S. Wu[4], S.Q. Xi[1,3], J. Xia[4,14], G.M. Xiang[1,3,30], D.X. Xiao[15], G. Xiao[1,3], Y.F. Xiao[17], B.H. Xie[11], F. Xie[35], Y.L. Xin[11], H.D. Xing[1,2,3], Y. Xing[16], D.R. Xiong[29], B.N. Xu[1,3], C.Y. Xu[25], D.L. Xu[7], R.X. Xu[34], S.S. Xu[1,3], L. Xue[26], D.H. Yan[17], T. Yan[1,3], C. Yang[1,2,3], C.Y. Yang[29], F.F. Yang[1,3,13], L.L. Yang[21], M.J. Yang[1,3], R.Z. Yang[4], W.X. Yang[8], Z.H. Yang[7], Z.G. Yao[1,3], X.A. Ye[14], L.Q. Yin[1,3], N. Yin[26], X.H. You[1,3], Z.Y. You[1,3], Y.H. Yu[24], Q. Yuan[14], H. Yue[1,2,3], H.D. Zeng[14], T.X. Zeng[1,3,13], W. Zeng[17], X.T. Zeng[21], M. Zha[1,3], B. Zhang[22], B.B. Zhang[19], B.T. Zhang[1,3], C. Zhang[19], H. Zhang[7], H.M. Zhang[35], H.Y. Zhang[17], J.L. Zhang[20], J.Y. Zhang[1,2,3], L.Y. Zhang[32], Li Zhang[17], P.F. Zhang[17], R. Zhang[14], R.Y. Zhang[24], S.R. Zhang[15], S.S. Zhang[1,3], S.Y. Zhang[15], W. Zhang[1,3], X. Zhang[37], X.L. Zhang[1,2,3], X.P. Zhang[1,3], Yi Zhang[14], Yong Zhang[1,3], Z.P. Zhang[4], J. Zhao[1,3], L. Zhao[13,4], L.Z. Zhao[15], X.H. Zhao[29], F. Zheng[39], T.C. Zheng[1,3], B. Zhou[1,3], H. Zhou[7], J.N. Zhou[16], L. Zhou[32], M. Zhou[33], P. Zhou[19], R. Zhou[31], X.X. Zhou[1,2,3], X.X. Zhou[11], B.Y. Zhu[4,14], C.G. Zhu[26], F.R. Zhu[11], H. Zhu[20], K.J. Zhu[1,2,3,13], Y.F. Zhu[1,3], Z.F. Zhu[9], Y.C. Zou[32], X. Zuo[1,3],

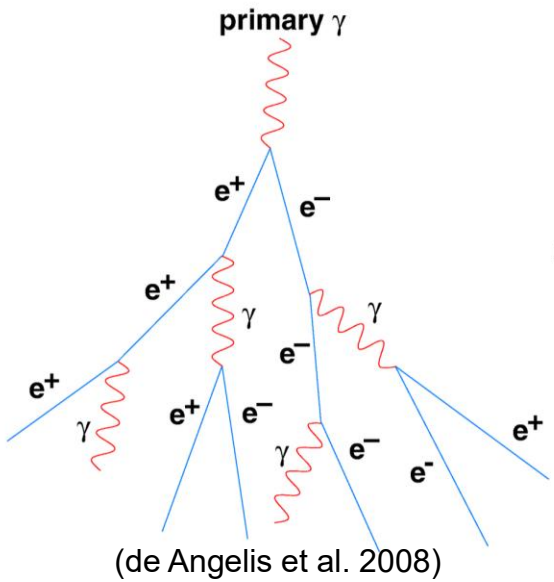
[1] State Key Laboratory of Particle Astrophysics & Experimental Physics Division & Computing Center, Institute of High Energy Physics, Chinese Academy of Sciences, 100049 Beijing, China
[2] University of Chinese Academy of Sciences, 100049 Beijing, China
[3] Tianfu Cosmic Ray Research Center, 610000 Chengdu, Sichuan, China
[4] University of Science and Technology of China, 230026 Hefei, Anhui, China
[5] Yerevan State University, 1 Alek Manukyan Street, Yerevan 0025, Armenia
[6] Max-Planck-Institut for Nuclear Physics, P.O. Box 103980, 69029 Heidelberg, Germany
[7] Tsung-Dao Lee Institute & School of Physics and Astronomy, Shanghai Jiao Tong University, 200240 Shanghai, China
[8] Center for Astrophysics, Guangzhou University, 510006 Guangzhou, Guangdong, China
[9] APC, Universit'e Paris Cit'e, CNRS/IN2P3, CEA/IRFU, Observatoire de Paris, 119 75205 Paris, France
[10] Institute for Nuclear Research of Russian Academy of Sciences, 117312 Moscow, Russia
[11] School of Physical Science and Technology & School of Information Science and Technology, Southwest Jiaotong University, 610031 Chengdu, Sichuan, China
[12] Department of Physics, The Chinese University of Hong Kong, Shatin, New Territories, Hong Kong, China
[13] State Key Laboratory of Particle Detection and Electronics, China
[14] Key Laboratory of Dark Matter and Space Astronomy, Purple Mountain Observatory, Chinese Academy of Sciences, 210023 Nanjing, Jiangsu, China
[15] Hebei Normal University, 050024 Shijiazhuang, Hebei, China
[16] Shanghai Astronomical Observatory, Chinese Academy of Sciences, 200030 Shanghai, China
[17] School of Physics and Astronomy, Yunnan University, 650091 Kunming, Yunnan, China
[18] Key Laboratory of Cosmic Rays (Tibet University), Ministry of Education, 850000 Lhasa, Tibet, China
[19] School of Astronomy and Space Science, Nanjing University, 210023 Nanjing, Jiangsu, China
[20] Key Laboratory of Radio Astronomy and Technology, National Astronomical Observatories, CAS, Beijing 100101, China
[21] School of Physics and Astronomy & School of Physics (Guangzhou), Sun Yat-sen University, 519000 Zhuhai, Guangdong, China
[22] The Hong Kong Institute for Astronomy and Astrophysics & Department of Physics, The University of Hong Kong, Pokfulam Road, Hong Kong SAR, China
[23] School of Physics and Electronic Science, Guizhou Normal University, 550025 Guiyang, Guizhou, China
[24] School of Physics, Henan Normal University, 453007 Xinxiang, Henan, China
[25] Research Center for Computational Earth and Space Science, Zhejiang Laboratory, 311121 Hangzhou, Zhejiang, China
[26] Institute of Frontier and Interdisciplinary Science, Shandong University, 266237 Qingdao, Shandong, China
[27] Department of Astronomy, Xiamen University, 361005 Xiamen, Fujian, China
[28] Department of Engineering Physics & Department of Physics & Department of Astronomy, Tsinghua University, 100084 Beijing, China
[29] Yunnan Observatories, Chinese Academy of Sciences, 650216 Kunming, Yunnan, China
[30] China Center of Advanced Science and Technology, Beijing 100190, China
[31] College of Physics, Sichuan University, 610065 Chengdu, Sichuan, China
[32] School of Physics, Huazhong University of Science and Technology, Wuhan 430074, Hubei, China
[33] Center for Relativistic Astrophysics and High Energy Physics, School of Physics and Materials Science & Institute of Space Science and Technology, Nanchang University, 330031 Nanchang, Jiangxi, China
[34] School of Physics & Kavli Institute for Astronomy and Astrophysics, Peking University, 100871 Beijing, China
[35] Guangxi Key Laboratory for Relativistic Astrophysics, School of Physical Science and Technology, Guangxi University, Nanning 530004, China
[36] Department of Physics, Faculty of Science, Mahidol University, Bangkok 10400, Thailand
[37] School of Physics and Technology, Nanjing Normal University, 210023 Nanjing, Jiangsu, China
[38] Moscow Institute of Physics and Technology, 141700 Moscow, Russia
[39] National Space Science Center, Chinese Academy of Sciences, 100190 Beijing, China

# Outline

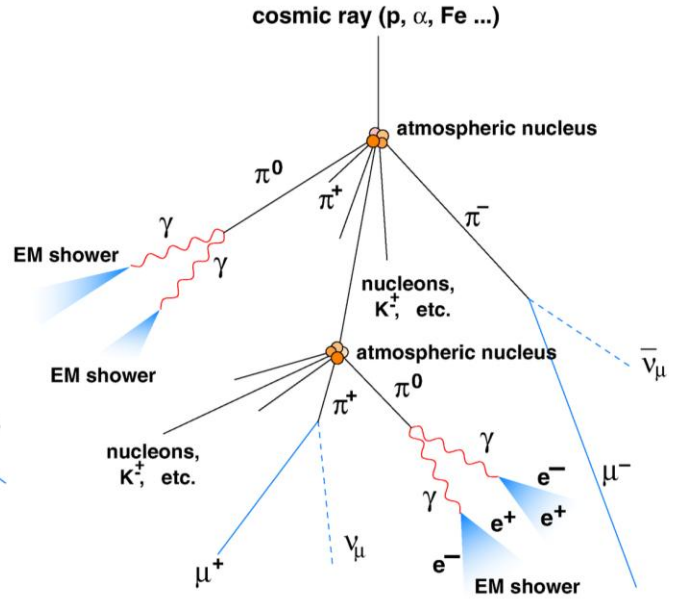
1. **Introduction:** The LHAASO Observatory
2. **Cosmic-Ray Energy Spectra:** Probing the Knee Region
3. **Cosmic-Ray Anisotropy (Focus):**
   - Large-scale dipole & quadrupole anisotropy
   - Rigidity-dependent evolution across species
   - Medium-scale structures & energy-dependent centroid shifts
   - Transient anisotropy driven by ICME
4. **Galactic Diffuse Emission:** UHE $\gamma$-Ray Mapping along the Galactic Plane
5. **Galactic Particle Accelerators (PeVatrons):**
   - Supernova Remnants (SNRs)
   - Pulsar Wind Nebulae (PWNe) & Pulsar Halos
   - Young Massive Star Clusters (YMSCs)
   - Binaries (Microquasars & $\gamma$-Ray Binaries)
6. **Summary & Outlook**

# LHAASO: Large High Altitude Air Shower Observatory

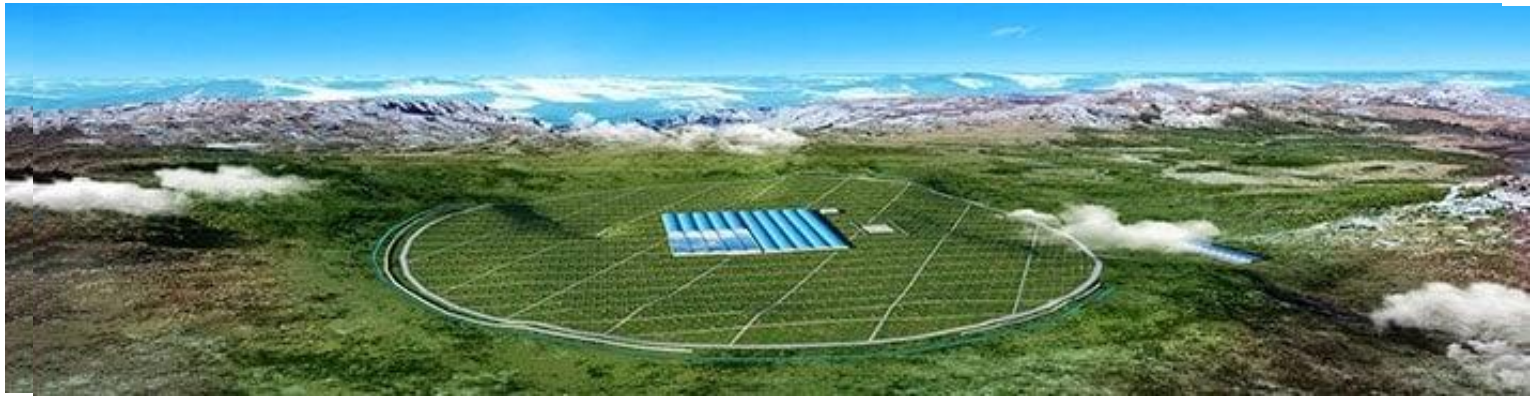



(de Angelis et al. 2008)




- Haizi mountain, Sichuan Province, China
- **4410m** above the sea level
- A large-scale dual-purpose experiment for CR and γ-ray observations.
- Hybrid detector arrays to detect secondary products from CR air showers and γ-ray air shower.
- Full operation since July 2021



# Layout of LHAASO

高海拔宇宙线观测站
Large High Altitude Air Shower Observatory

**Square Kilometer Array (KM2A)**

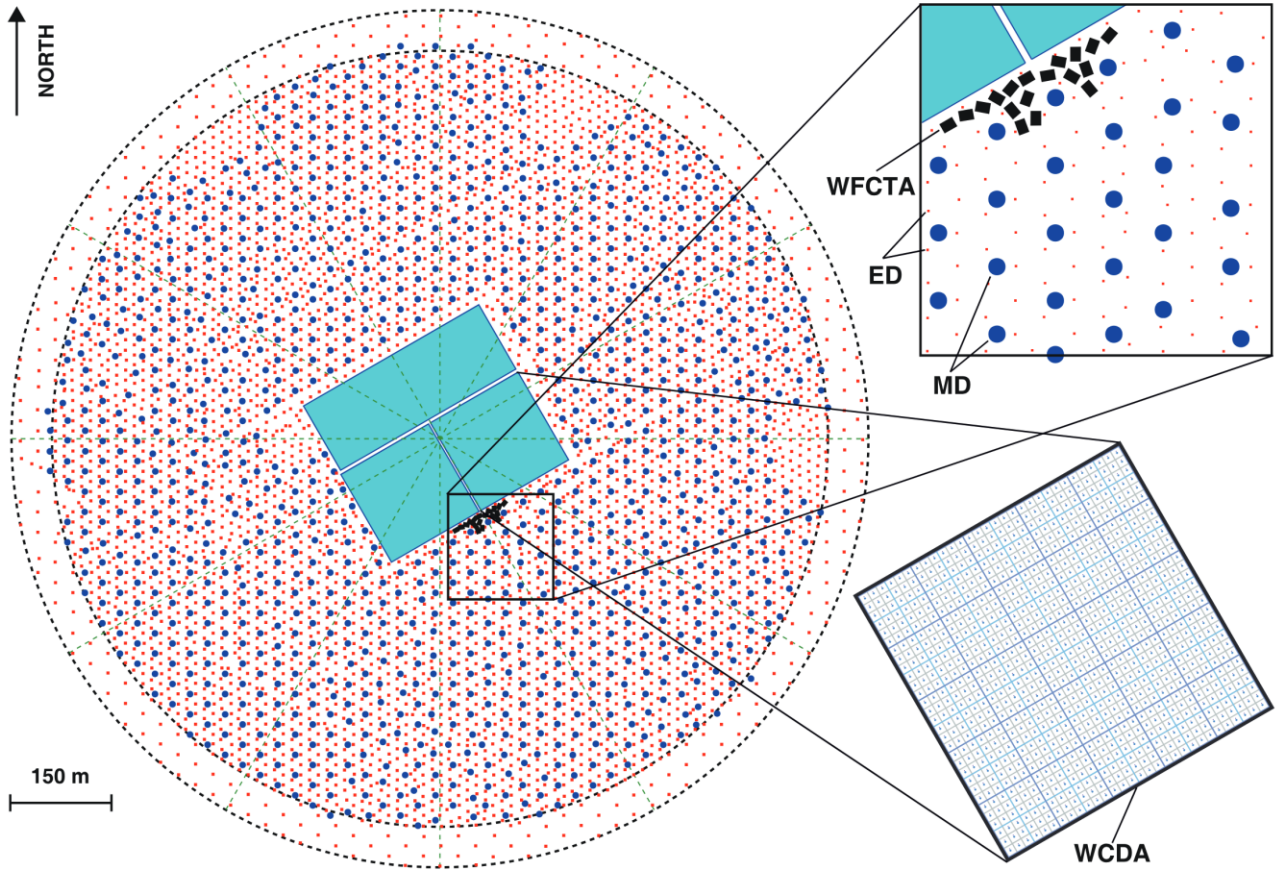
- **1.3 km² area**
- **5216 EDs** for energy and direction reconstruction
- **1188 MDs** to distinguish gamma/hadron
- Energy coverage: **~10 TeV - 100 PeV**

**Water Cherenkov Detector Array (WCDA)**

- **78000 m² water tanks**
- **3120 WCDs** to detect Cherenkov light produced by air shower particles in water
- Energy coverage: **100s GeV-10s TeV**

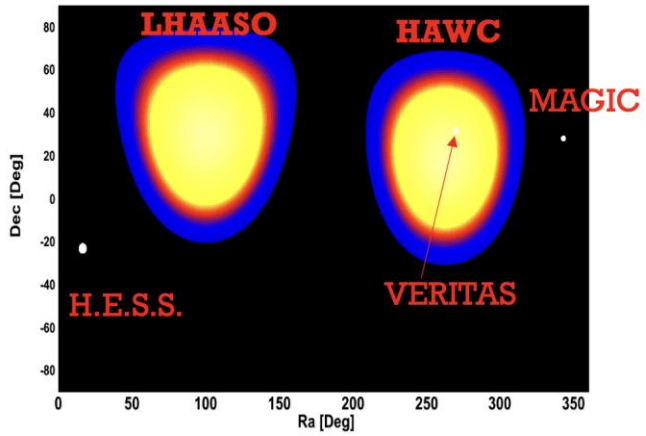
**Wide Field-of-view Cherenkov Telescope Array (WFCTA)**

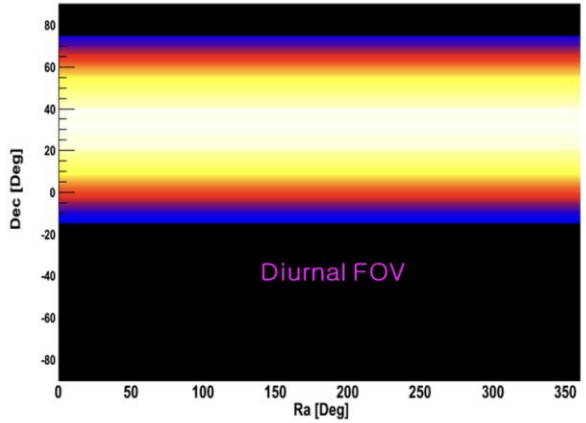
- **18 WFCTs** to distinguish particles with different mass, each one has an area of 4.7 m² and covers a square sky with area 16°×16°
- Dedicated to CR observations.

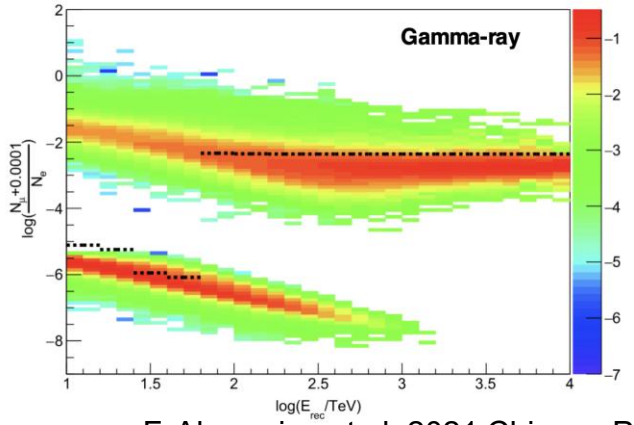


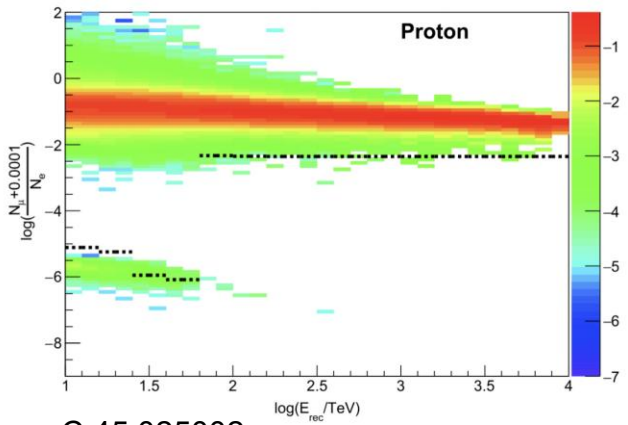

Chinese Physics C Vol. 46, No. 3 (2022) 030001

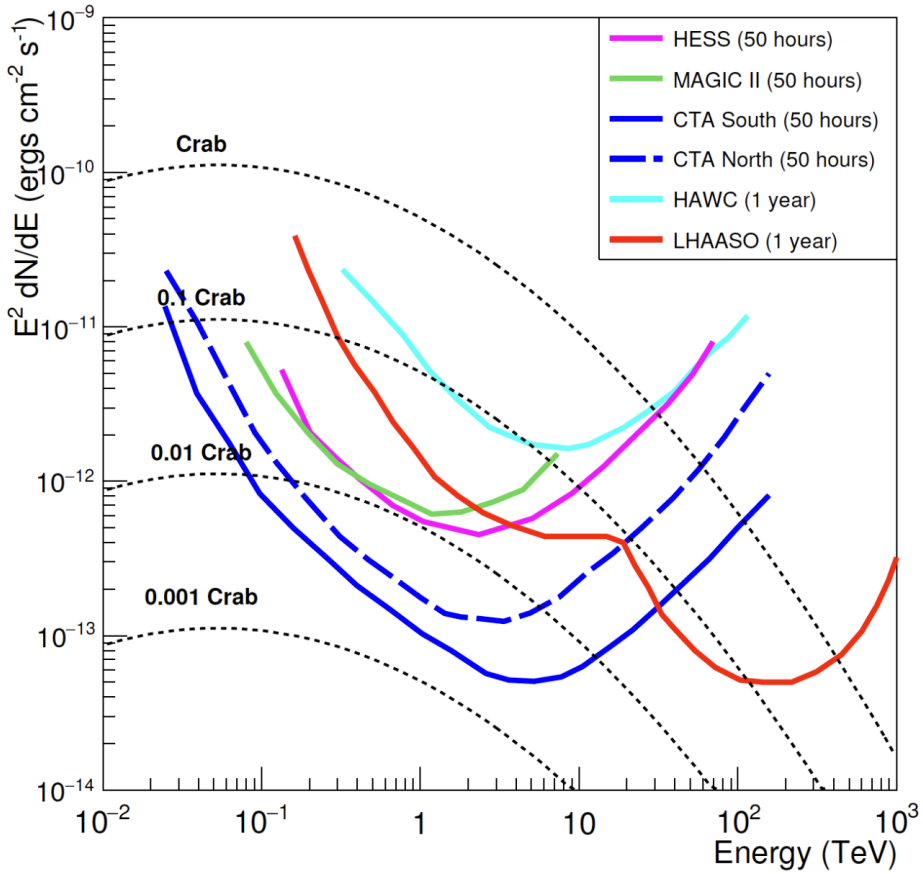
# Performance of LHAASO




F. Aharonian et al. 2021 Chinese Phys. C 45 025002

- Large effective area, wide FOV, powerful γ/hadron discrimination

→ **Excellent sensitivity at multi-TeV to PeV energies**

→**Exploring the origin of GCRs (knee region, PeVatrons).**

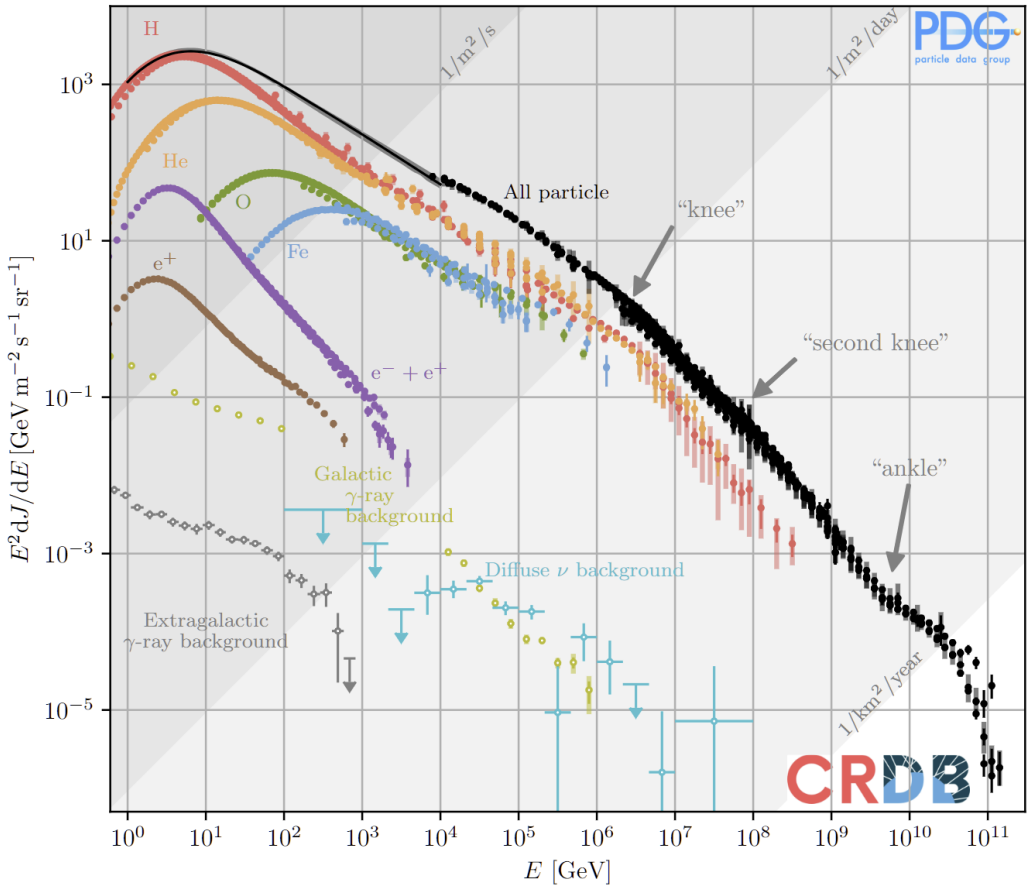
# Outline

1. **Introduction:** The LHAASO Observatory
2. **Cosmic-Ray Energy Spectra:** Probing the Knee Region
3. **Cosmic-Ray Anisotropy (Focus):**
   - Large-scale dipole & quadrupole anisotropy
   - Rigidity-dependent evolution across species
   - Medium-scale structures & energy-dependent centroid shifts
   - Transient anisotropy driven by ICME
4. **Galactic Diffuse Emission:** UHE $\gamma$-Ray Mapping along the Galactic Plane
5. **Galactic Particle Accelerators (PeVatrons):**
   - Supernova Remnants (SNRs)
   - Pulsar Wind Nebulae (PWNe) & Pulsar Halos
   - Young Massive Star Clusters (YMSCs)
   - Binaries (Microquasars & $\gamma$-Ray Binaries)
6. **Summary & Outlook**

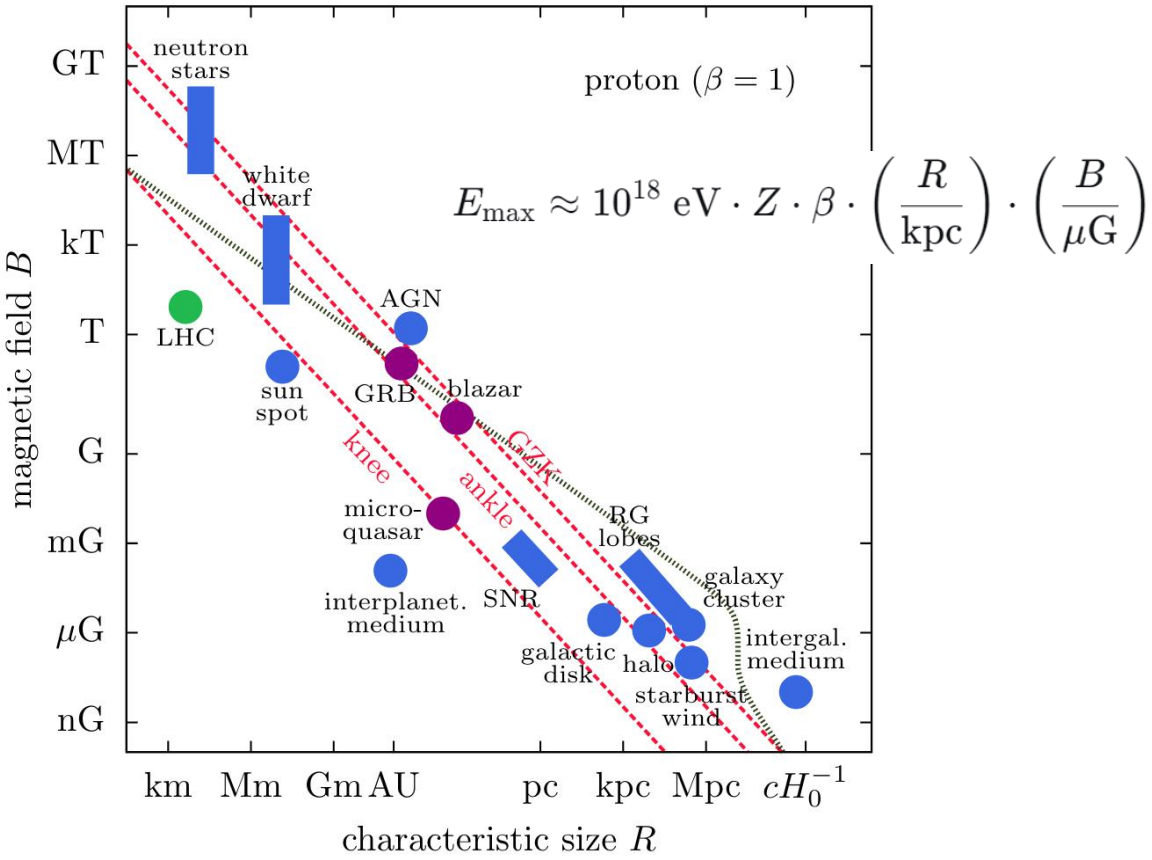
# The Galactic Cosmic Ray Landscape: Spectrum and Acceleration Limits



**Power required (0.3–1) × $10^{41}$ erg/s for GCR**




## Hillas Plot



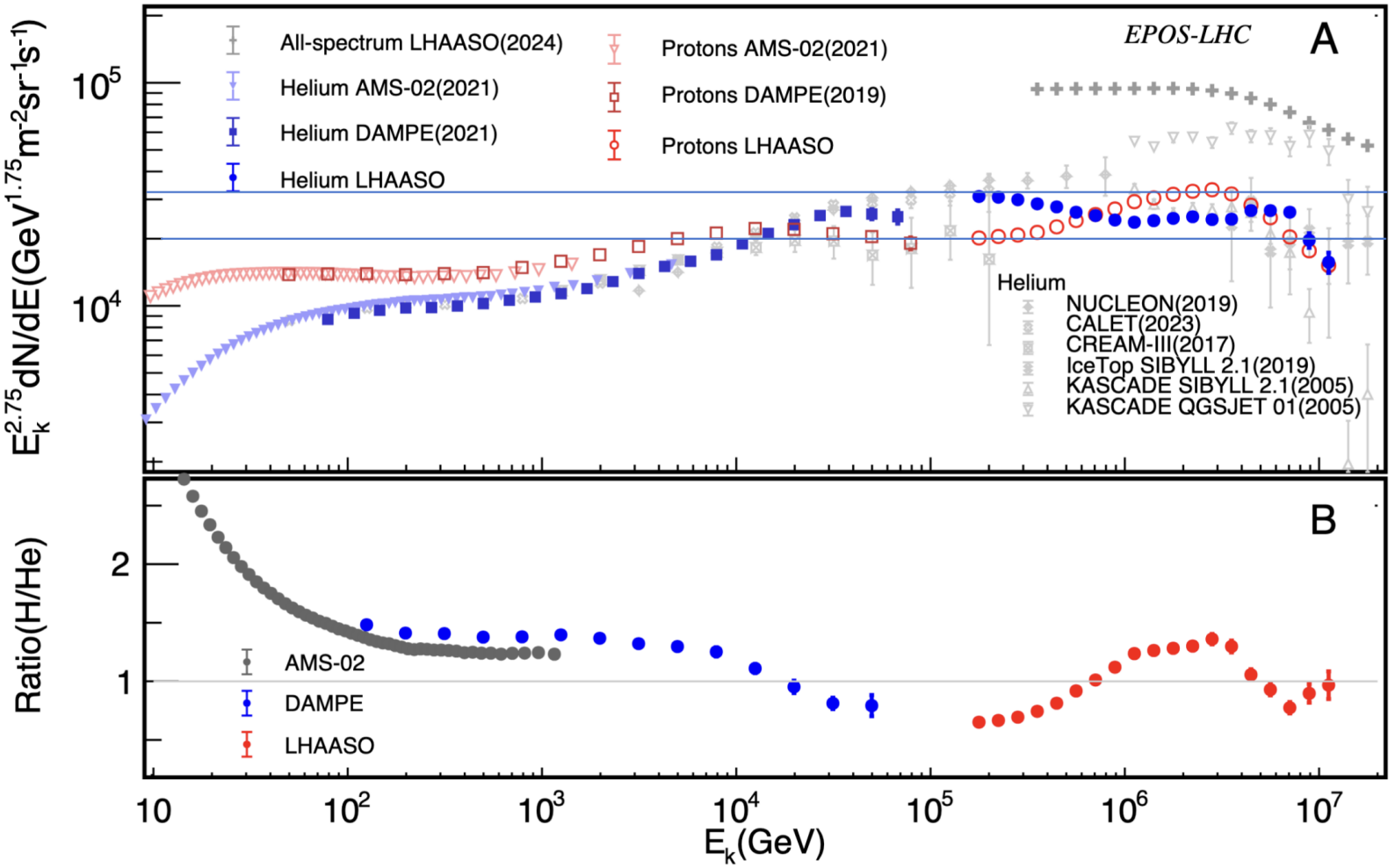

**CRs** are high-energy particles from outer space, those with E<~3 PeV (around "knee" region) are believed to be accelerated within our Galaxy.

- Which kinds of Galactic sources are PeVatrons that can accelerate particles (especially protons) to the PeV regime?
- $E_{max,p} \gtrsim$ PeV (via p-p interactions) → $E_\gamma \gtrsim$100 TeV

# LHAASO's Measurements of Proton and Helium Spectra

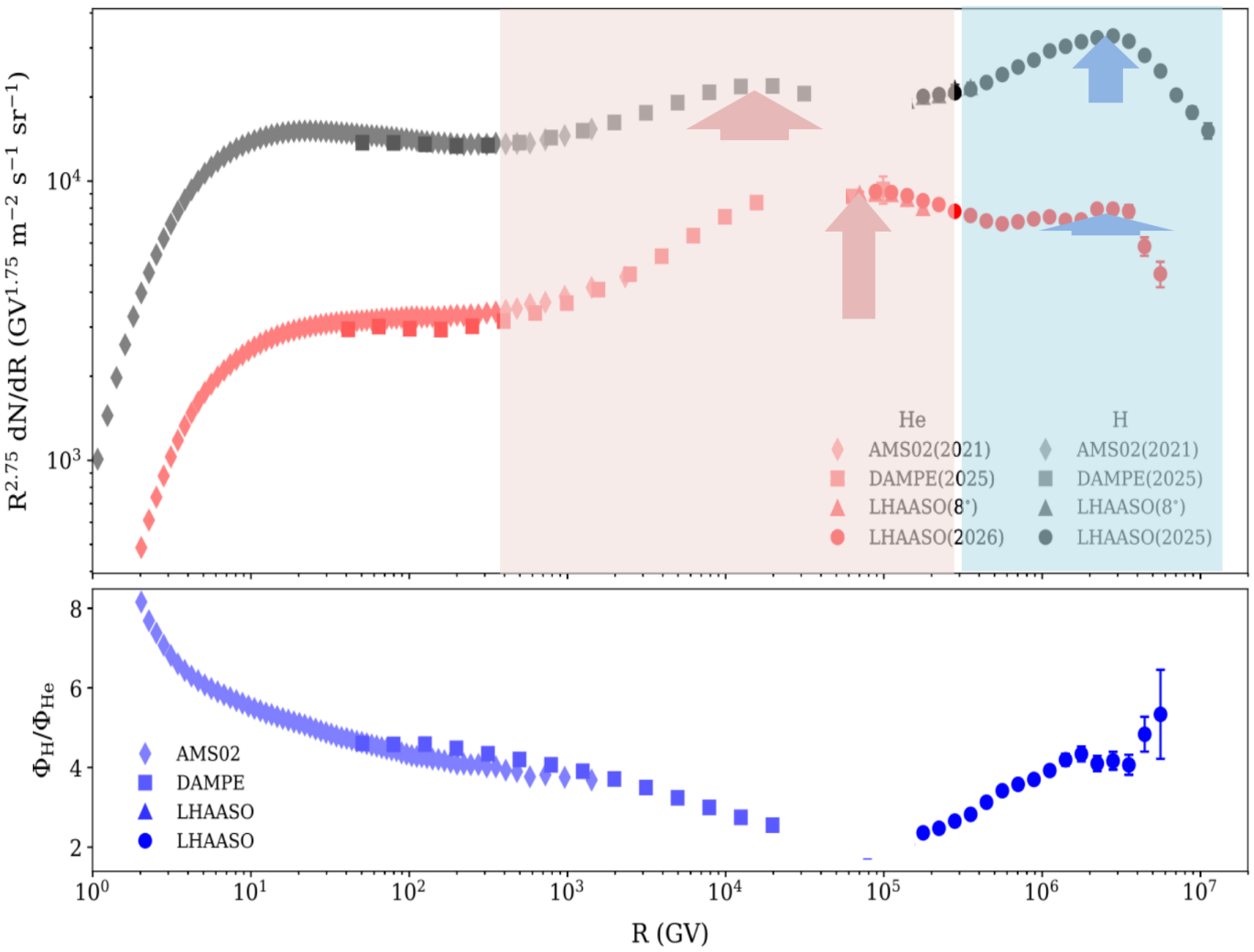
- The "Knee" is a complex feature; p and He exhibit distinct spectral structures and characteristic break energies.
- P: hardening at ~340 TeV, softening (knee) at ~3.3 PeV
- He: hardening at ~ 1.1 PeV, softening (knee) at ~7 PeV
- p/He ratio reverses at least 3 times over the energy rage from 10 TeV to 10 PeV (He-rich ~0.1 PeV, P-rich ~3 PeV)

## Latest p and He energy spectra measurements




LHAASO, Science Bulletin, 70, 24 (2025) arXiv: 2505.14447
LHAASO, PRL, 136, 121001 (2026) arXiv: 2511.05013

# Physical Implications of the P and He Spectra




- **No Strict Rigidity Dependence:** The $p$ and He spectra cannot be explained by a single rigidity-dependent mechanism.

- **Ratio Reversal:** The $p$/He ratio decreases from 10 GV to $\sim 100$TV, then steadily increases up to a few PV.

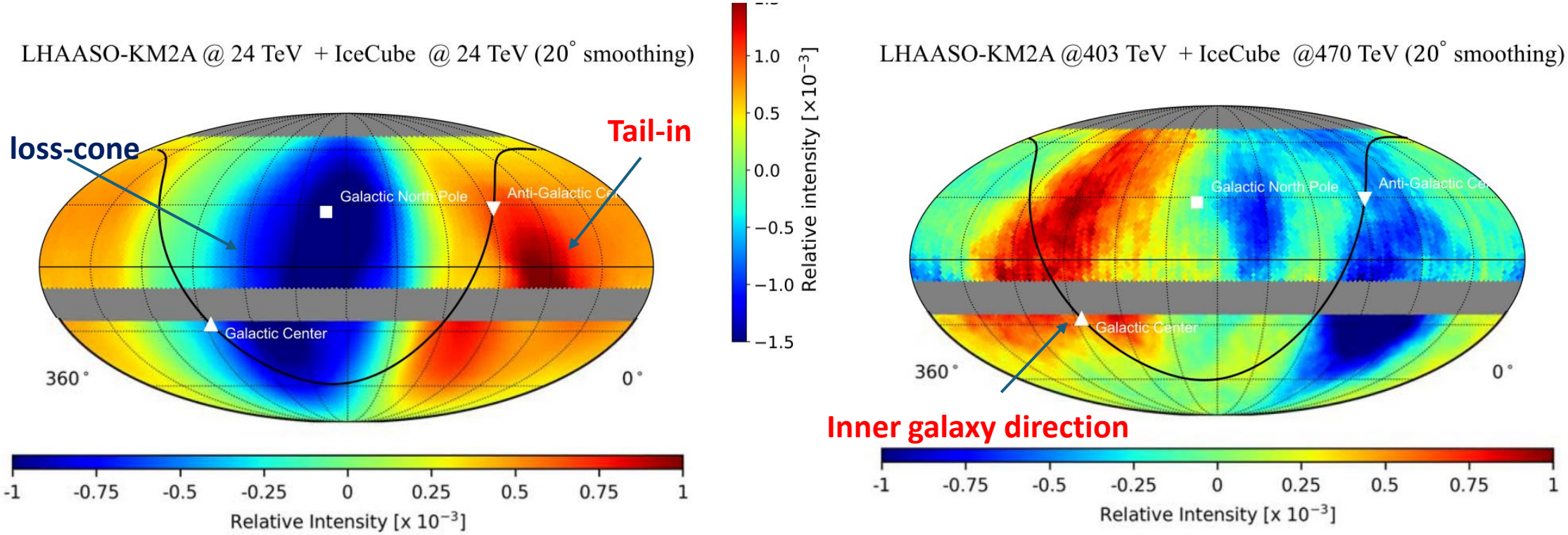
- **Evidence of Multiple Origins:** Two major rigidity components suggest different astrophysical sources:
- **0.1 – 100 TV:** Features a strong He flux enhancement →**He-rich population**.
- **0.1 – 10 PV:** Features a strong $p$ flux enhancement (near the Knee) → **$p$-rich population**.

LHAASO, Science Bulletin, 70, 24 (2025) arXiv: 2505.14447
LHAASO, PRL, 136, 121001 (2026) arXiv: 2511.05013

# Outline

1. **Introduction:** The LHAASO Observatory
2. **Cosmic-Ray Energy Spectra:** Probing the Knee Region
3. **Cosmic-Ray Anisotropy (Focus):**
   - Large-scale anisotropy and energy evolution
   - Rigidity-dependent evolution across species
   - Medium-scale structures & energy-dependent centroid shifts
   - Transient anisotropy driven by ICME
4. **Galactic Diffuse Emission:** UHE $\gamma$-Ray Mapping along the Galactic Plane
5. **Galactic Particle Accelerators (PeVatrons):**
   - Supernova Remnants (SNRs)
   - Pulsar Wind Nebulae (PWNe) & Pulsar Halos
   - Young Massive Star Clusters (YMSCs)
   - Binaries (Microquasars & $\gamma$-Ray Binaries)
6. **Summary & Outlook**

# The All-Sky View: Tens of TeV vs. subPeV



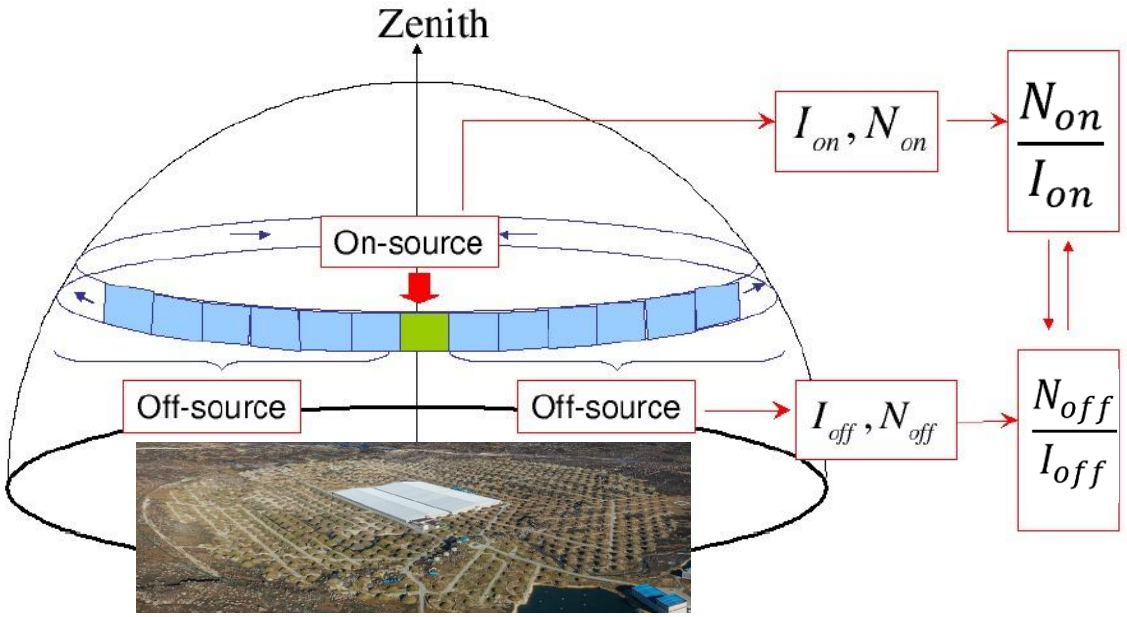

## The Full-Sky Morphological Shift:

**~20 TeV:** A distinct large-scale structure dominated by the classic "tail-in" excess and "loss-cone" deficit.
**~400 TeV:** The global morphology completely inverts, confirming that the 100 TeV phase flip is a coherent, all-sky phenomenon.

# Methodology: All-Distance Equi-Zenith Angle Method

**Relative Intensity Estimation**

- **Method:** Iterative $\chi^2$ approach based on the all-distance equi-zenith method
- **Local-frame binning:**
- 180 time bins
- 40 zenith rings, each divided into equal solid-angle bins in azimuth
- **Celestial mapping:** 2°×2° resolution in equatorial coordinates



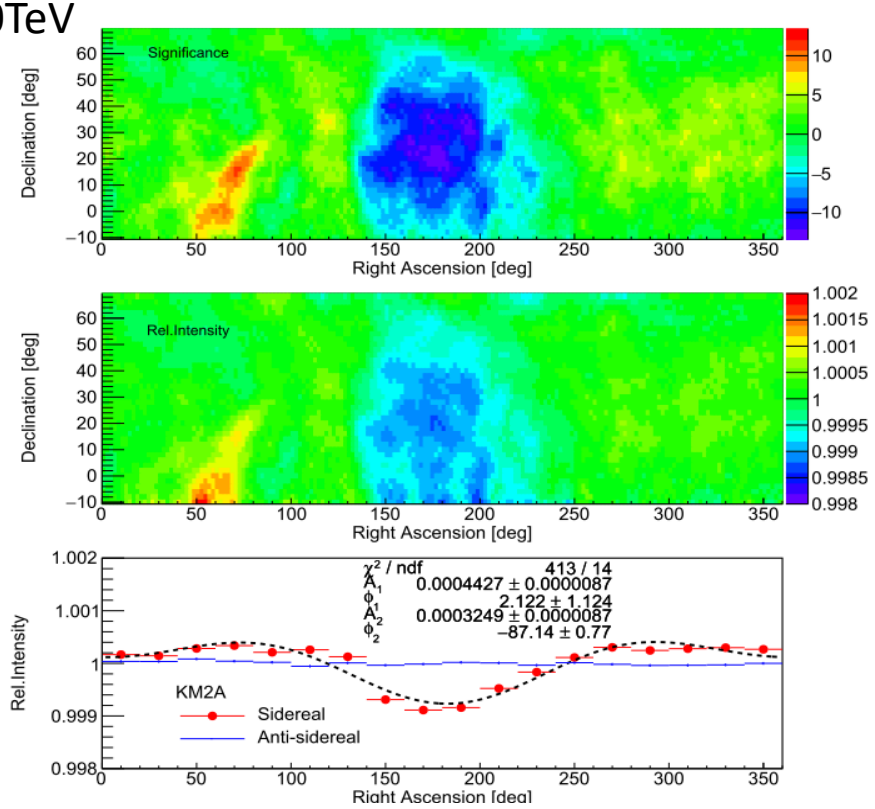

$$\chi^2 = \sum_{t,\theta,\phi} \frac{\left( \frac{N_{t,\theta,\phi}}{I_{i,j}} - \frac{1}{n_\theta - 1} \sum_{\phi' \neq \phi}^{n_\theta} \frac{N_{t,\theta,\phi}}{I_{i',j'}} \right)^2}{\sigma^2_{t,\theta,\phi}}$$

Amenomori, M. et al. ApJ 836, 153 (2017)

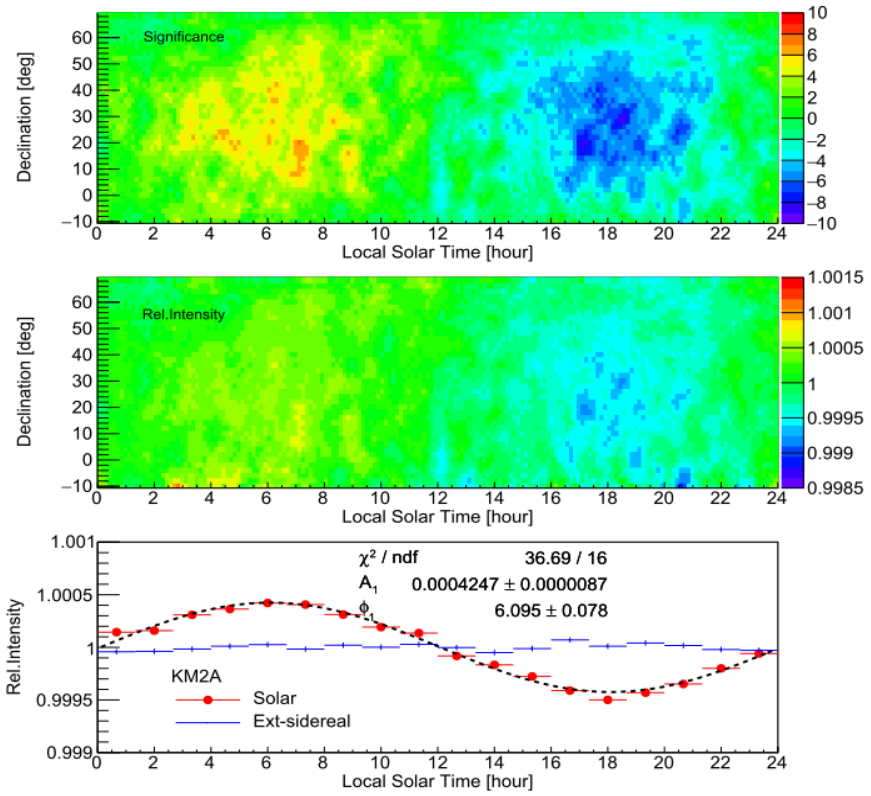
# LHAASO Anisotropy in local Sidereal & Solar Time

- **Dataset:** Full array (V3), 2021/07/20 – 2024/07/19 (3-year data set)
- **Selection Criteria:**
  - $\theta_{\mathrm{rec}} < 40°$
  - $N_{\mathrm{ED}} \geq 20$(triggered electromagnetic detectors)
  - Core contained within array

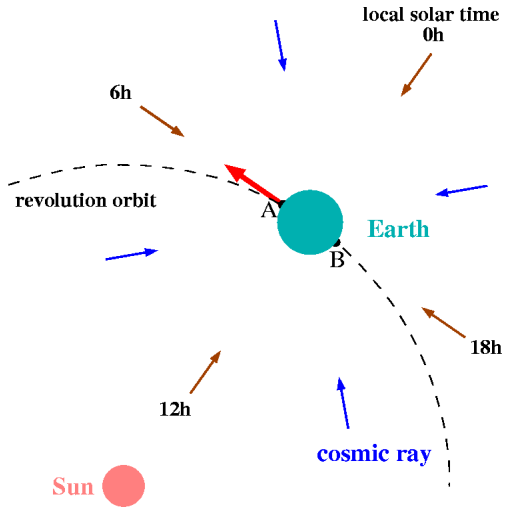
E: 60TeV



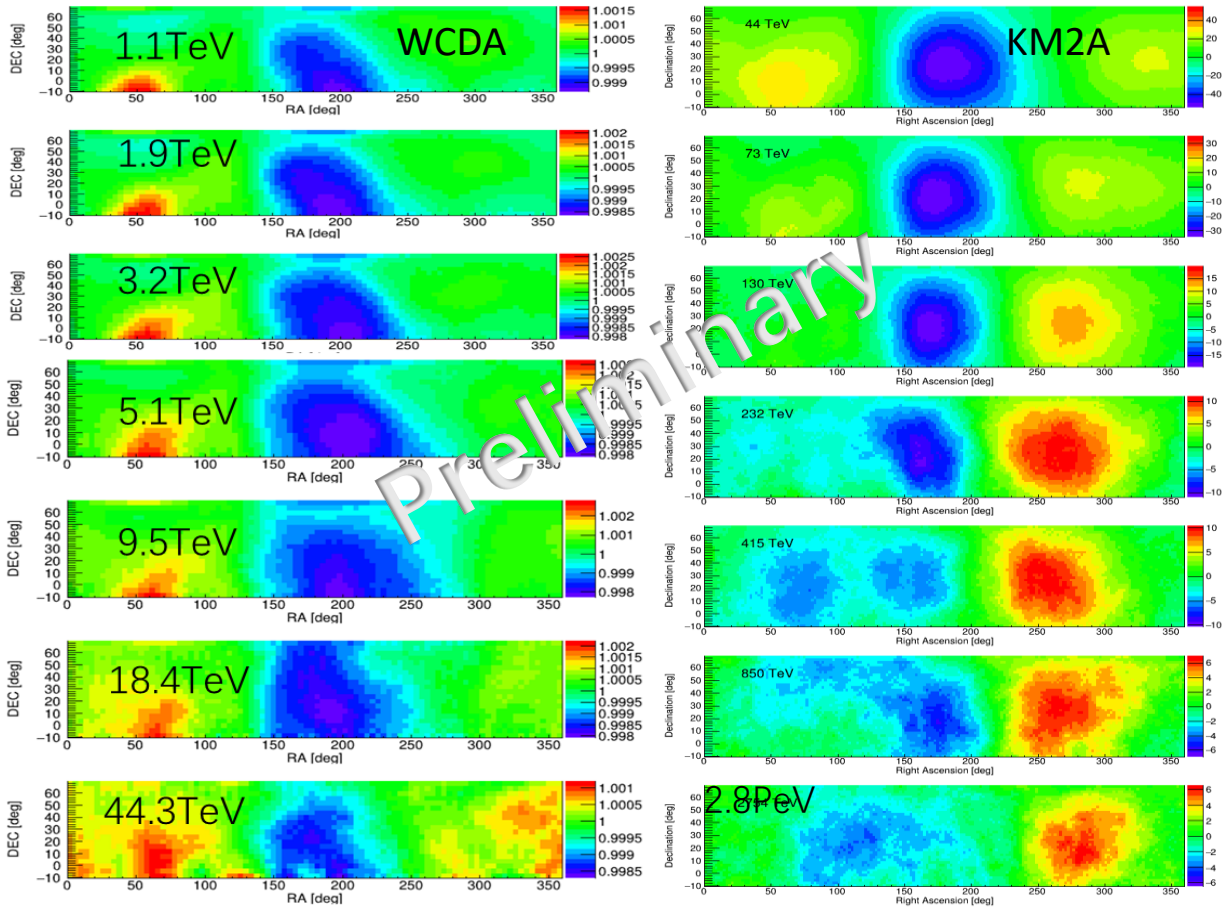

Sidereal time anisotropy

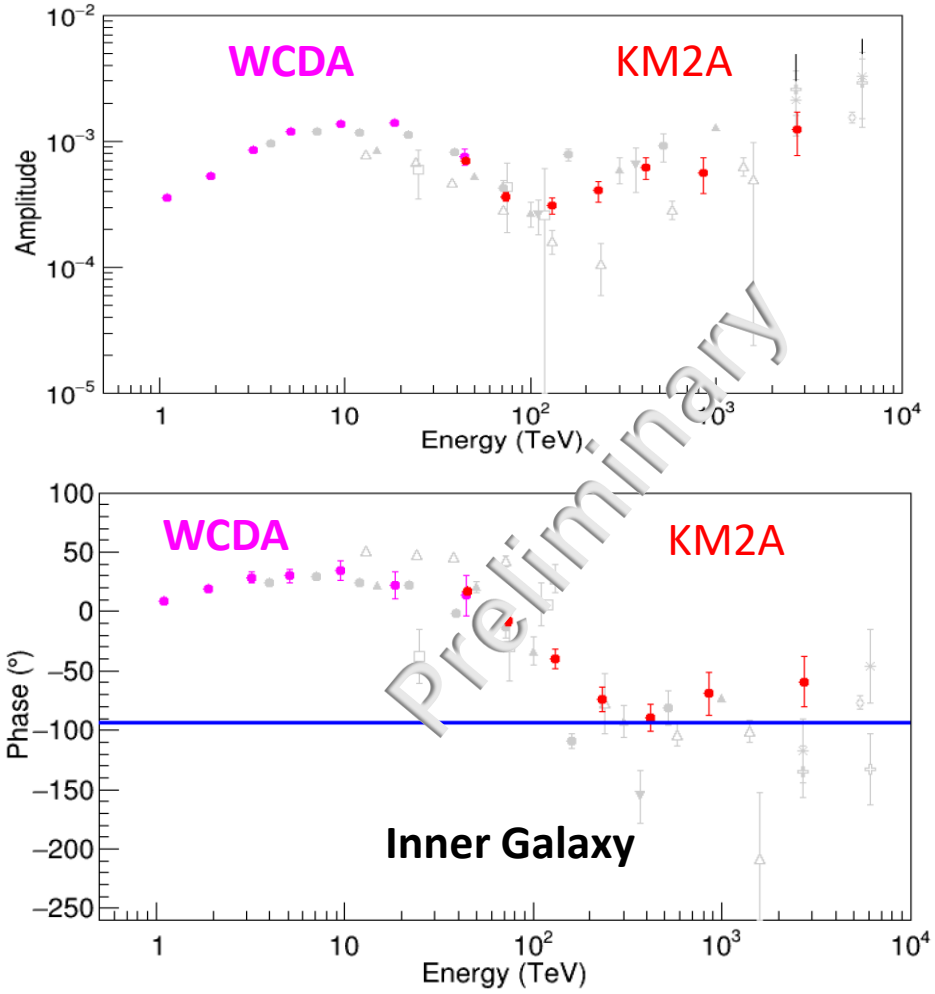



Compton-Getting effect



# Energy Dependence of Cosmic-Ray Anisotropy



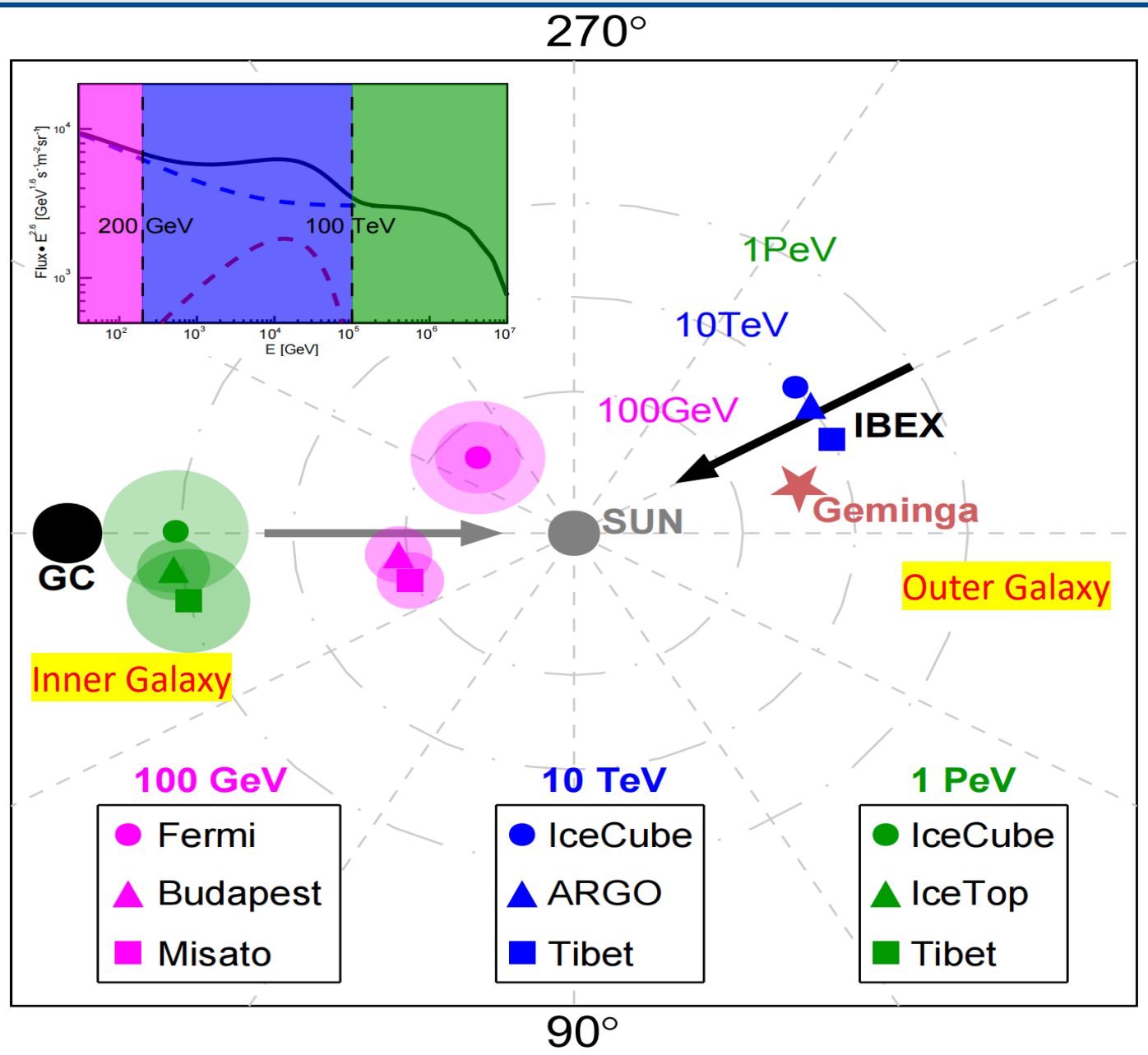

**Broadband Evolution:**

- Reveals a distinct, energy-dependent evolution spanning **1 TeV to 2.8 PeV**, observed continuously by a single facility.
- Both the amplitude and phase transition smoothly across three orders of magnitude in energy.

**Detector Consistency:**

- WCDA and KM2A measurements show excellent agreement in their overlapping energy regime.

# Physical Interpretation: The 100 TeV Phase Flip as a Competing Source




**The Two Competing Environments:**

- **Inner Galaxy:** Dense accelerator population (e.g., SNRs) driving a steady, global background
- **Outer Galaxy:** Powerful nearby sources (e.g., Vela, Geminga) driving an intense, localized flux.

**Low Energies (< 100 TeV): The Nearby Source Dominates**

- Proximity allows the nearby source to completely outshine the Galactic background.
- Guided by the LIMF, this creates a dipole excess pointing toward the Outer Galaxy.

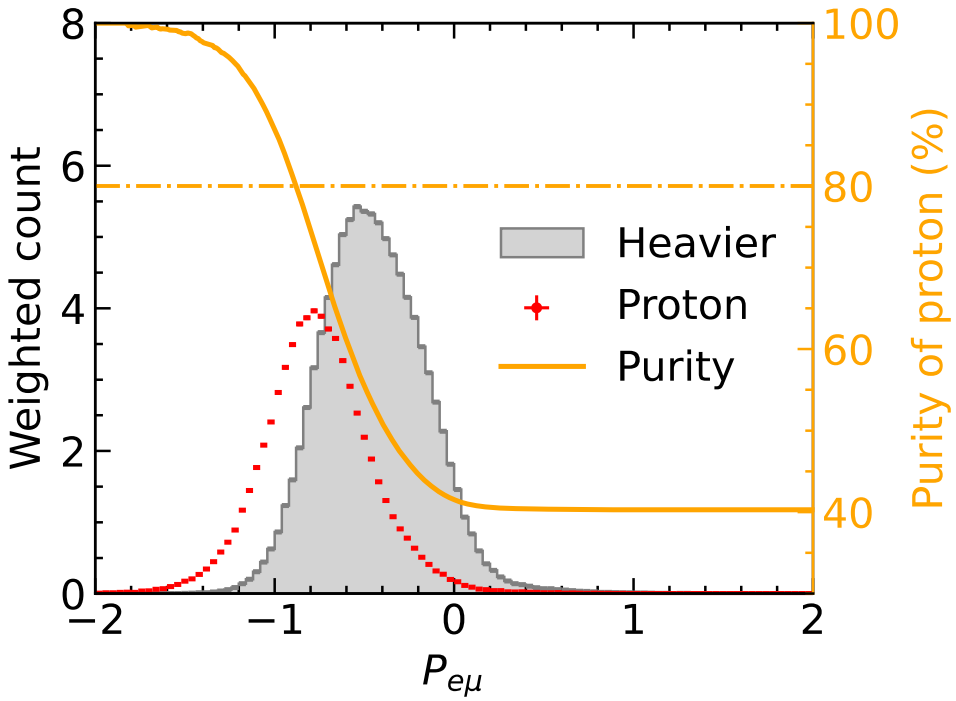
**High Energies (> 100 TeV): The Inner Galaxy Takes Over**

- Cumulative flux from the Inner Galaxy accelerators becomes the dominant component.
- Also modulated by the LIMF, this background shift drives the ~180° phase flip, pointing toward the Inner Galaxy.

# Outline

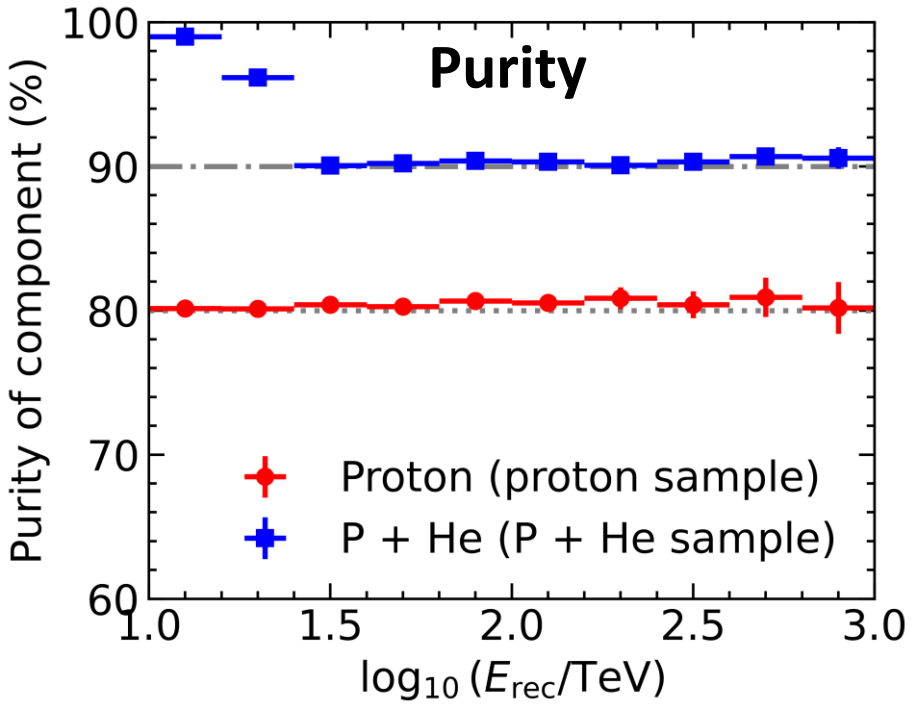
1. **Introduction:** The LHAASO Observatory
2. **Cosmic-Ray Energy Spectra:** Probing the Knee Region
3. **Cosmic-Ray Anisotropy (Focus):**
    - Large-scale anisotropy and energy evolution
    - **Rigidity-dependent evolution across species**
    - Medium-scale structures & energy-dependent centroid shifts
    - Transient anisotropy driven by ICME
4. **Galactic Diffuse Emission:** UHE $\gamma$-Ray Mapping along the Galactic Plane
5. **Galactic Particle Accelerators (PeVatrons):**
    - Supernova Remnants (SNRs)
    - Pulsar Wind Nebulae (PWNe) & Pulsar Halos
    - Young Massive Star Clusters (YMSCs)
    - Binaries (Microquasars & $\gamma$-Ray Binaries)
6. **Summary & Outlook**

# Data Analysis: Mass Composition / Primary Particle Selection




**Particle identity parameter:**

$$P_{e\mu} = \log_{10} \frac{N_\mu + 10^{-4}}{N_e}$$



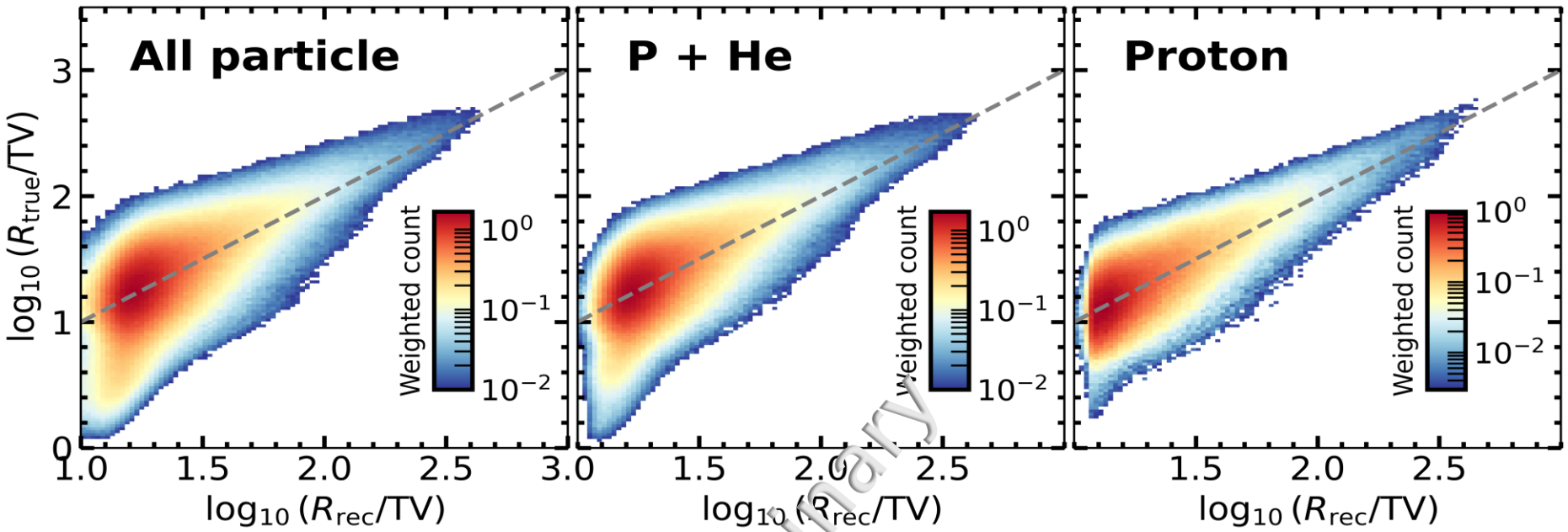

**Particle Identification (PID) Strategy:**

- **Light component** ($p$ + He)**:** $> 90\%$purity
- **Pure proton sample** ($p$)**:** $> 80\%$purity

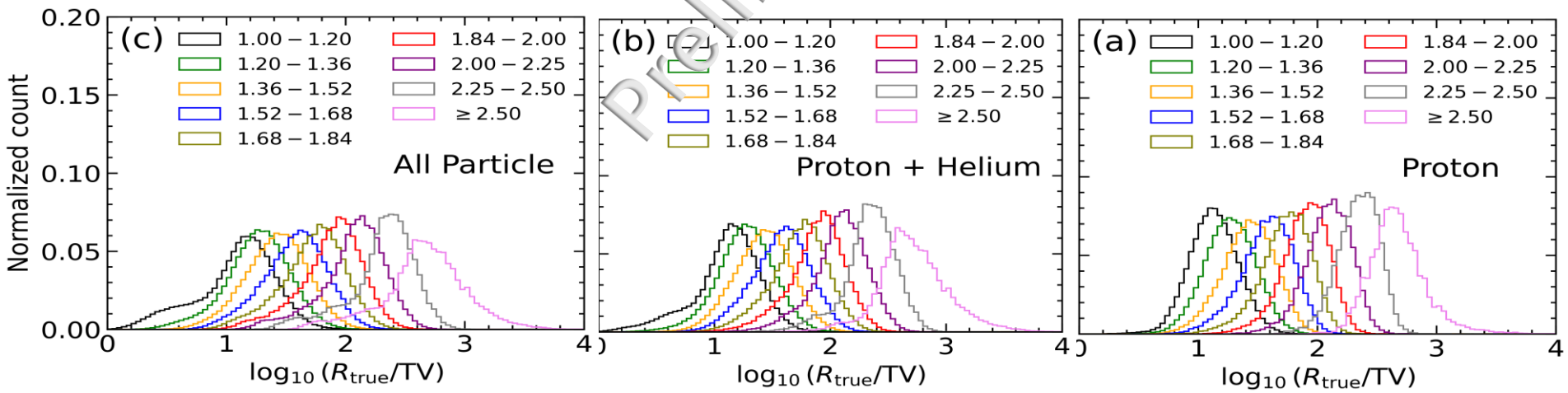
# Rigidity Reconstruction Method

New rigidity reconstruction method based on:

$N_\mu, N_e, S_{50}, \theta$

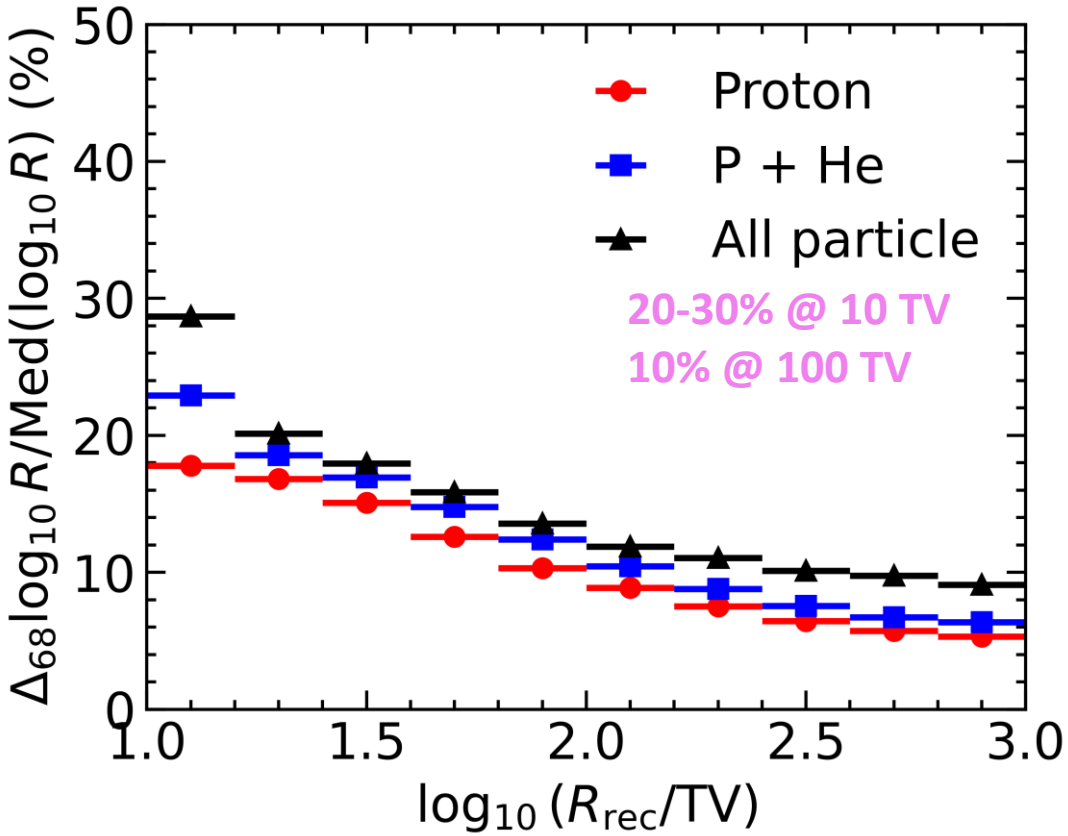



**Correlation: True vs. Reconstructed Rigidity.**

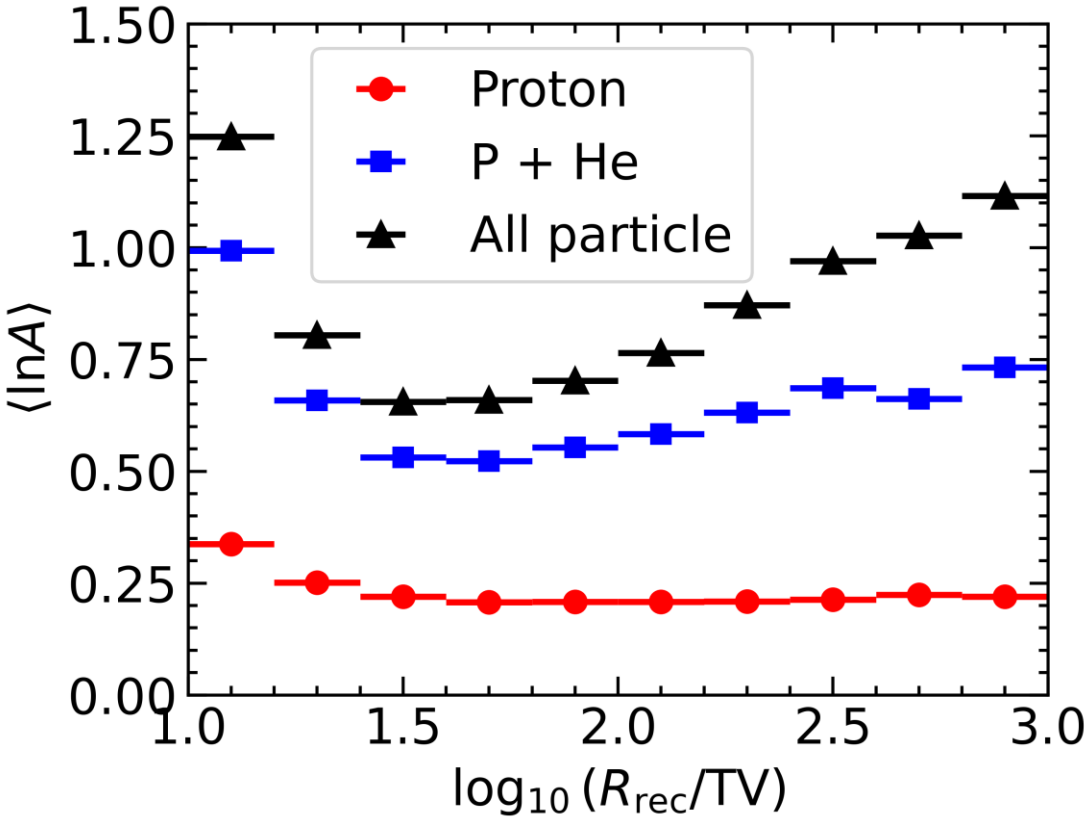



**True rigidity distributions for reconstructed bins.**

# Data Analysis: Rigidity Reconstruction & Performance



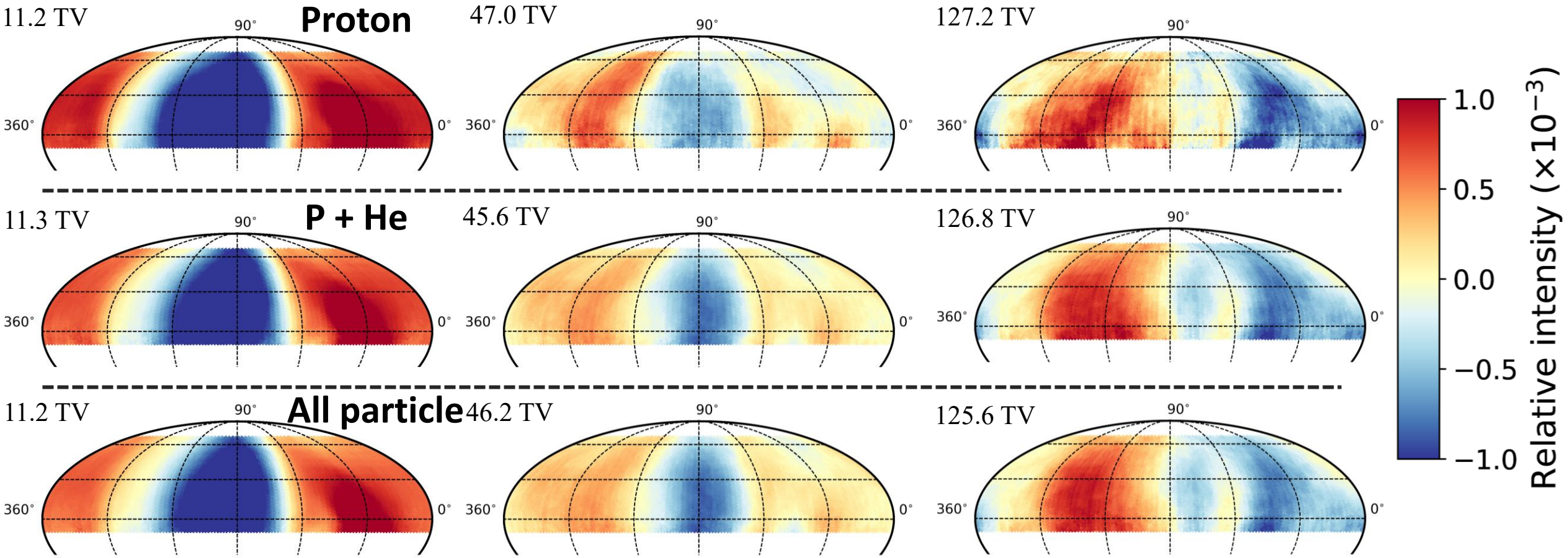

**Rigidity resolution and dispersion evaluated via detector simulation**




**Mass composition of selected samples across rigidity bins**

# Results: 2D Anisotropy Sky Maps

Top-hat smooth with a 20-degree radius.




- **Morphology:** Different primary samples exhibit remarkably consistent anisotropy patterns.
- **Transition Energy:** A distinct pattern transition is observed around 50 TV.

# Dipole Amplitude & Phase: Rigidity Scaling

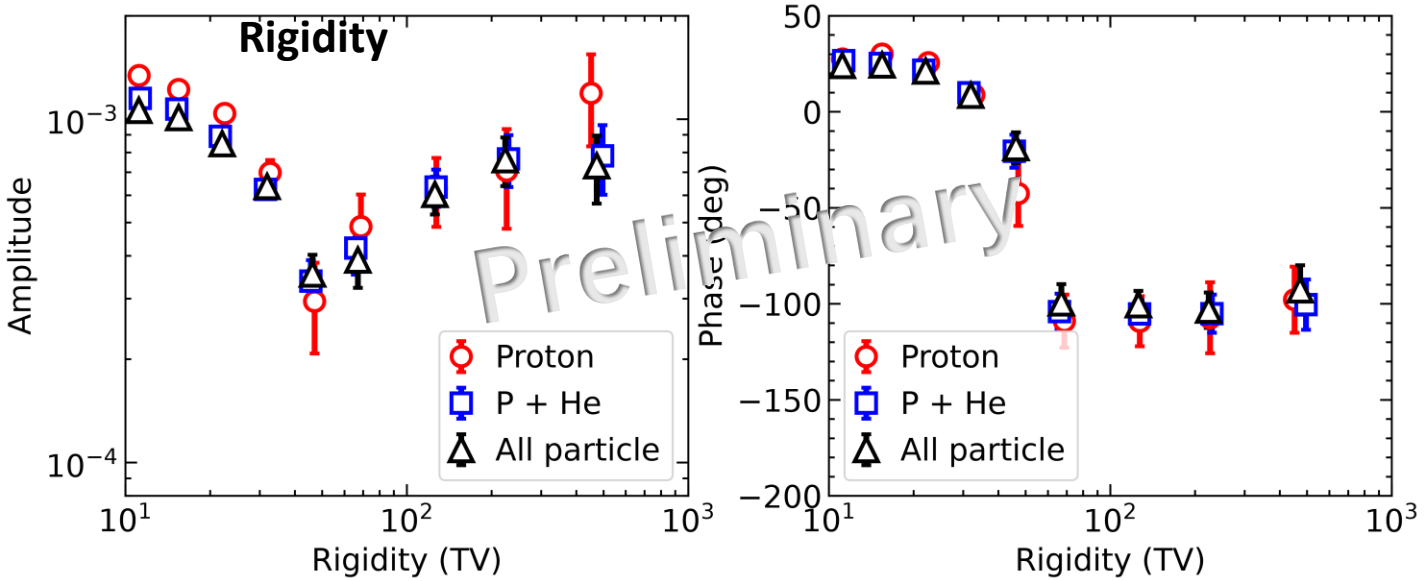
**Harmonic Analysis:**

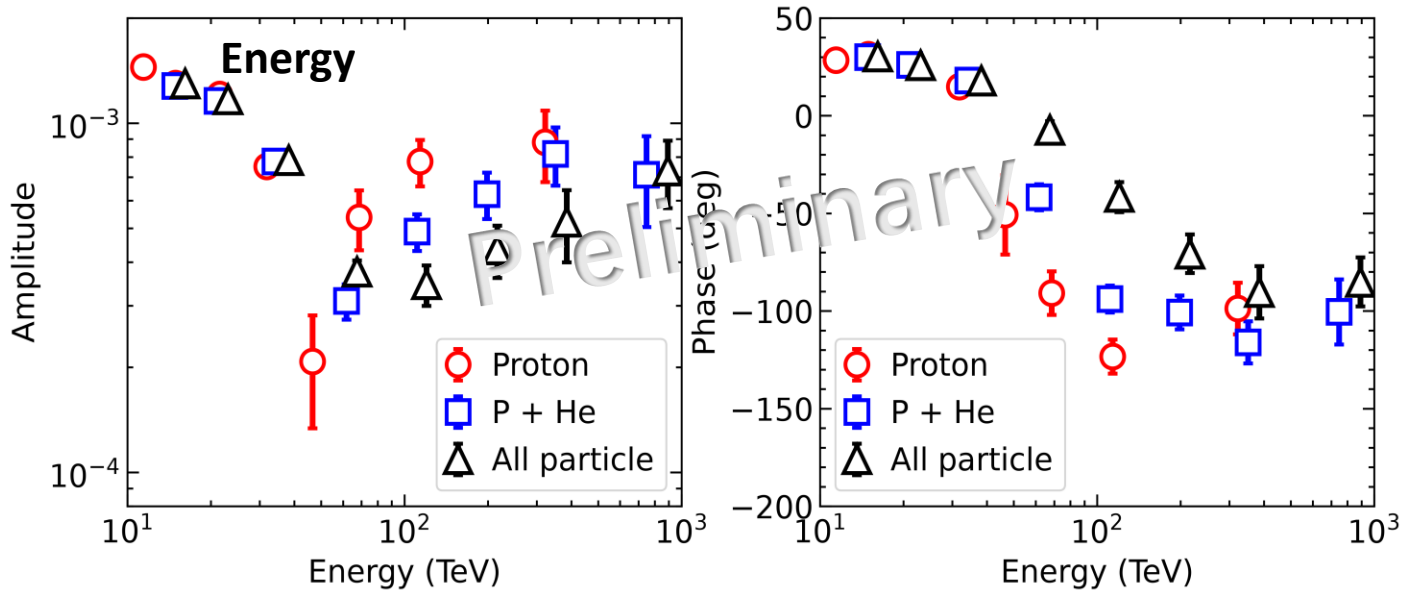
- 1D relative intensity profiles projected along Right Ascension ($\alpha$):
- $I(\alpha) = 1 + \sum_{k=1}^{2} A_k \cos[k(\alpha - \phi_k)]$

*(where $A_1, \phi_1$ denote the dipole amplitude and phase)*

**Rigidity-dependent:** Different mass samples align and share a **common rigidity-dependent evolution**

Demonstrates that the transition scales with **magnetic rigidity ($R = E/Z$)** rather than primary energy alone



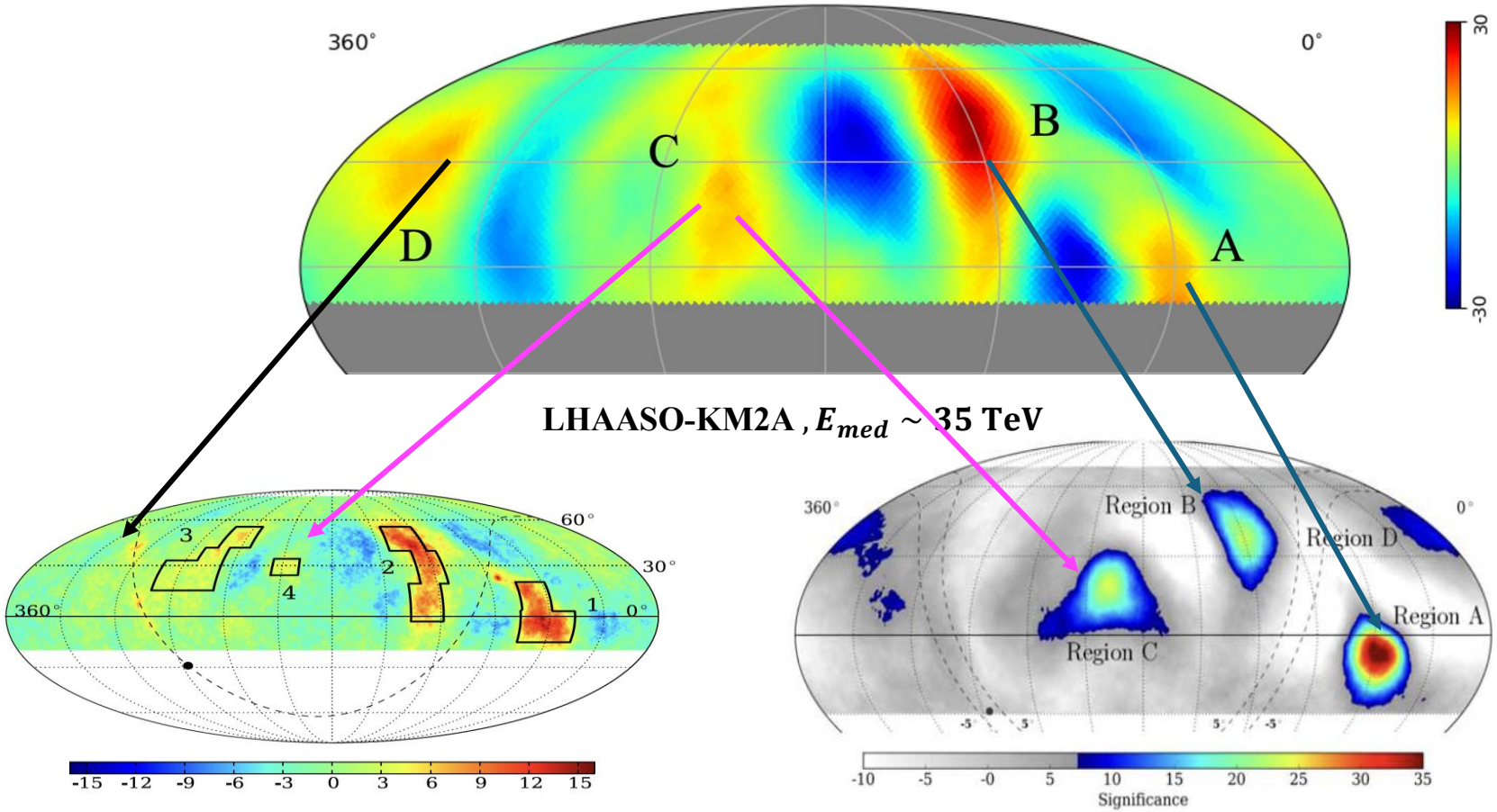



# Outline

1. **Introduction:** The LHAASO Observatory
2. **Cosmic-Ray Energy Spectra:** Probing the Knee Region
3. **Cosmic-Ray Anisotropy (Focus):**
   - Large-scale anisotropy and energy evolution
   - Rigidity-dependent evolution across species
   - Medium-scale structures & energy-dependent centroid shifts
   - Transient anisotropy driven by ICME
4. **Galactic Diffuse Emission:** UHE $\gamma$-Ray Mapping along the Galactic Plane
5. **Galactic Particle Accelerators (PeVatrons):**
   - Supernova Remnants (SNRs)
   - Pulsar Wind Nebulae (PWNe) & Pulsar Halos
   - Young Massive Star Clusters (YMSCs)
   - Binaries (Microquasars & $\gamma$-Ray Binaries)
6. **Summary & Outlook**

# LHAASO Observation of Medium--scale anisotropy

$$\delta I(\alpha,\delta) = \sum_{l=0}^{3}\sum_{m=-l}^{l} a_{lm} Y_{lm}\left(\frac{\pi}{2}-\delta,\alpha\right),\ \text{Subtract } l \le 2$$



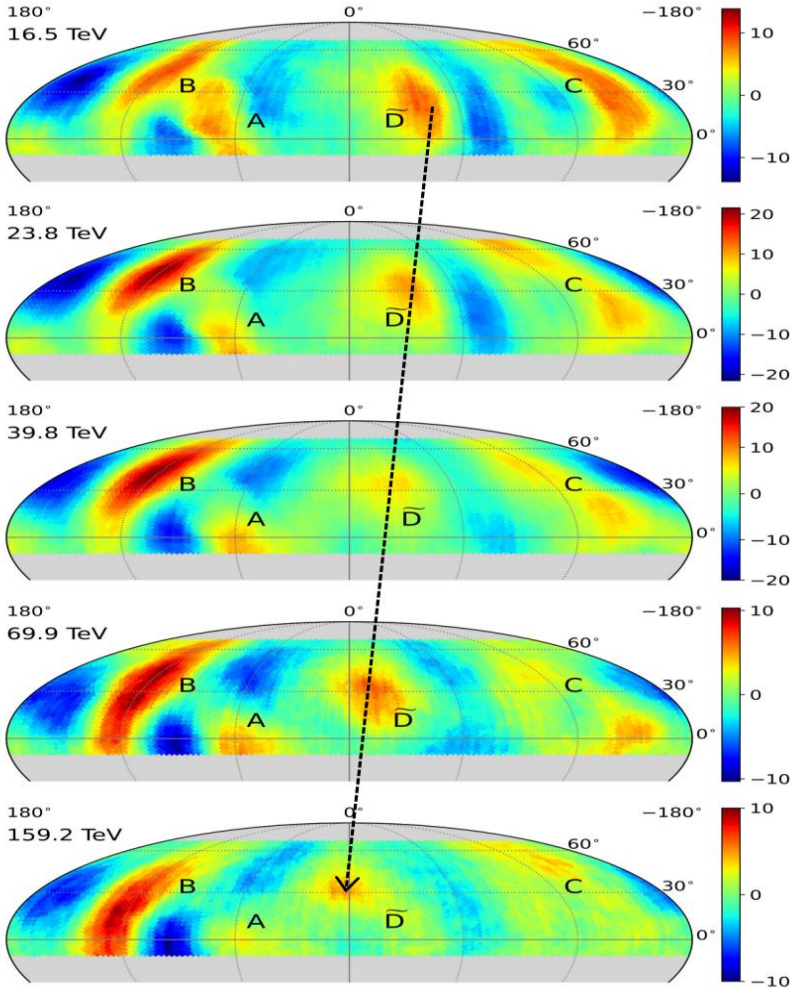

**ARGO-YBJ 2011** @~ 2 TeV

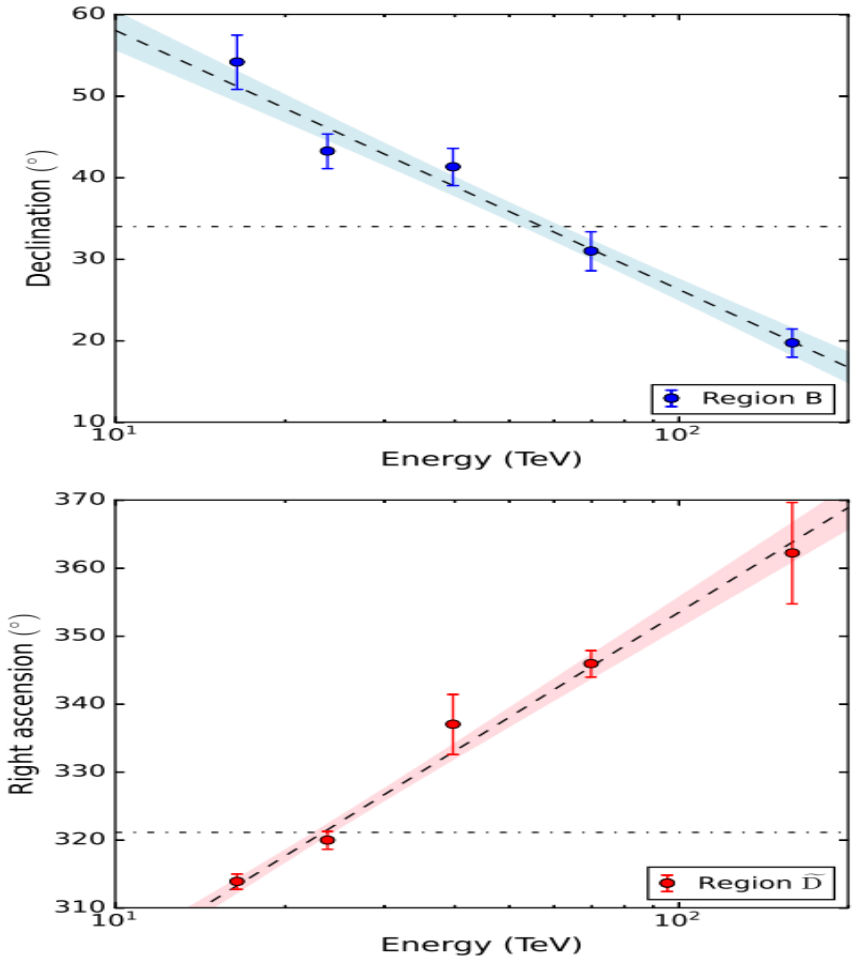
**HAWC 2018** @~ 2 TeV

Four regions are detected by LHAASO; Region A and B are consistent with results from other experiments. Region C was also observed by HAWC and ARGO, and ARGO-YBJ shows hints of Region D.

# Positional Evolution of MSA Regions with Energy



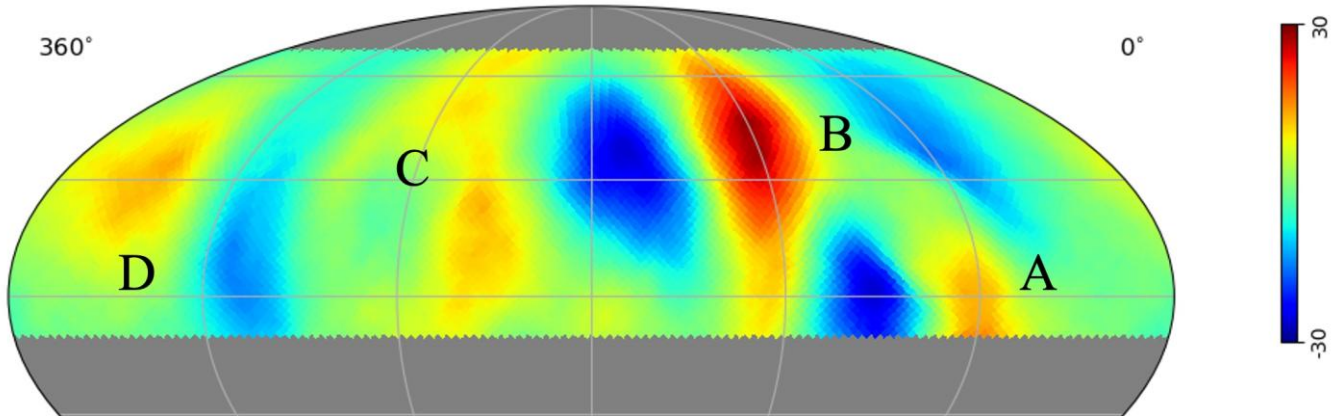


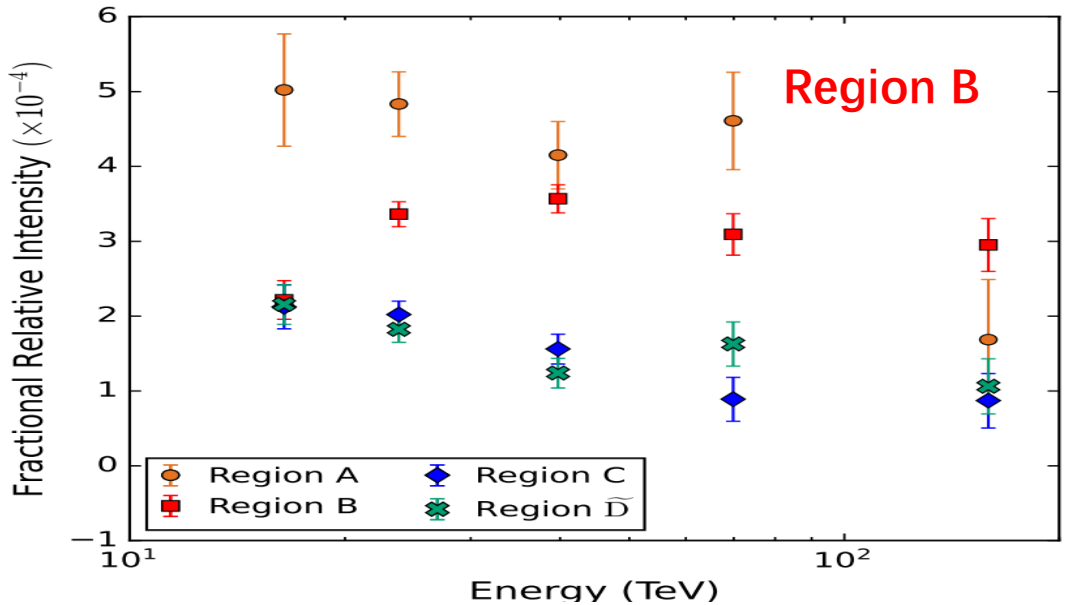




- First observation of significant energy-dependent positional shifts in MSA excess regions (10 to over 100 TeV).
- Reproduced by models, suggesting that MSA is shaped by specific local turbulent magnetic field realizations.

LHAASO collaboration, Phys. Rev. Lett. **137**, 051004 (2026)

# Energy dependence of Medium--scale anisotropy




- Certain regions persist up to 200 TeV, whereas other features gradually fade.
- This persistence rules out heliospheric/solar effects as the dominant driver of the observed anisotropy.

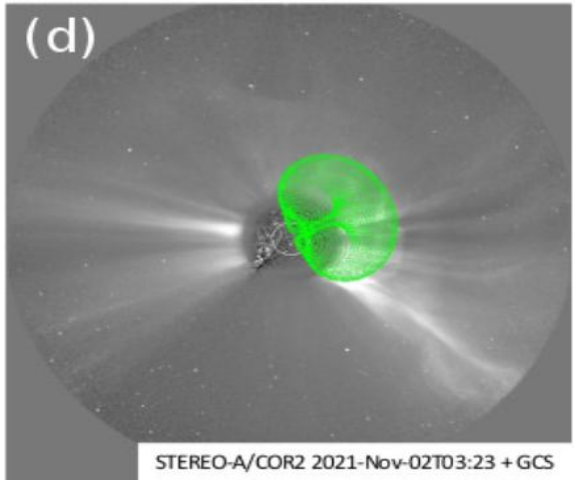
LHAASO collaboration, Phys. Rev. Lett. **137**, 051004 (2026)

# Outline

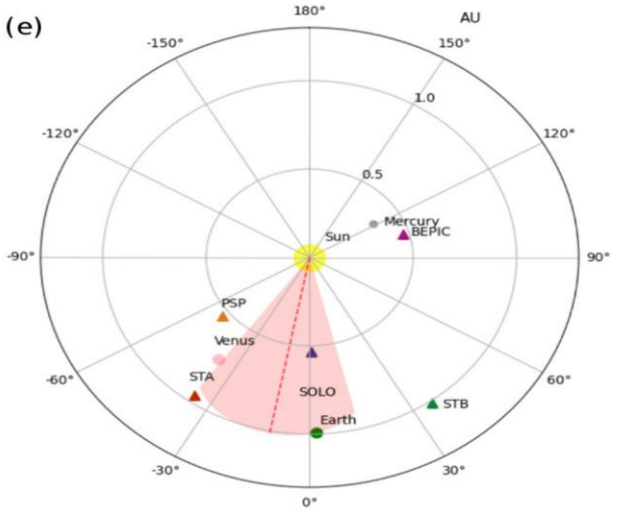
1. **Introduction:** The LHAASO Observatory
2. **Cosmic-Ray Energy Spectra:** Probing the Knee Region
3. **Cosmic-Ray Anisotropy (Focus):**
   - Large-scale anisotropy and energy evolution
   - Rigidity-dependent evolution across species
   - Medium-scale structures & energy-dependent centroid shifts
   - Transient anisotropy driven by ICME
4. **Galactic Diffuse Emission:** UHE $\gamma$-Ray Mapping along the Galactic Plane
5. **Galactic Particle Accelerators (PeVatrons):**
   - Supernova Remnants (SNRs)
   - Pulsar Wind Nebulae (PWNe) & Pulsar Halos
   - Young Massive Star Clusters (YMSCs)
   - Binaries (Microquasars & $\gamma$-Ray Binaries)
6. **Summary & Outlook**

# Bidirectional anisotropy produced by an ICME

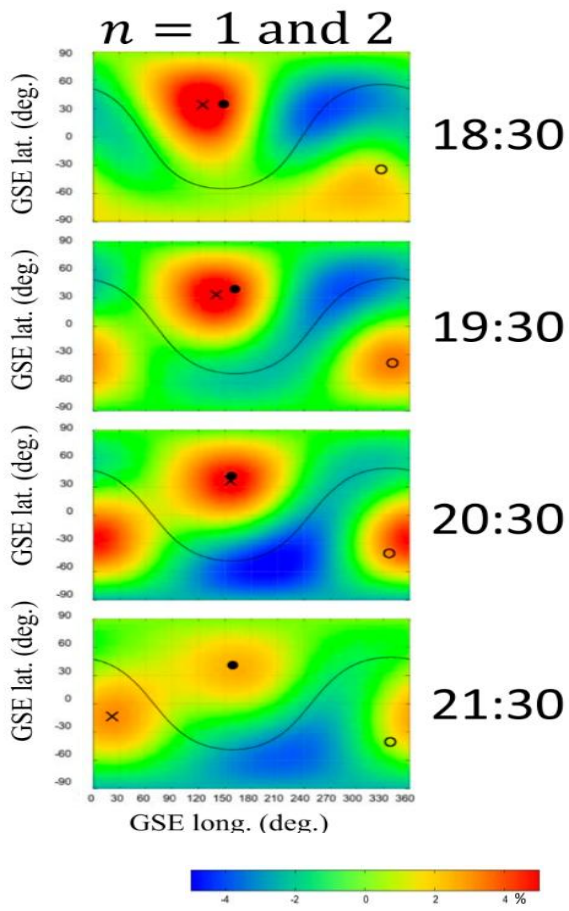
- The ICME on 2021 November 4-5 (see images) produced an unusually strong bidirectional anisotropy, as observed by neutron monitors (median 15+ GV) and muon detectors (median 65+ GV), with more ions moving along **B** or **–B** [Munakata+22].
- Possible mechanisms (involve gyro-orbits within flux rope:
  - Adiabatic focusing/deceleration due to flux rope expansion
  - Ions drifting into one leg of the flux rope
- To our knowledge, **transient effects on cosmic rays have never been observed above ~150 GeV,** other than on the Sun shadow.
- To search for transient cosmic ray anisotropy >100 GeV, we developed techniques to examine hourly anisotropy in LHAASO data.




[Thalmann+23]




@ 15 GV, 2021 Nov 4

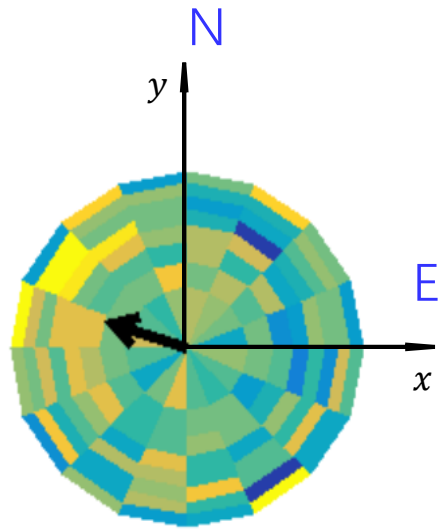



[Munakata+22]

# Analysis Method

1. Only consider hours with a standard number of events (100-120 million per hour)
2. Divide hourly skymap of intensity into "pizza slices" of equal solid angle: $I_{t,\theta,\varphi}^{on,off}$
   - 16 values of azimuthal angle $\varphi$
   - 8 values of zenith angle $\theta$, equally spaced in cos $\theta$, up to $\theta$ = 45 deg
3. $N_{t,\theta,\varphi}^{on}$ : Counts at some hour $t$ and direction $\theta, \varphi$ on the skymap of a specific day.
4. $N_{t,\theta,\varphi}^{off}$: Average for same hour during preceding and following 2 days,

   for a total of **4** days as background for the specific hour.




5. $I_{t,\theta,\varphi} = \frac{N_{t,\theta,\varphi}^{on}}{N_{t,\theta,\varphi}^{off}}$ : Hourly skymap of relative intensity.

$$g = \sqrt{g_x^2 + g_y^2}$$

6. $I_{t,\theta,\phi}^{Final} = \frac{I_{t,\theta,\varphi}}{\frac{1}{16}\sum_{\varphi=1}^{16} I_{t,\theta,\varphi}}$ : Normalize intensity by average at that zenith angle.

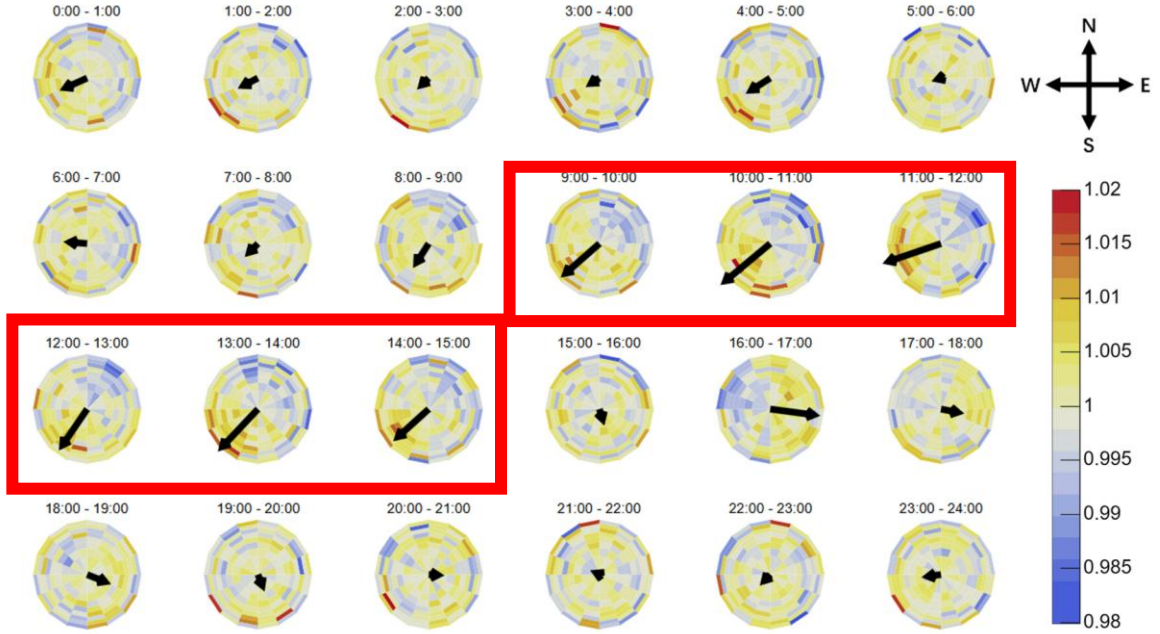
7. **Define gradient.** $x_i = sin\theta_i cos\varphi_i$, $y_i = sin\theta_i sin\varphi_i$ $\theta_i, \varphi_i$ are the values of the zenith angle and azimuth angle for the i[th] bin.

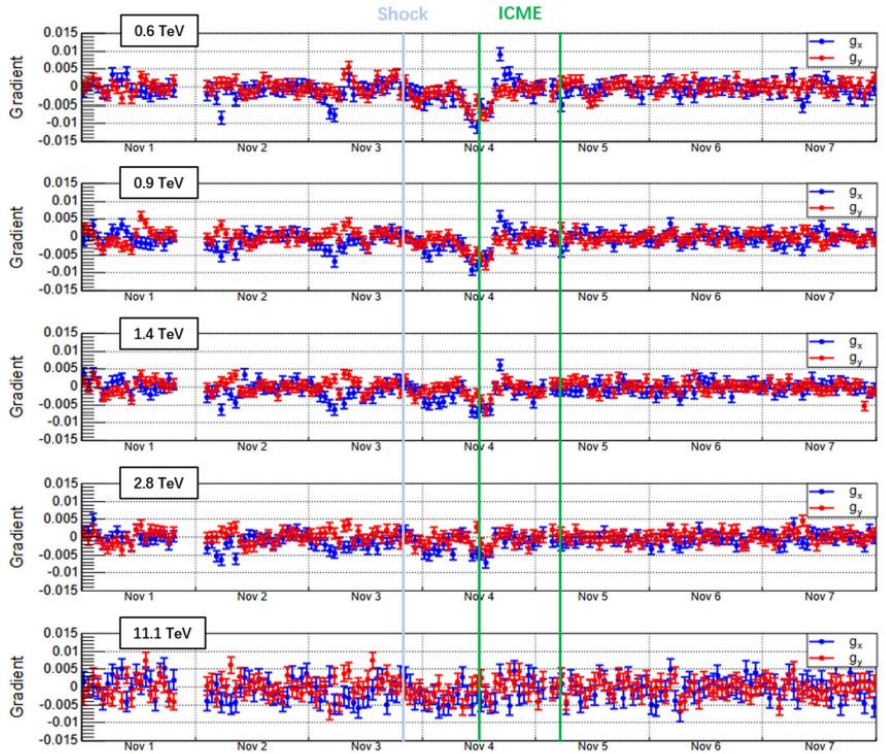
Define: $f = 1 + g_x x_i + g_y y_i$, $g_x, g_y$ are the components of the gradient vector

Minimum: $\chi^2 = \sum_{i=1}^{n} \frac{[I_i - (1 + g_x x_i + g_y y_i)]^2}{\sigma^2(I_i)}$

# ICME-Induced TeV Anisotropy

| Disturbance Y/M/D (UT) (a) | ICME Plasma/Field Start, End Y/M/D (UT) (b) | | Comp. Start, End (Hrs wrt. Plasma/ Field) (c) | | MC Start, End (Hrs wrt. Plasma/ Field) (d) | | BDE? (e) | BIF? (f) | Qual. (g) | dV (km/s) (h) | V_ICME (km/s) (i) | V_max (km/s) (j) | B (nT) (k) | MC? (l) | Dst (nT) (m) | V_transit (km/s) (n) |
|---|---|---|---|---|---|---|---|---|---|---|---|---|---|---|---|---|
| 2021/10/12 0226 | 2021/10/12 1600 | 2021/10/14 0000 | ... | ... | ... | ... | Y | ... | 2 | 60 | 440 | 490 | 6 | 1 | -65 P | 620 |
| 2021/11/03 1942 | 2021/11/04 0700 | 2021/11/05 0500 | ... | ... | ... | ... | Y | ... | 1 | 250 | 650 | 770 | 17 | 2 | -105 P | 630-1100 |

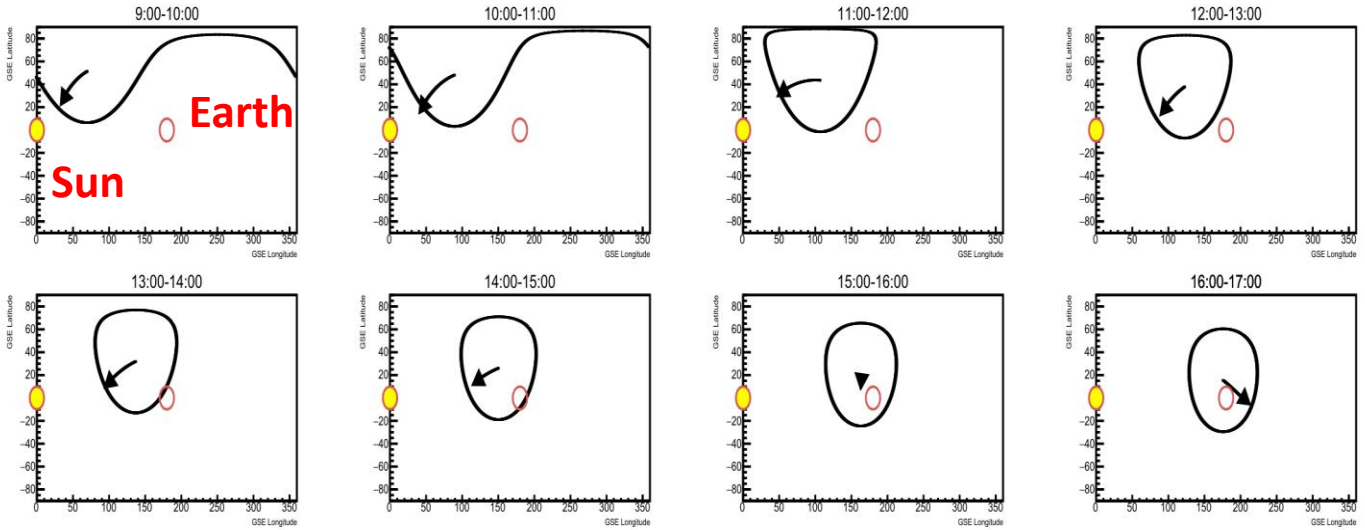


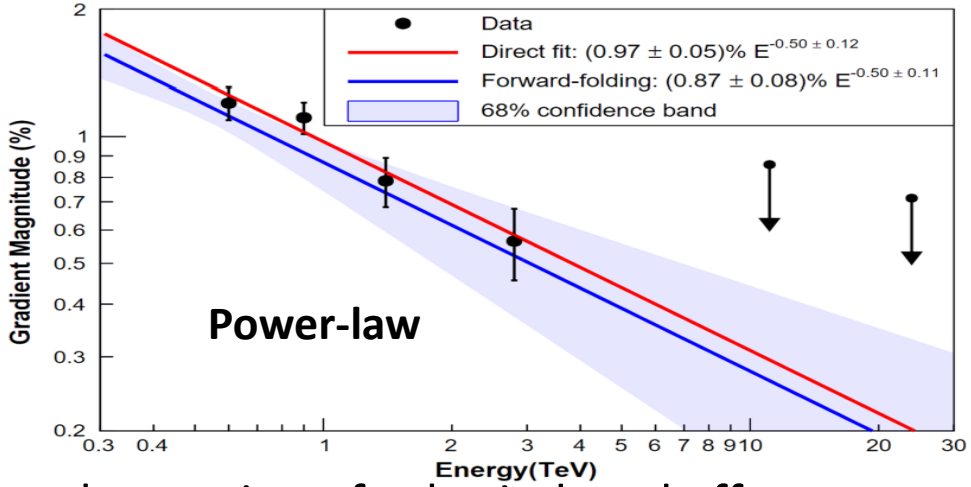

- Hourly skymaps of relative CR intensity measured by WCDA.
- The ICME impact occurred at ~12:00 UT (highlighted by red boxes).
- Black arrows represent gradient vectors, where the arrow length indicates magnitude and the direction points toward intensity enhancements.

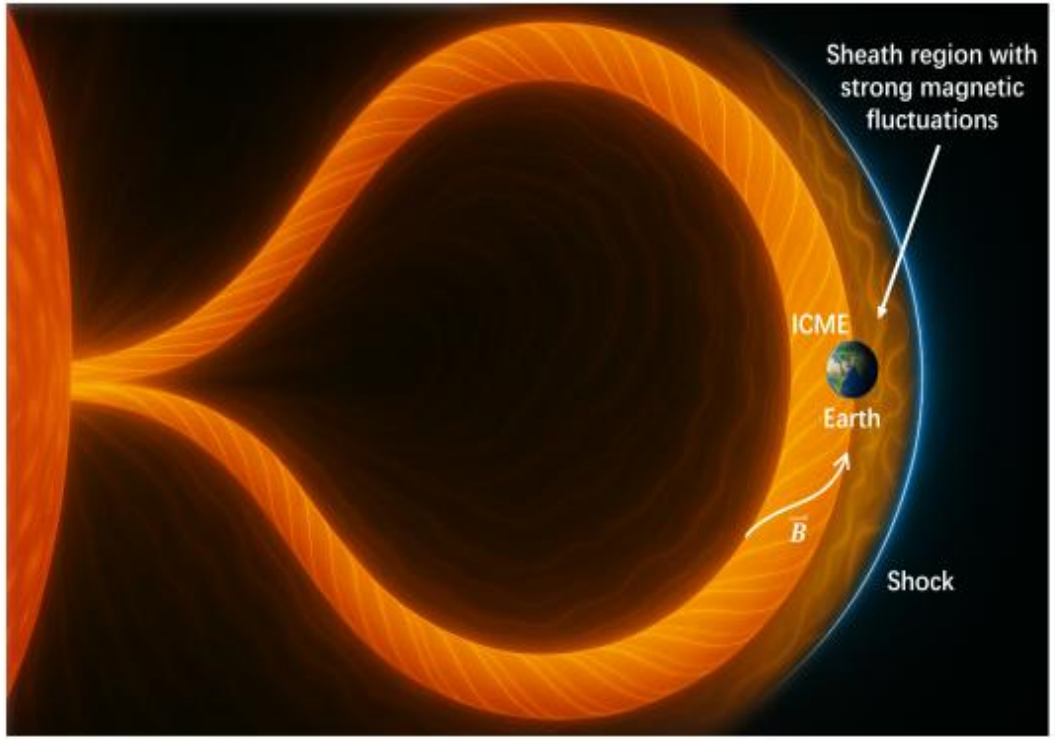
Gradient vectors as a function of time for five energy bins.

# ICME-Induced TeV Anisotropy




Gradient vectors in GSE coordinates.




Schematic of an ICME flux rope passing Earth (Nov 4, 2021), preceded by an interplanetary shock and a turbulent sheath region.

- First observation of solar-induced effects on transient TeV large-scale anisotropy.
- Suggests TeV cosmic rays scattering by intense magnetic fluctuations in the sheath region.

The LHAASO Collaboration, Phys. Rev. Lett. 136, 251002 (2026)

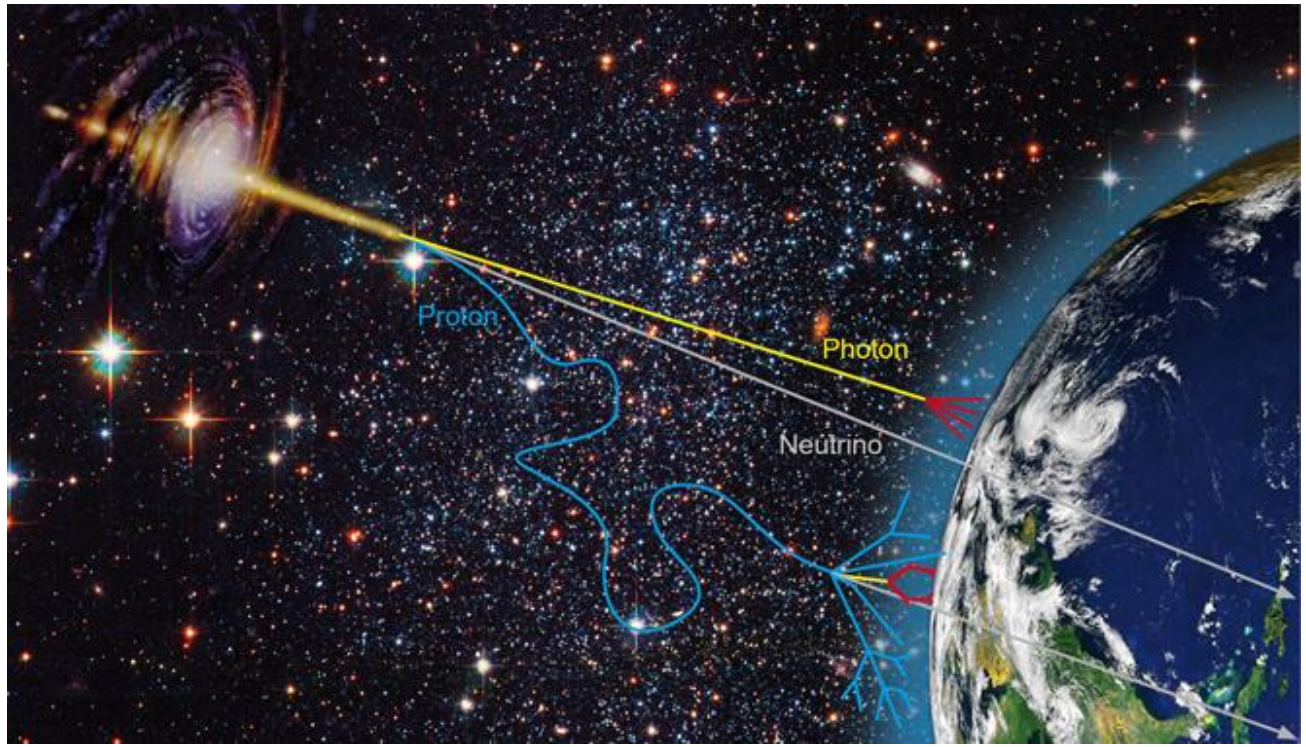
# Insights from Cosmic Rays & The Need for Neutral Messengers

LHAASO 高海拔宇宙线观测站 Large High Altitude Air Shower Observatory

## Insights from Direct CR Observations:

- **From Energy Spectra:** The spectral structures suggest the existence of at least two distinct source populations below the "Knee" region.

- **From Anisotropy:** The arrival direction distributions hint at the presence of a dominant nearby source, combined with a large concentration of sources towards the inner galaxy direction.




Charged cosmic rays are deflected by interstellar magnetic fields, almost completely losing their original directional information.

Since magnetic fields scramble the paths of charged particles, tracing them back to their origins requires neutral messengers—**making gamma-ray observations our most powerful and viable tool for pinpointing Galactic accelerators.**

# Outline

1. **Introduction:** The LHAASO Observatory
2. **Cosmic-Ray Energy Spectra:** Probing the Knee Region
3. **Cosmic-Ray Anisotropy (Focus):**
   - Large-scale anisotropy and energy evolution
   - Rigidity-dependent evolution across species
   - Medium-scale structures & energy-dependent centroid shifts
   - Transient anisotropy driven by ICME
4. **Galactic Diffuse Emission:** UHE $\gamma$-Ray Mapping along the Galactic Plane
5. **Galactic Particle Accelerators (PeVatrons):**
   - Supernova Remnants (SNRs)
   - Pulsar Wind Nebulae (PWNe) & Pulsar Halos
   - Young Massive Star Clusters (YMSCs)
   - Binaries (Microquasars & $\gamma$-Ray Binaries)
6. **Summary & Outlook**

# The GDE Spectrum: Confronting Models with the Observed Flux Excess

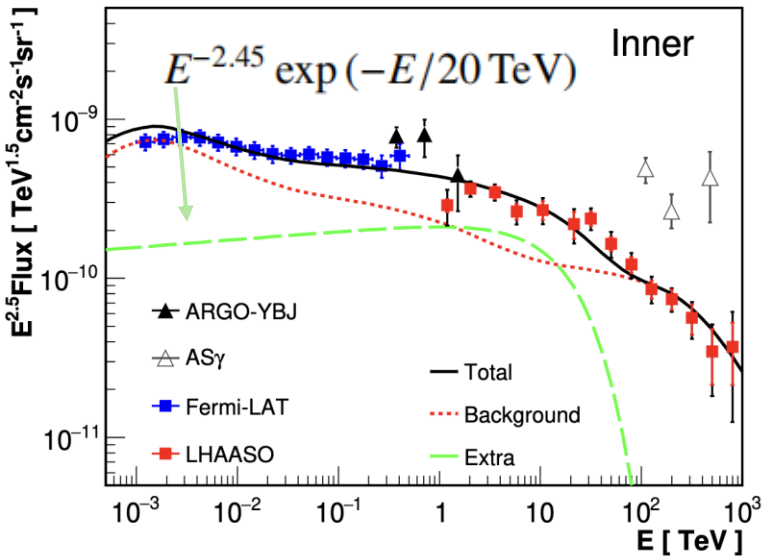
- Measured fluxes > model prediction ( local CR spectra+gas column density), roughly consistent with gas distributions for b, but show significant deviation for l .

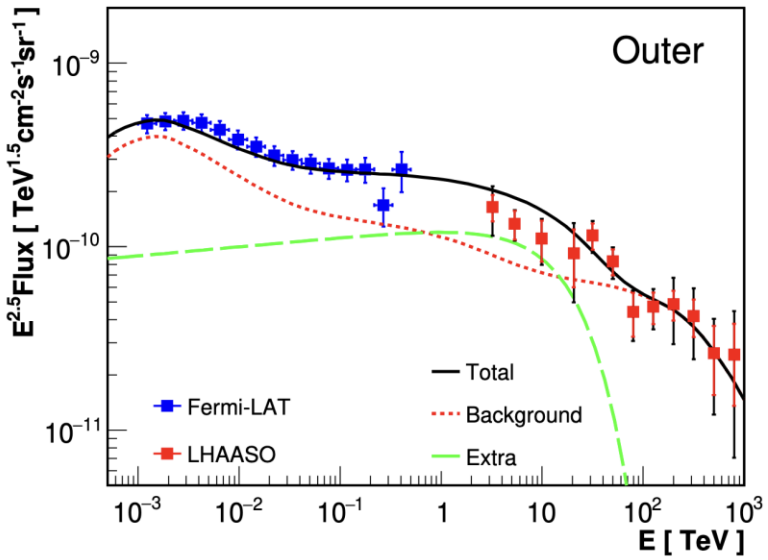
- Inner region: break around 30 TeV **(indices changing from ~2.7 to ~3.1), , while continuous emission persists as expected.**

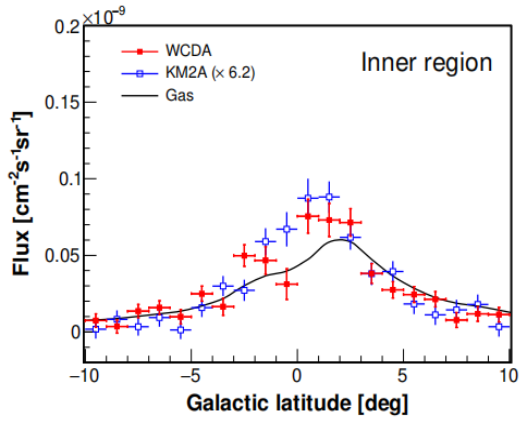
- An empirical component with spectrum ∝ $E^{-2.45}$ exp (−E/20 TeV) added to CR propagation model can fit the measured excess.

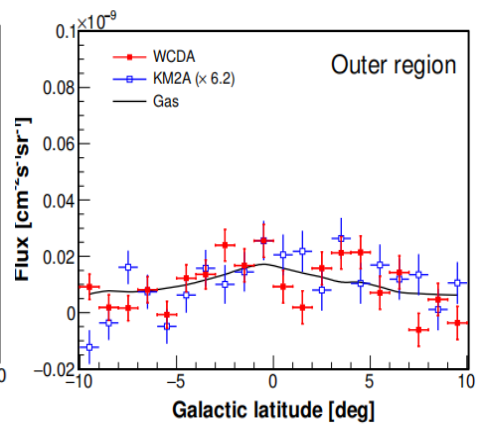
***Possible explanations:***

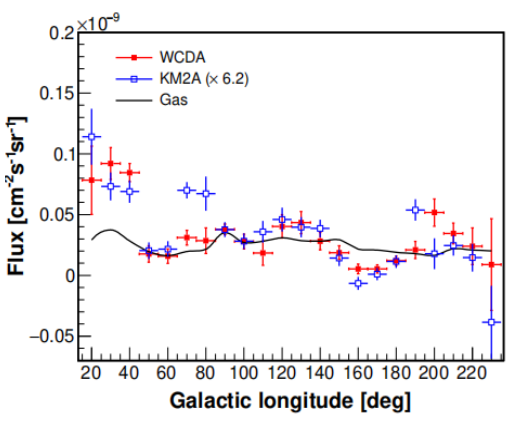
- Unresolved sources? (PWN/pulsar halo, YMCs...)
- Confinement and interaction of CRs around acceleration sites?
- Change of the canonical propagation scenario?




LHAASO, PRL, 134, 081002 (2025) arXiv: 2411.16021

# Outline

1. **Introduction:** The LHAASO Observatory
2. **Cosmic-Ray Energy Spectra:** Probing the Knee Region
3. **Cosmic-Ray Anisotropy (Focus):**
    - Large-scale anisotropy and energy evolution
    - Rigidity-dependent evolution across species
    - Medium-scale structures & energy-dependent centroid shifts
    - Transient anisotropy driven by ICME
4. **Galactic Diffuse Emission:** UHE $\gamma$-Ray Mapping along the Galactic Plane
5. **Galactic Particle Accelerators (PeVatrons):**
    - Supernova Remnants (SNRs)
    - Pulsar Wind Nebulae (PWNe) & Pulsar Halos
    - Young Massive Star Clusters (YMSCs)
    - Binaries (Microquasars & $\gamma$-Ray Binaries)
6. **Summary & Outlook**

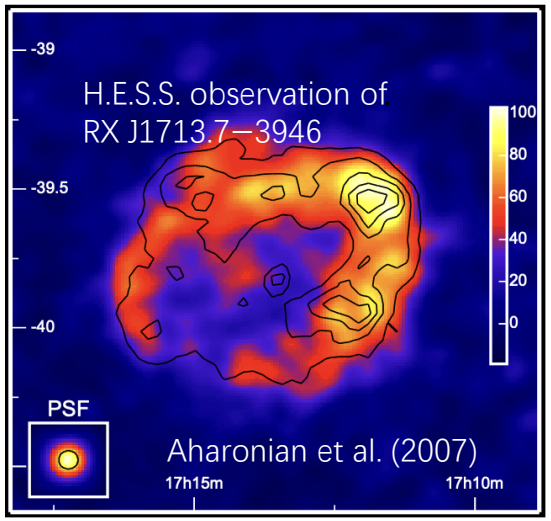
# SNRs: the leading candidates for GCRs

## The SNR Paradigm

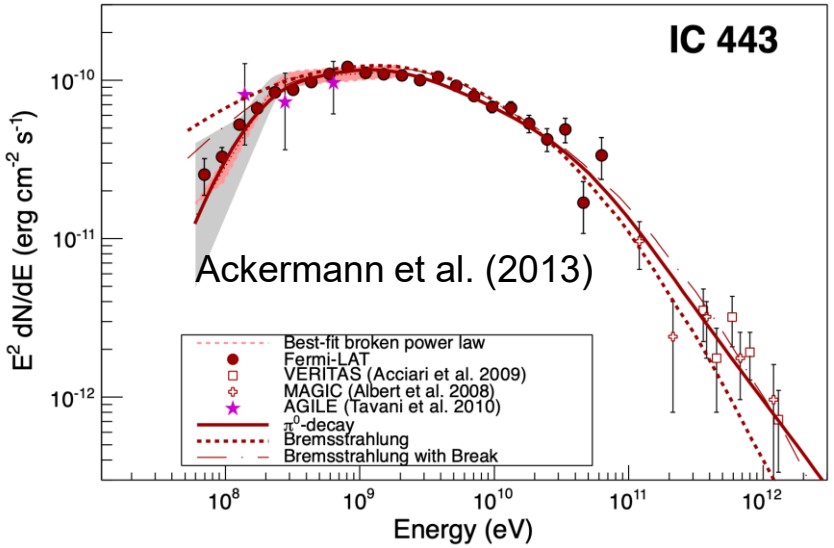
Energy budget: $E_{SN}\sim 10^{51}$ erg, ~3/century, $\eta \sim 10\% \rightarrow L_{GCR}\sim 10^{41}$ erg/s

Theories: DSA, $N(E)\propto E^{-\alpha}$ ,$D(E)\propto E^{\delta}$ ($\delta$=0.3−0.7) →local CR spectra, $\Gamma$~2.7-2.8.

- Clear evidences from multi-wavelength observations show SNRs are **GeV–TeV** CR accelerators.
- The biggest challenge of the SNR paradigm is the **"PeVatron"** or maximum energy problem.




Spatial correlation between TeV gamma-ray emission and molecular clouds




$\pi^0$-decay bump at sub-GeV energies in IC 443 provides a smoking-gun signature for proton acceleration.

*COSMIC RAYS FROM SUPER-NOVAE*

By W. Baade and F. Zwicky

Mount Wilson Observatory, Carnegie Institution of Washington and California Institute of Technology, Pasadena

Communicated March 19, 1934

happenings in a super-nova now confronts us. With all reserve we advance the view that a super-nova represents the transition of an ordinary star into a *neutron star*, consisting mainly of neutrons. Such a star may possess a very small radius and high density. Gravitation within it can be packed much more closely than in ordinary matter. Provisionally we shall refer to the neutron star as the end-product of the super-nova. In the present note we wish to discuss briefly the possibility that the super-nova process represents the conversion of ordinary matter into neutrons, and to point out that the release of packing energy may be sufficient to account for the cosmic-ray energy.



Baade & Zwicky (1934) :
SN → NS & CRs

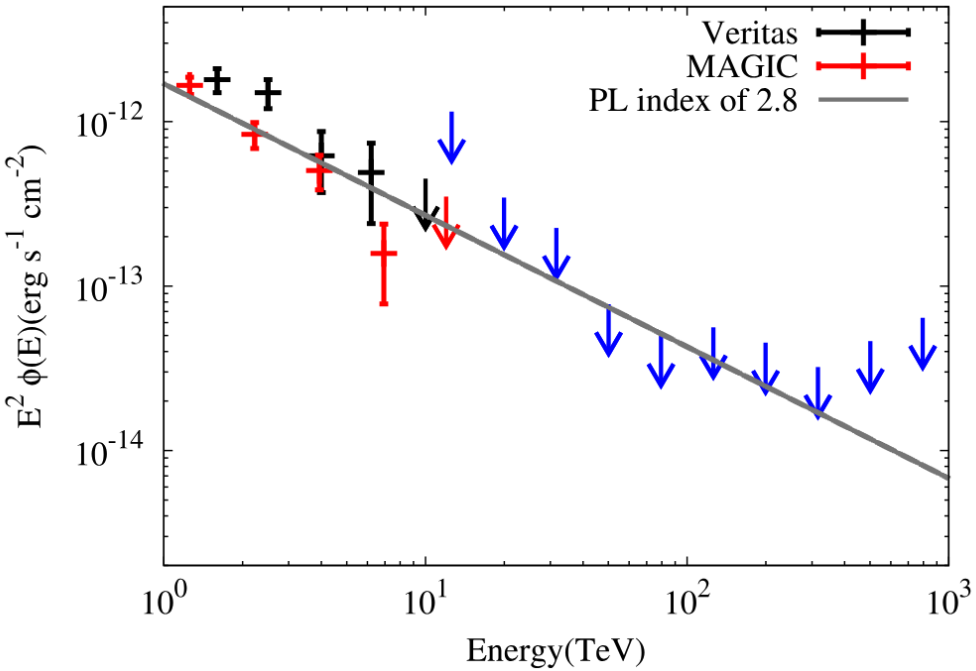
D. *Conclusions.*—From the above discussion of the various types of nuclear transformations the following picture of the super-nova process suggests itself.

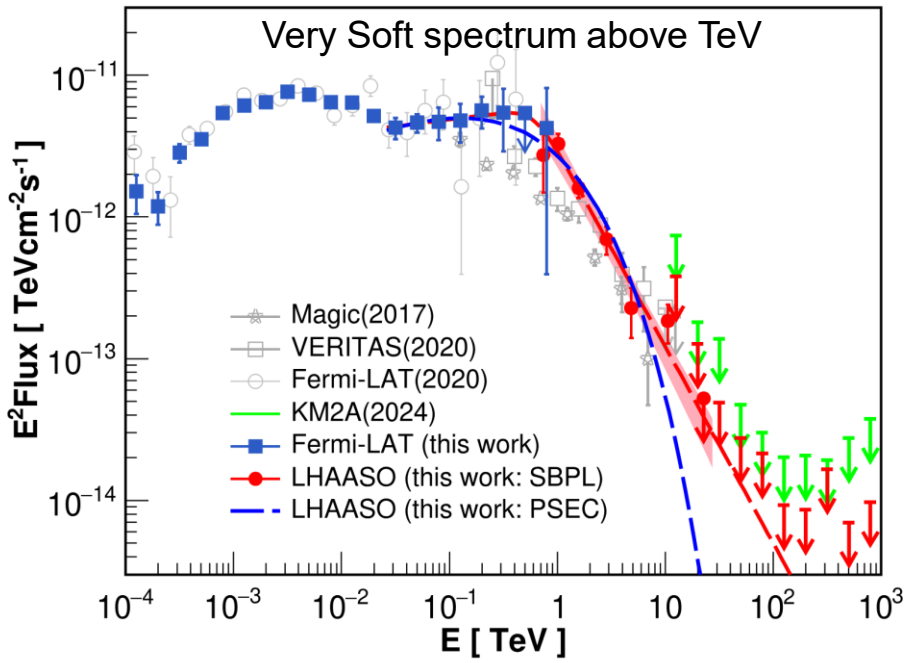
(1) Mass may be *annihilated* in bulk, leaving behind a star consisting of atoms whose total mass is $M$ may lose in the form of electromagnetic radiation and kinetic energy an amount of energy $E_T$ which probably cannot be accounted for by the liberation of known nuclear packing fractions. Several interpretations of this result are possible and will be published in another place.

(2) The hypothesis that *super-novae emit cosmic rays* leads to a very satisfactory agreement with some of the major observations on cosmic rays.

# Young SNR: Cas A

**Cas A:** age~350 yr, R~2.5', d~3.4 kpc

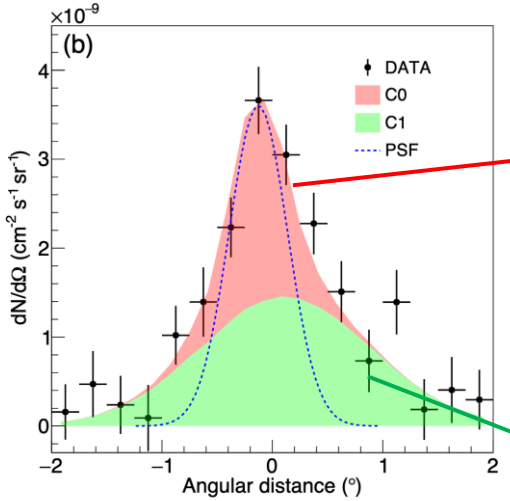


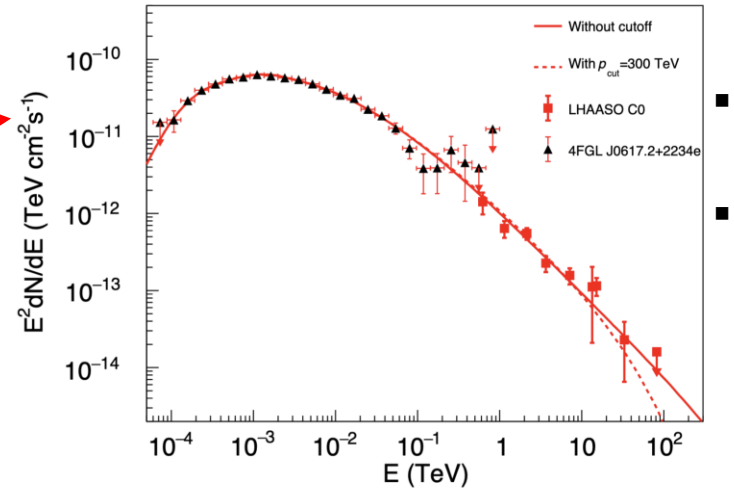



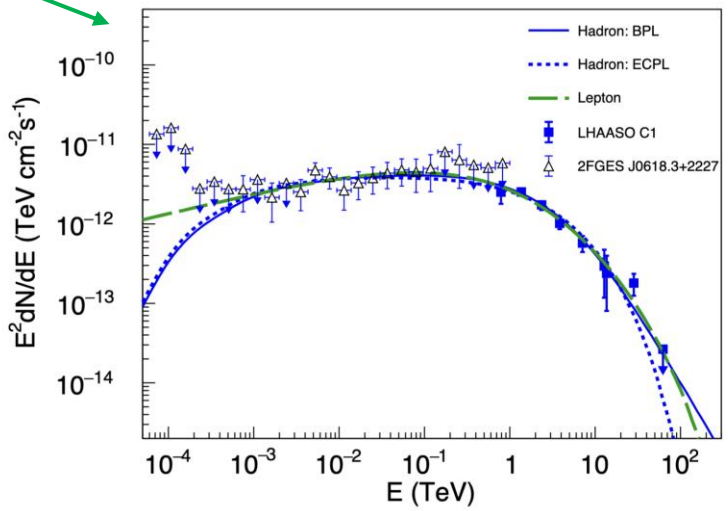

- $E_{\gamma,break}$~1 TeV, and no strong emission above 10 TeV detected yet: challenges Cas A-type young SNR as PeVatron.

LHAASO, ApJL, 961, L43 (2024) arXiv: 2310.17082
LHAASO, ApJL, 982, L33 (2025) arXiv: 2502.04848

# Middle-aged SNR: IC 443




**IC 443**

- Age~3-30 kyr, d~1.5 kpc.
- Evidence of MC interaction
- Hadronic emission detected (pion-bump feature by GeV observations).

Compact component C0:

- The γ-ray SED: PL with index~3.0 without apparent cutoff.
- PP model: the 95% lower limit of $E_p$ ~300 TeV →Hadronic sub-PeV particles are likely accelerated by IC 443.

Extended component C1:

- The γ-ray SED: PL with index ~2.5 and $E_{\gamma,cut}$~20 TeV
- PP/IC model with $E_{p/e}$ reaching 100s of TeV.
- Possible origin: IC 443, SNR G189.6+3.3, or putative PWN CXOU J061705.3+222127

❑ LHAASO observation resolved the emission around IC443 into two components:

1. point-like compact source (C0)
2. extended source (C1) with r39=0.67◦±0.07◦

LHAASO, PRL, 136, 161002 (2026) arxiv: 2510.26112

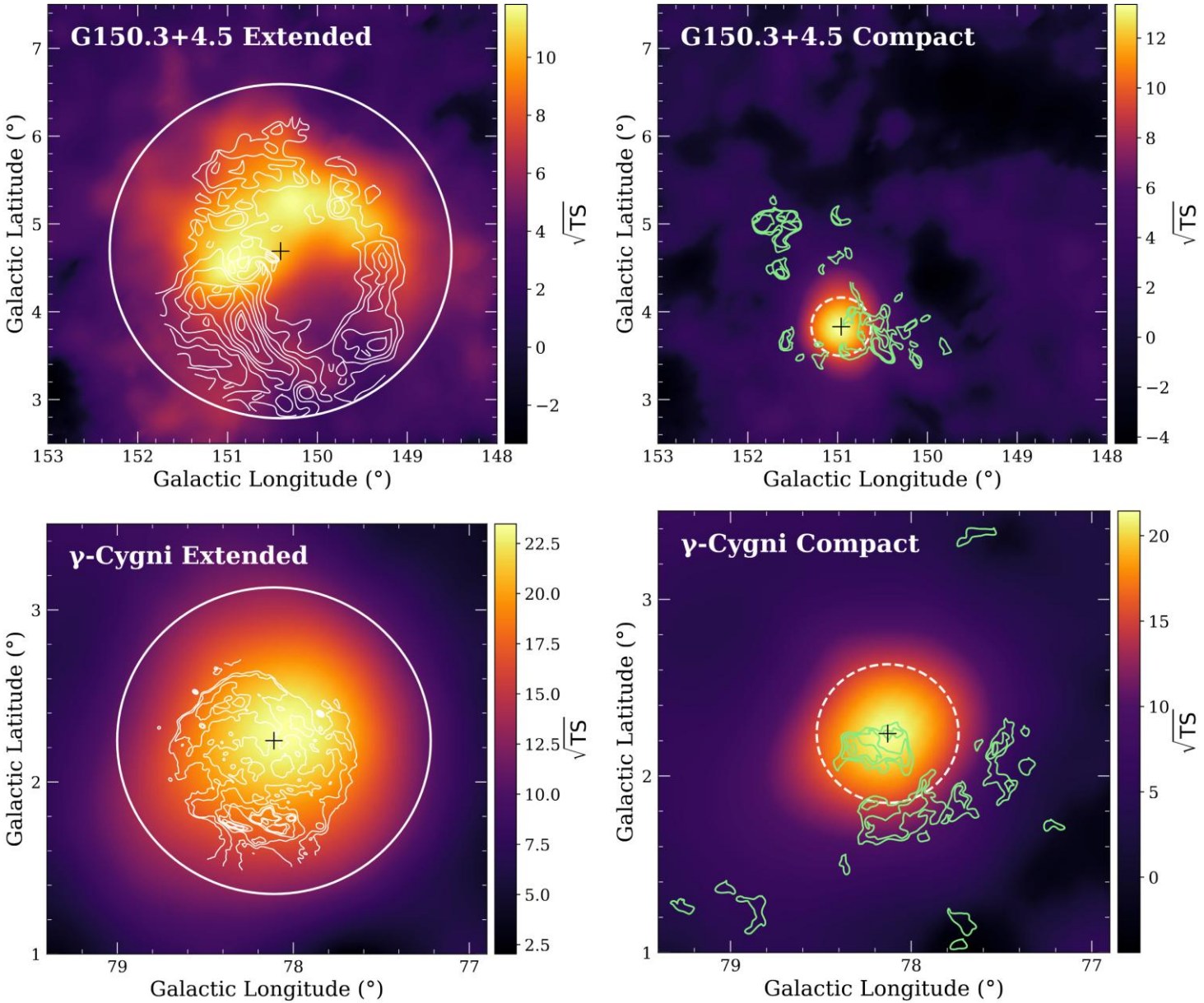
# Middle-aged SNR: G150.3+4.5, γ-Cygni

- **G150.3+4.5:** R~1.3°, age~(1−18)×$10^4$ yr, d ~740 pc
- **γ-Cygni:** R~0.5°, age~7 kyr, d~1.7 kpc

**LHAASO observation results:**

- ❑ γ rays with E>100TeV detected (>3σ).
- ❑ The emission was resolved into 2 (G150.3) or 3 (γ-Cygni) components:
  - Extended low-energy components coincide with the SNR shell
    → Trapped particles?
  - Compacter high-energy components coincide with nearby clouds
    → Escaped particles illuminating the clouds?

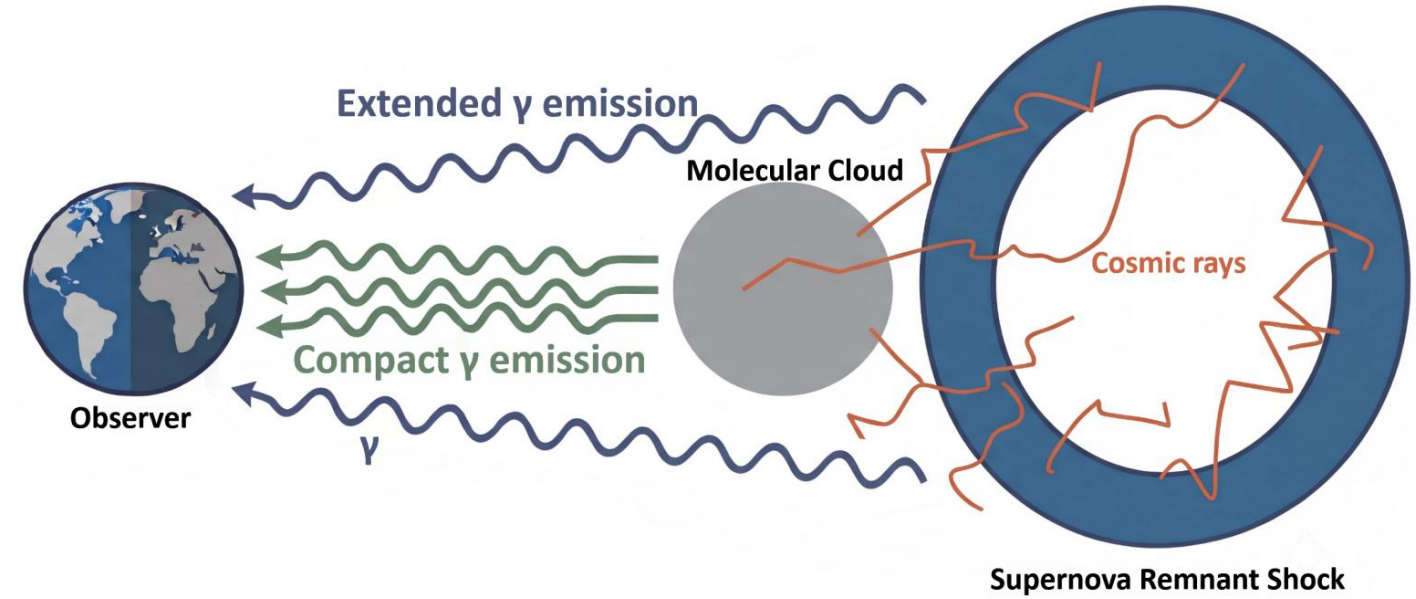
LHAASO (2026) arxiv: 2604.22621

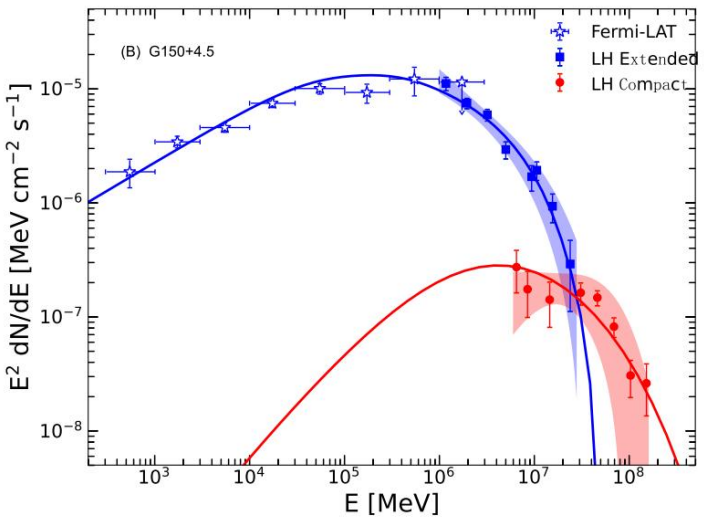


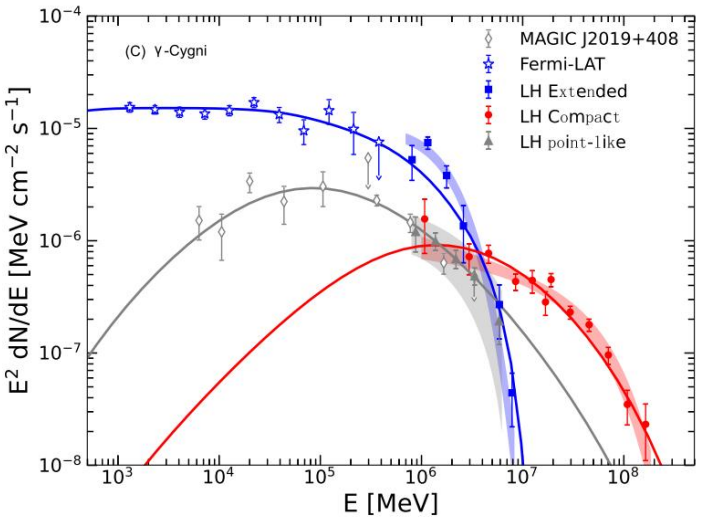
# Middle-aged SNR: G150.3+4.5, γ-Cygni

**The γ-ray SED modeling:**

- IC (extended) +PP (compact)
- Particles were accelerated at early stage and then injected instantaneously.
- Injected spectra:
  broken PL+ exponential cutoff
- $E_{p,cut}$~0.8 PeV → Hadronic PeVatron candidates

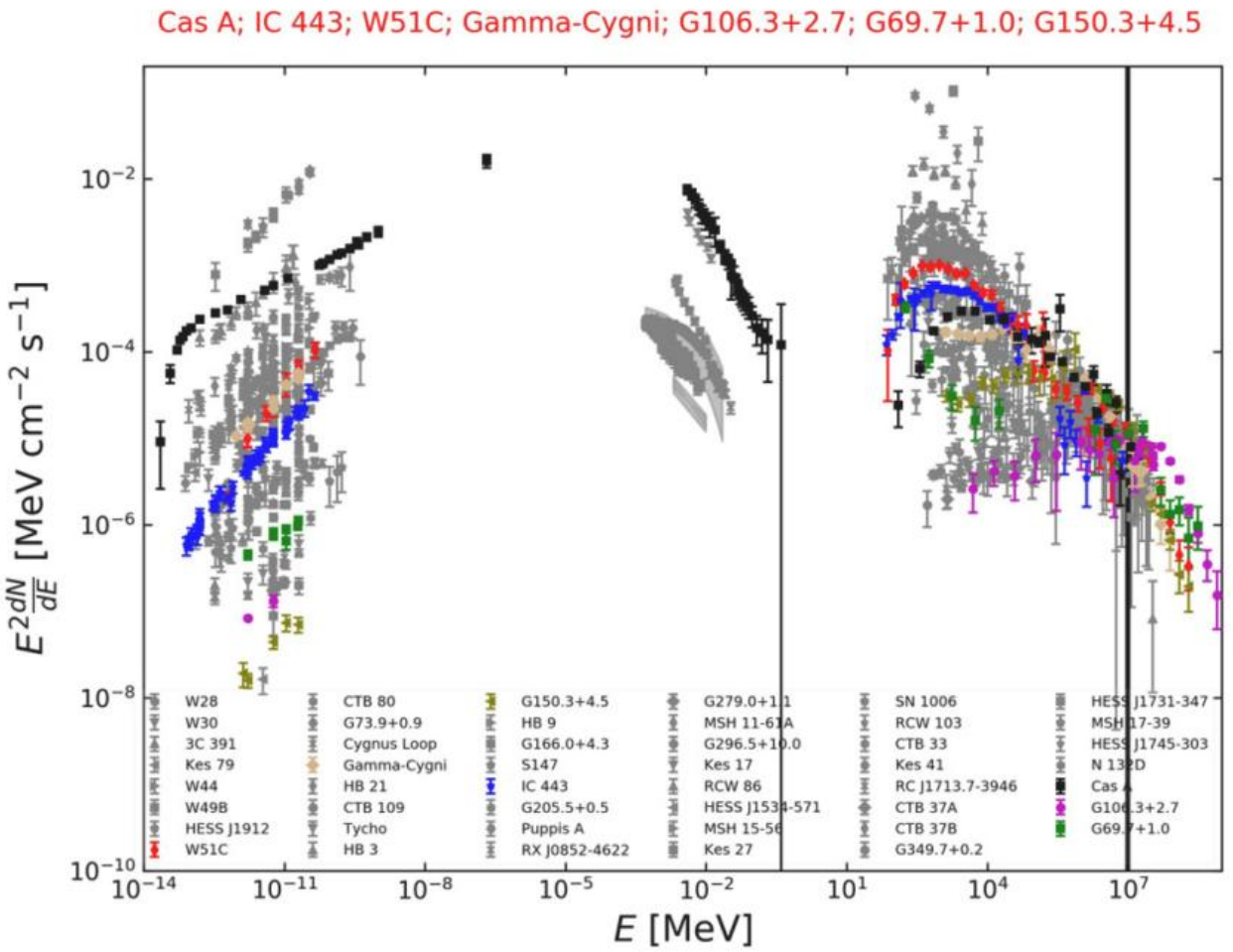



LHAASO (2026) arxiv: 2604.22621

# Summary of SNRs: Current Status and Limits as PeVatrons




- **Young SNRs fall short of PeV energies:**

Objects like Cas A show a spectral cutoff around 10 TeV ($E_{\mathrm{cut}} \sim 10$ TeV), indicating they are not current PeVatrons.

- **Middle-aged SNRs show sub-PeV/PeV potential:** Hadronic UHE emission is observed through two main mechanisms:
  - *Direct interaction* with molecular clouds (e.g., W51C, IC 443).
  - *Escaping particles illuminating* nearby clouds (e.g., G150.3+4.5, γ-Cygni).

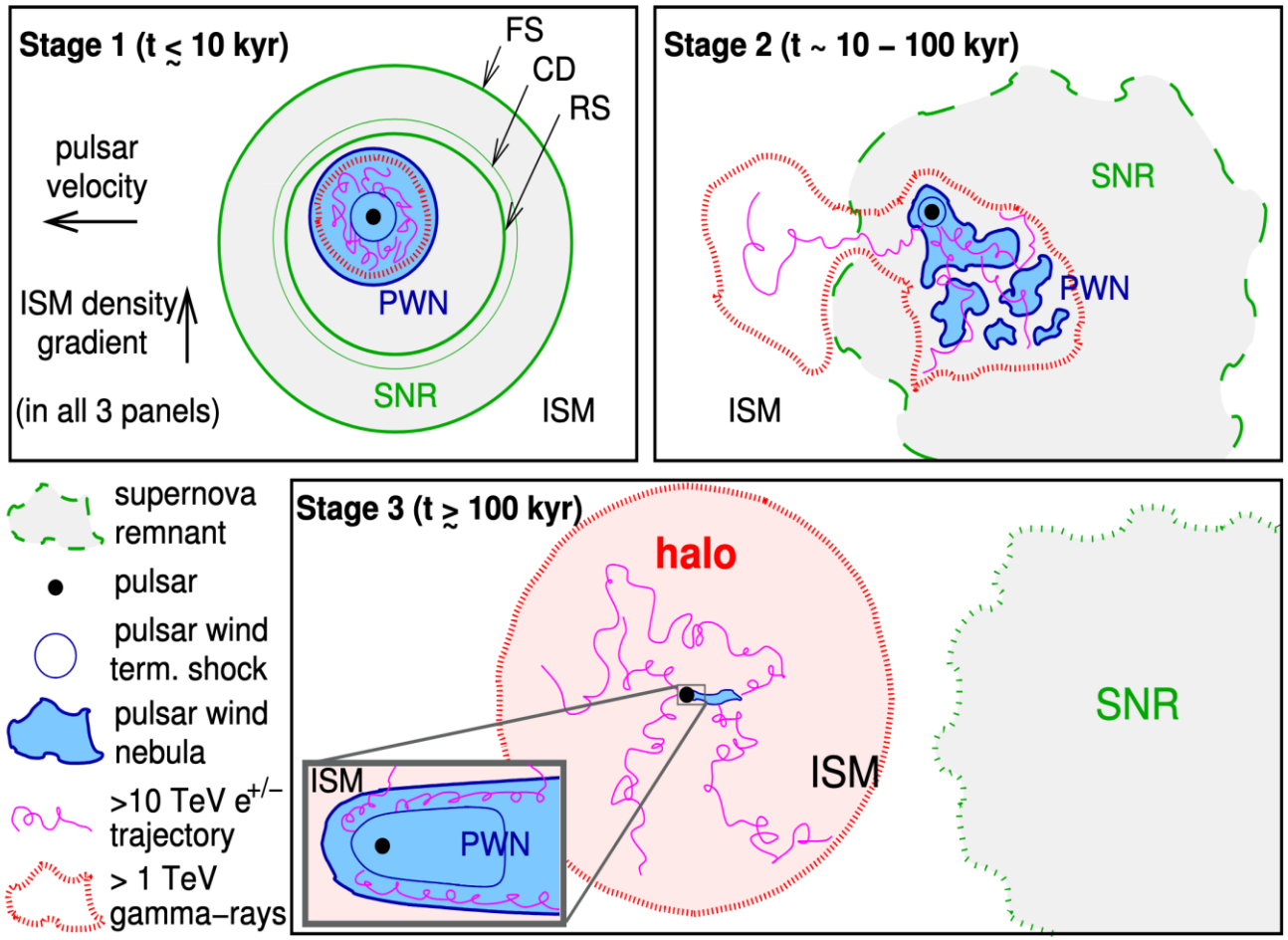
- **The "Knee" Problem:** Despite reaching the sub-PeV or PeV regime, SNRs likely do not contribute significantly to the cosmic ray spectrum above the knee.

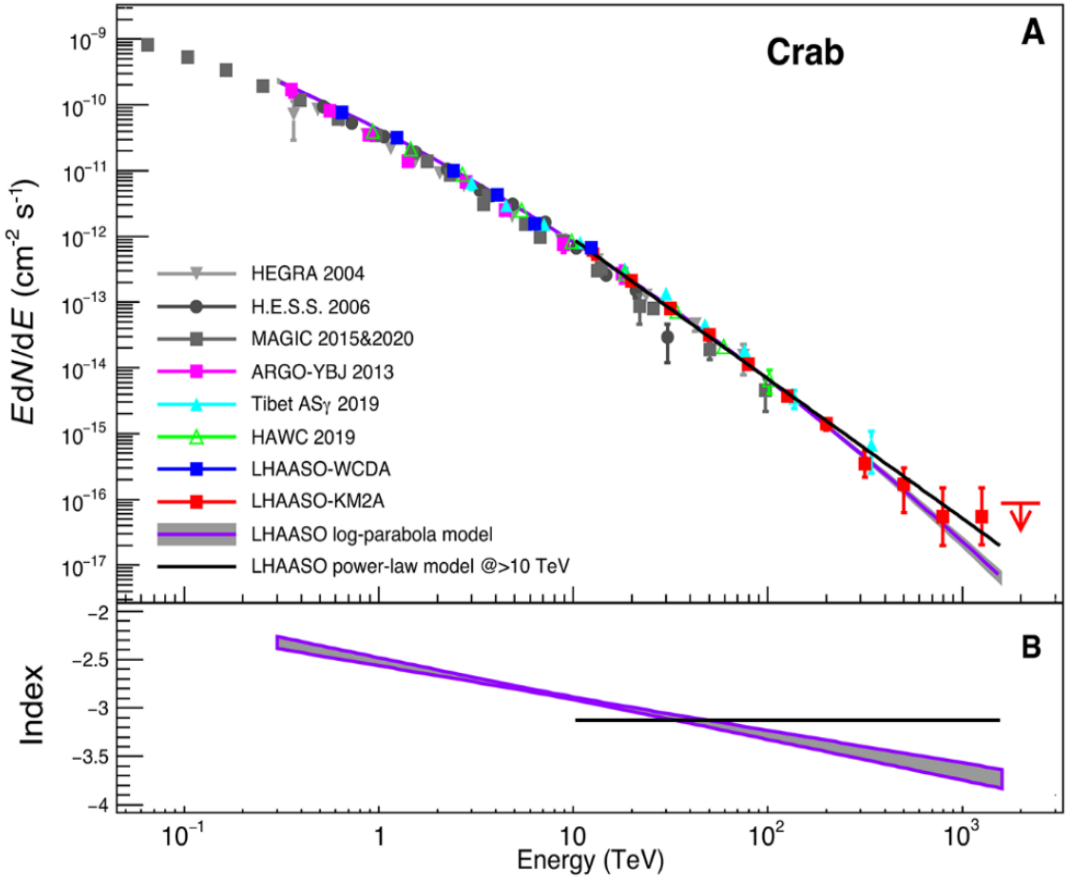
S.M. Liu, JHEA 44 (2024) 116–122

# Outline

1. **Introduction:** The LHAASO Observatory
2. **Cosmic-Ray Energy Spectra:** Probing the Knee Region
3. **Cosmic-Ray Anisotropy (Focus):**
   - Large-scale anisotropy and energy evolution
   - Rigidity-dependent evolution across species
   - Medium-scale structures & energy-dependent centroid shifts
   - Transient anisotropy driven by ICME
4. **Galactic Diffuse Emission:** UHE $\gamma$-Ray Mapping along the Galactic Plane
5. **Galactic Particle Accelerators (PeVatrons):**
   - Supernova Remnants (SNRs)
   - Pulsar Wind Nebulae (PWNe) & Pulsar Halos
   - Young Massive Star Clusters (YMSCs)
   - Binaries (Microquasars & $\gamma$-Ray Binaries)
6. **Summary & Outlook**

# Pulsar Wind Nebulae and pulsar halos




Science eabg5137 (2021)

- PWNe: one of the most numerous classes of Galactic TeV sources, samples to study the entire cycle from particle acceleration to particle escape and propagation.
- The PeV photons detected from the **Crab Nebula** demonstrated that young PWN could accelerate particles to the PeV regime.

# Extreme particle accelerator powered by PSR J1849-0001

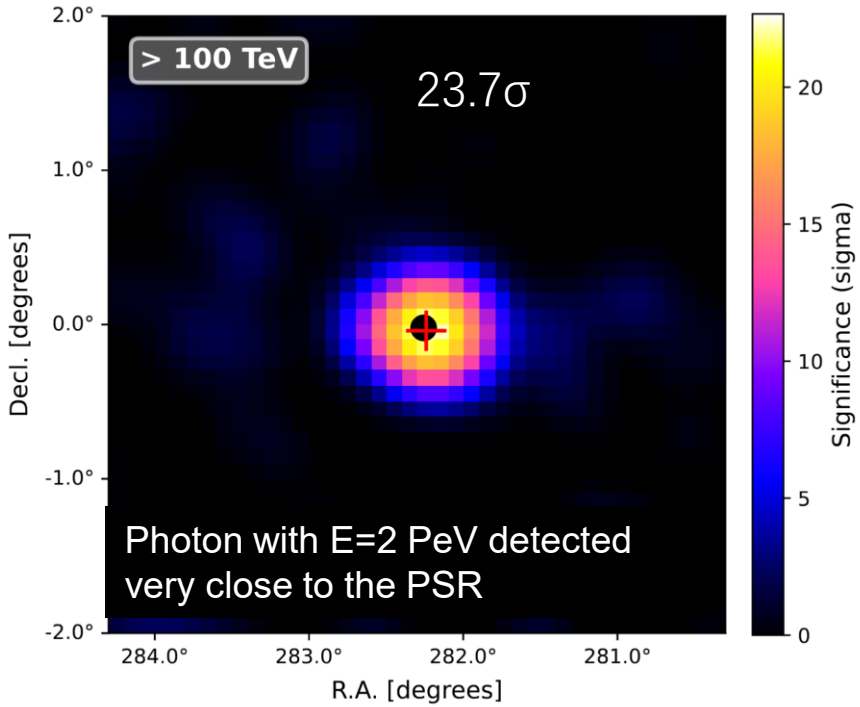
**PSR J1849-0001**:

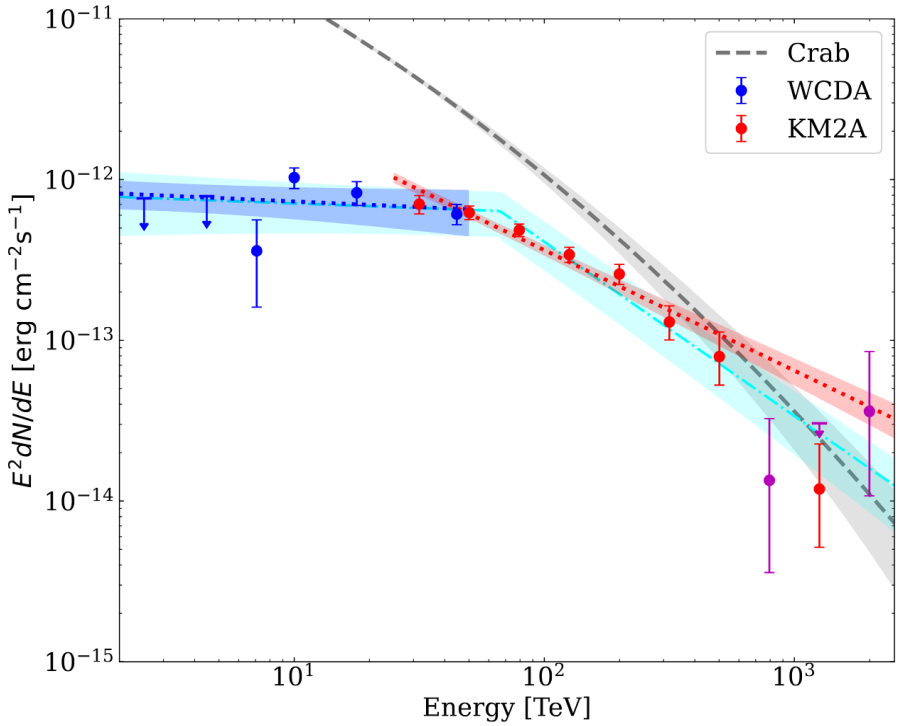
a fast-rotating pulsar initially discovered in the X-ray band.

d=7 kpc, $\tau_c$ = 43.1 kyr,

P = 38.5 ms (similar to Crab)

$L_{sd}$ = 9.8e36 erg/s (~1/50 Crab).

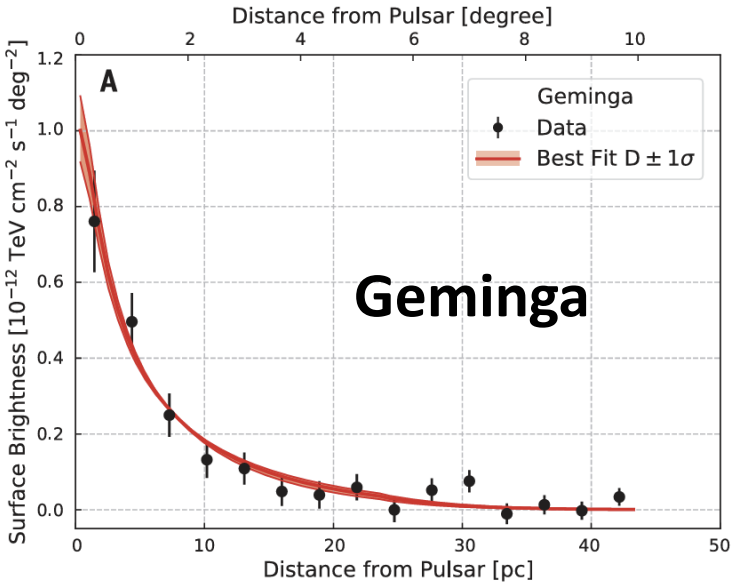


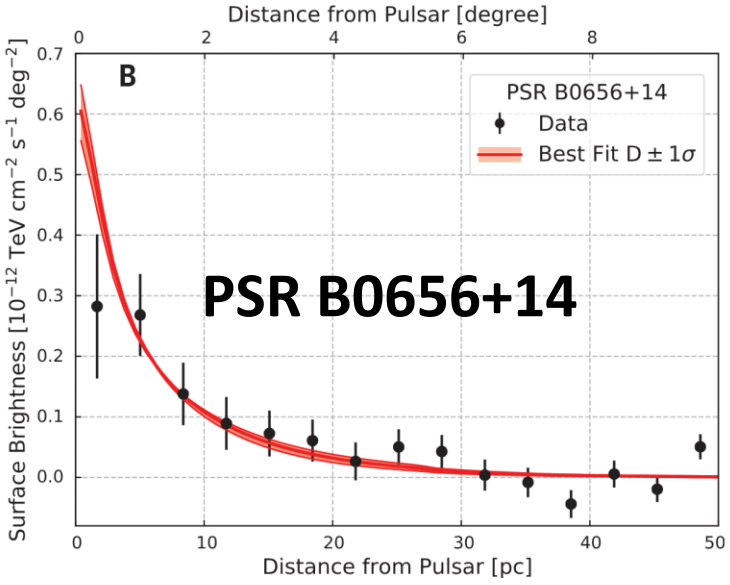



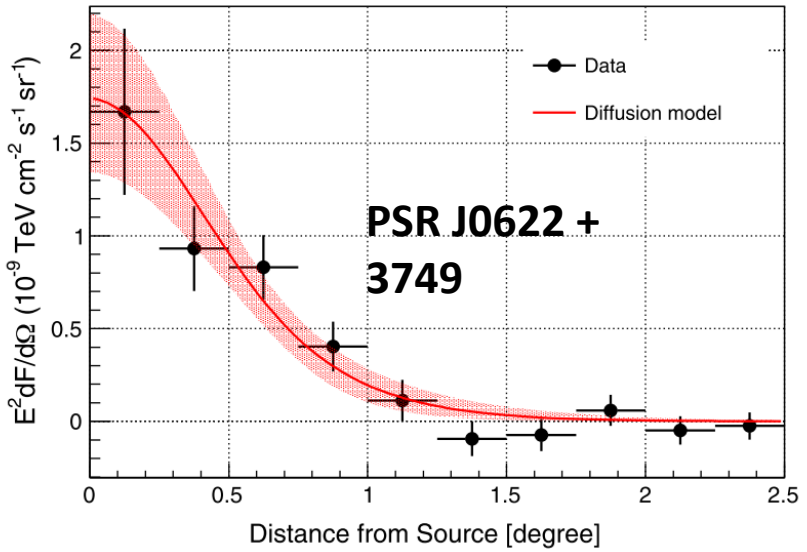

- LHAASO detected point-like UHE γ-ray source with spectrum up to PeV energies.
- The PeV luminosity is higher than that of the Crab Nebula.
- X-ray observations : B~3 μG within the PWN.
- Derived particle acceleration efficiency: approaching 1, challenging the particle acceleration theory in PWN.

LHAASO, NatAs, (2026) arXiv: 2603.15537

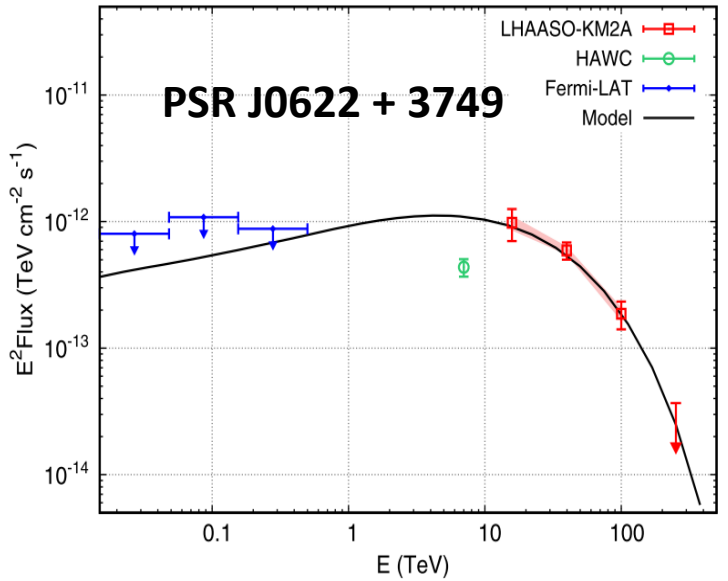
# Mid-Aged Pulsar Halos: Ubiquitous Slow Diffusion and UHE Emission




- **Anomalously Slow Diffusion:** Accelerated $e^{\pm}$pairs propagate within the vicinity at a diffusion coefficient ~ 2 orders of magnitude lower than the standard ISM value (derived from the B/C ratio).
- **A Ubiquitous Phenomenon:** These highly suppressed diffusion zones are universally present around mid-aged pulsars.
- **UHE Gamma-Ray Emission:** The resulting inverse-Compton emission extends up to ~ 100TeV.



# Summary: PWNe and Pulsar Halos as UHE Sources

- **A Major Class of UHE Sources:**
  - Recognized as a dominant population of ultra-high-energy (UHE) gamma-ray emitters.
- **Young PWNe as PeVatrons:**
  - Exhibit extreme particle acceleration and exceptionally high efficiency.
  - *Examples:* Crab Nebula, PSR J1849-0001.
- **Diverse Evolutionary Stages & Environments:**
  - Rich morphologies and physical behaviors observed across various stages of evolution and interstellar environments.
  - Highly suppressed diffusion zones around mid-aged Pulsar Halos.
- **Open Questions & Future Needs:**
  - Require a deeper understanding of the underlying **MHD physics**.
  - Call for refined models of **particle acceleration and propagation** mechanisms.

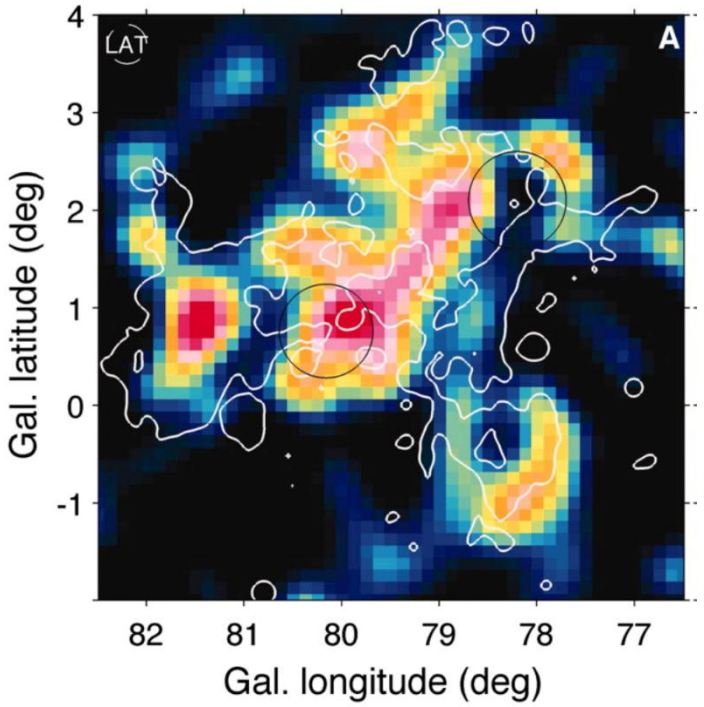
# Outline

1. **Introduction:** The LHAASO Observatory
2. **Cosmic-Ray Energy Spectra:** Probing the Knee Region
3. **Cosmic-Ray Anisotropy (Focus):**
    - Large-scale anisotropy and energy evolution
    - Rigidity-dependent evolution across species
    - Medium-scale structures & energy-dependent centroid shifts
    - Transient anisotropy driven by ICME
4. **Galactic Diffuse Emission:** UHE $\gamma$-Ray Mapping along the Galactic Plane
5. **Galactic Particle Accelerators (PeVatrons):**
    - Supernova Remnants (SNRs)
    - Pulsar Wind Nebulae (PWNe) & Pulsar Halos
    - Young Massive Star Clusters (YMSCs)
    - Binaries (Microquasars & $\gamma$-Ray Binaries)
6. **Summary & Outlook**

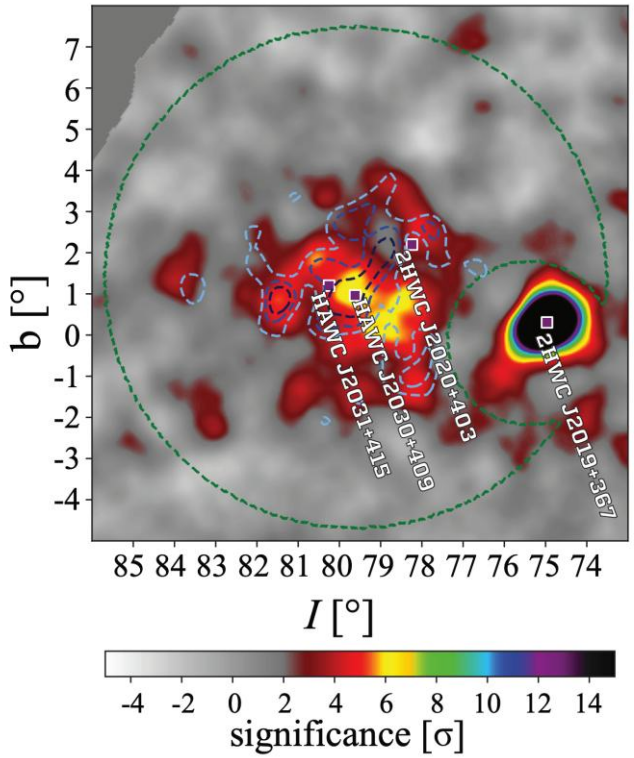
# Young massive clusters/star-forming regions

**Massive stars as important factories of GCRs:** Most of OB stars exist in associations or clusters, their stellar winds can accelerate particles and last much longer than SNR shocks (e.g., Cesarsky & Montmerle 83, Aharonian et al. 2019).

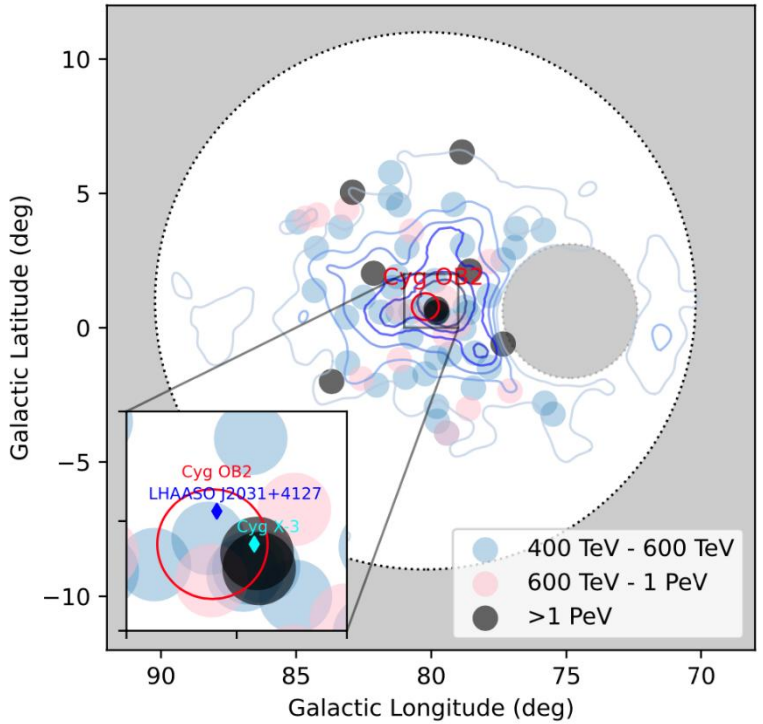
**Cygnus-X region:** potential of accelerating particles to TeV-multi PeV energies.




1-100 GeV gamma rays
Fermi-LAT, (2011) Science

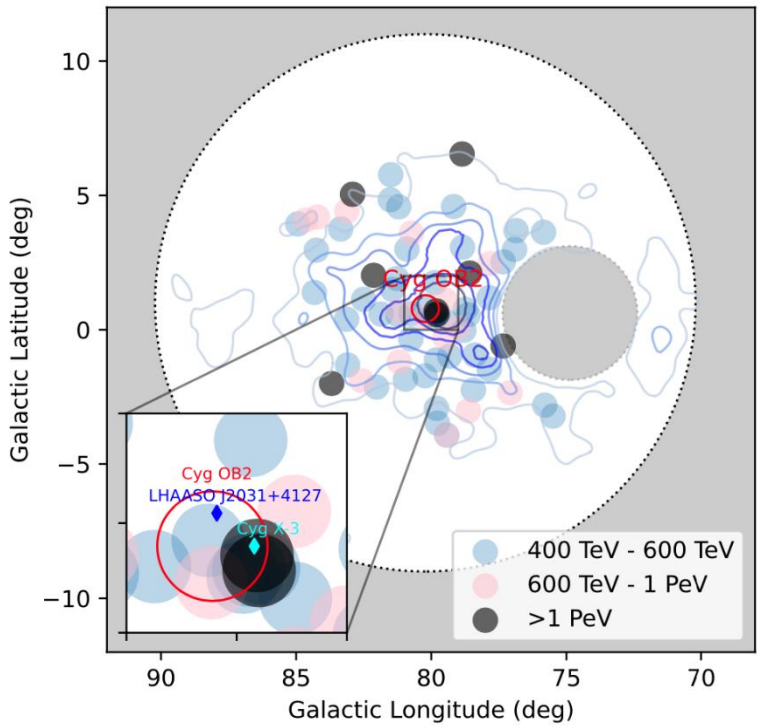


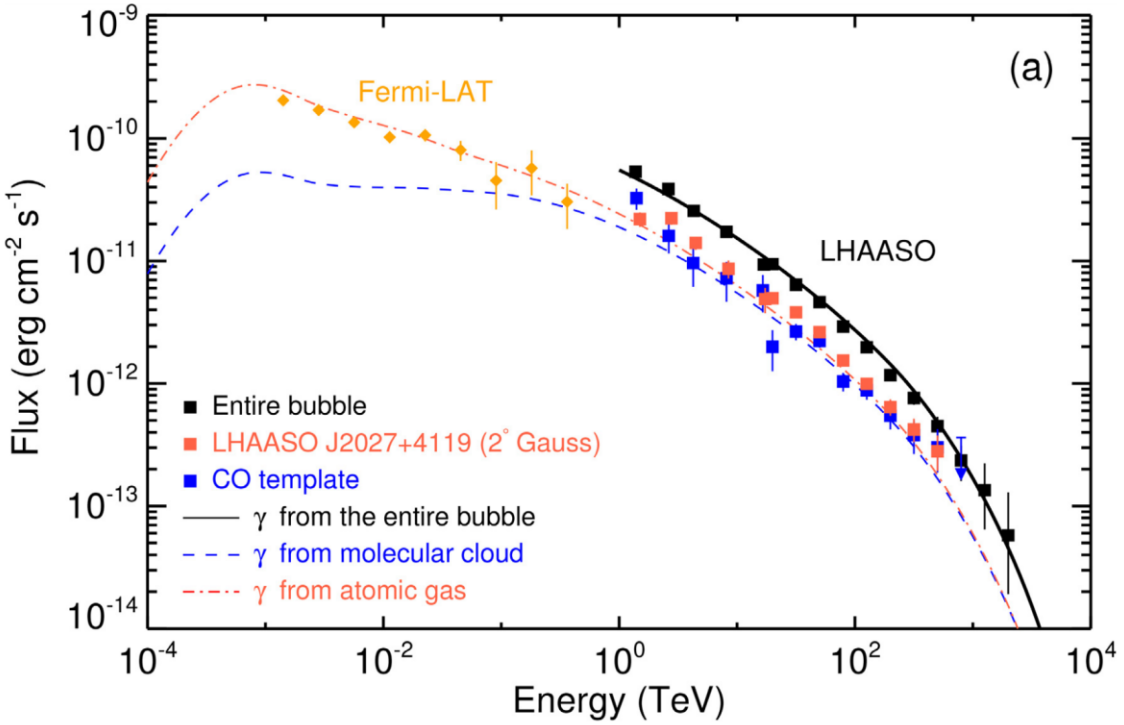

1-100 TeV gamma rays
HAWC, (2021) NA




100s TeV- PeV gamma rays
LHAASO, Science Bulletin, 69, 449 (2024)

# Cygnus-X region




✓Young massive star clusters: potentially sub-PeV to multi-PeV acceleration through collective stellar activity （e.g., Cygnus bubble, W43, G35.6-0.6) , but contributions from other sources need to be disentangled.

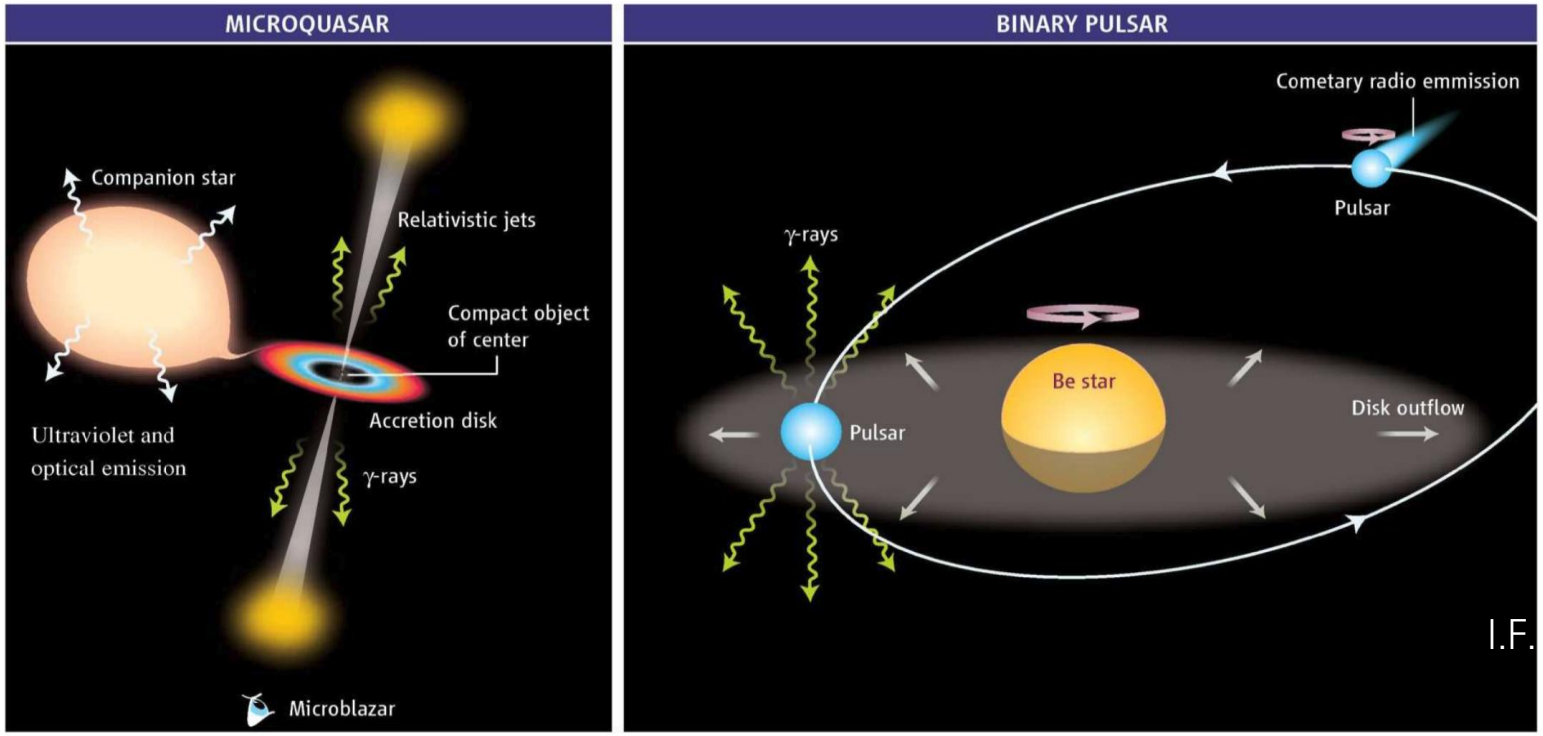
LHAASO, Science Bulletin, 69, 449 (2024)

# Outline

1. **Introduction:** The LHAASO Observatory
2. **Cosmic-Ray Energy Spectra:** Probing the Knee Region
3. **Cosmic-Ray Anisotropy (Focus):**
    - Large-scale anisotropy and energy evolution
    - Rigidity-dependent evolution across species
    - Medium-scale structures & energy-dependent centroid shifts
    - Transient anisotropy driven by ICME
4. **Galactic Diffuse Emission:** UHE $\gamma$-Ray Mapping along the Galactic Plane
5. **Galactic Particle Accelerators (PeVatrons):**
    - Supernova Remnants (SNRs)
    - Pulsar Wind Nebulae (PWNe) & Pulsar Halos
    - Young Massive Star Clusters (YMSCs)
    - Binaries (Microquasars & $\gamma$-Ray Binaries)
6. **Summary & Outlook**

# Binary systems






**Binary systems containing compact objects:**

extreme environment for particle acceleration

(strong magnetic fields, relativistic outflows, dense stellar environments... ) .

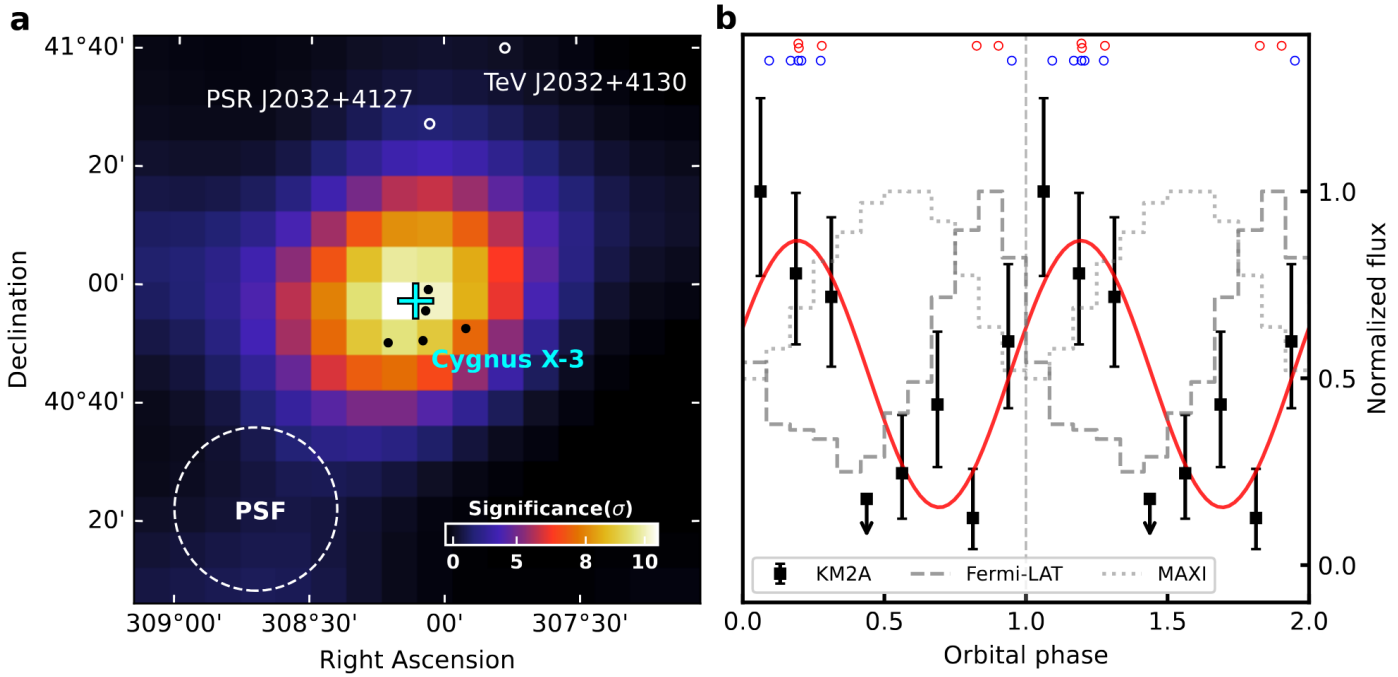
- **Micro-quasars:** accretion onto the compact object launch relativistic jets.
- **Gamma-ray binaries:** interaction between compact object and massive companion produces powerful non-thermal emission.

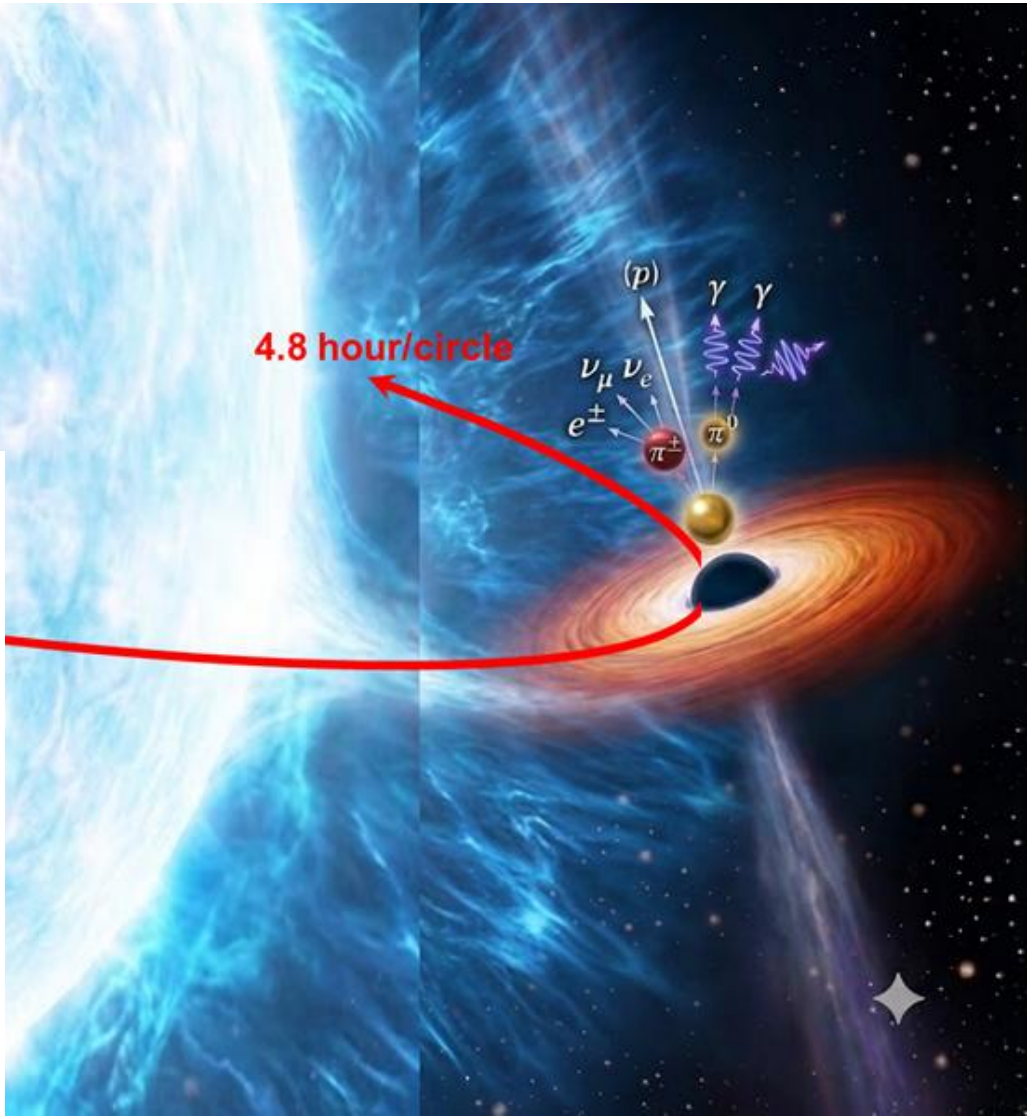
# Cygnus X-3: A variable Super PeVatron

**Cygnus X-3:** A high-mass X-ray binary system (WR star+compact object) with a very short period of 4.8 hours.

- LHAASO detected variable signal only at energies >100 TeV. (GeV-defined γ-ray high-state :11.5σ, low state: 2σ )
- Post-trial statistical significance of modulated signal: 3.2σ.

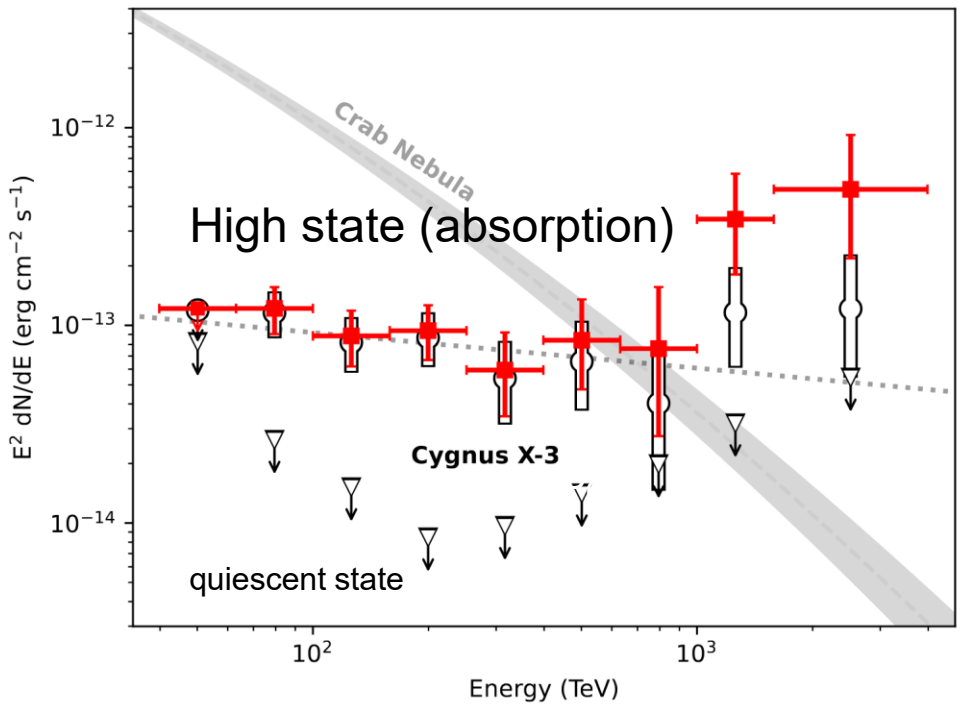
→The PeV γ-rays is produced within or close to the binary

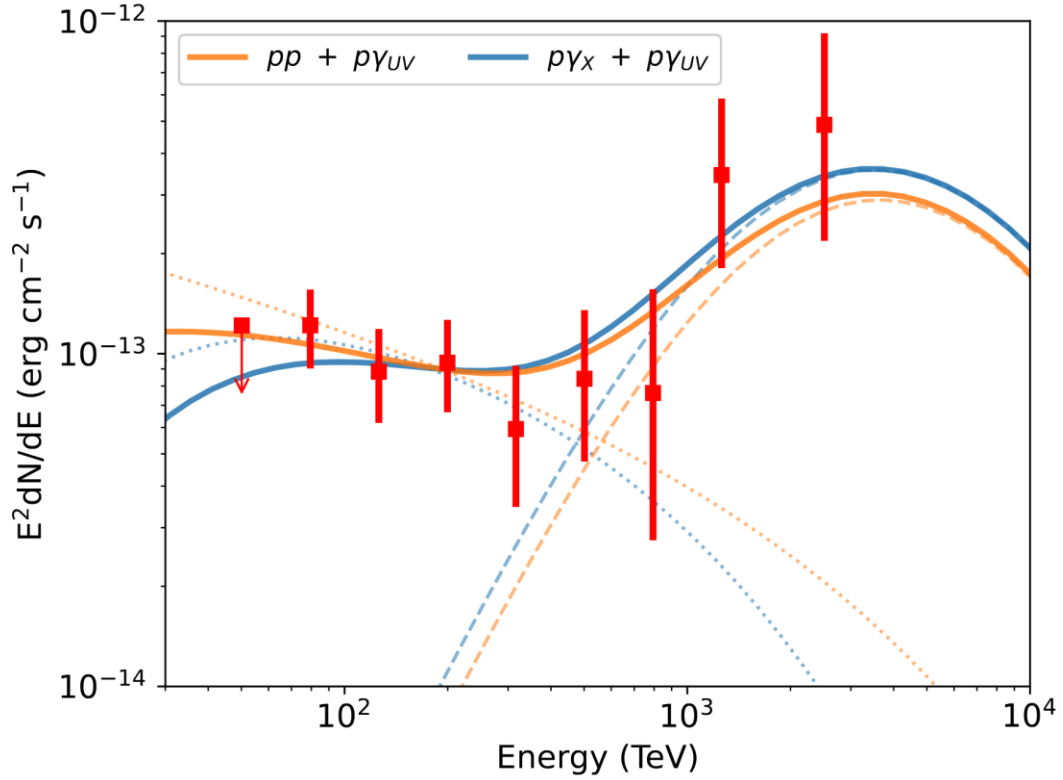



Significance map and orbital light curve of ≥ 0.1 PeV photons measured by LHAASO.

# Cygnus X-3: A variable Super PeVatron




- Particles with E > PeV accelerated within or close to the binary system (R ~3e11 cm) .
  - Hillas criterion (high B) + Synchrotron cooling effects (restrictive for e not for p)

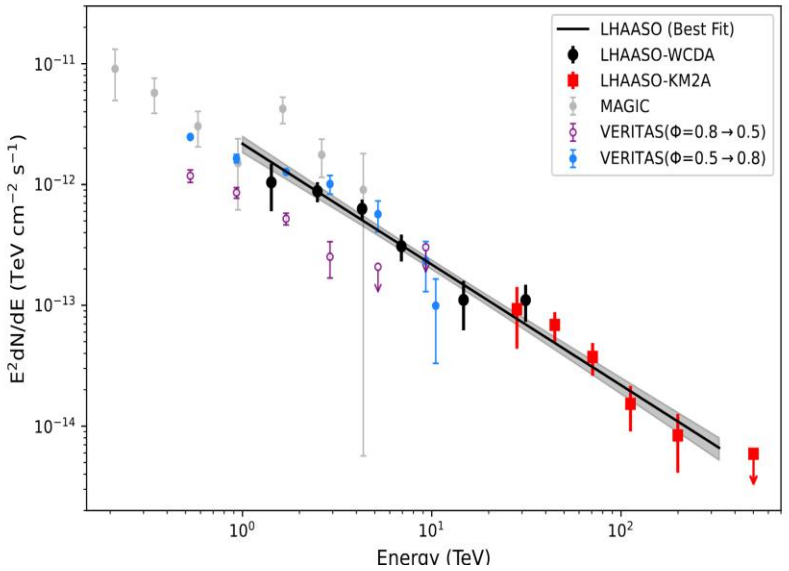
- Hadronic origin is favored: the proton energy can reach tens of PeV and produce PeV γ-rays via photo-meson processes.

LHAASO, National Science Review, (2026) arXiv: 2512.16638

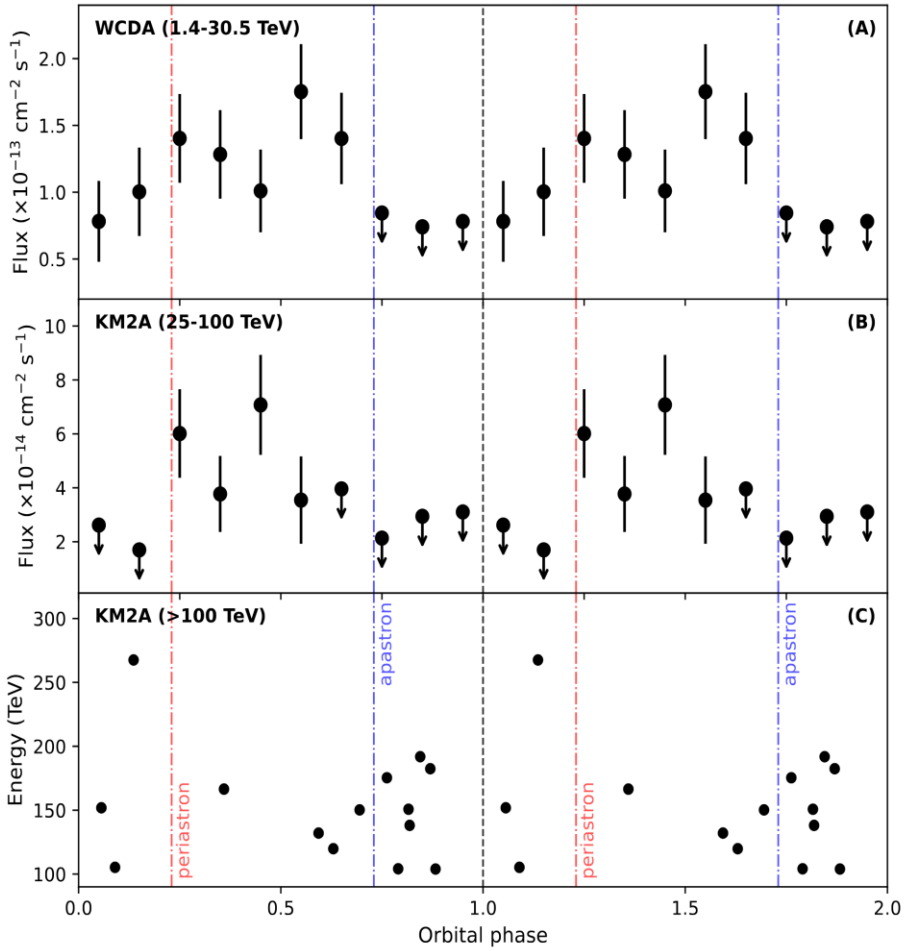
# UHE emission from LS I +61°303

**LS I +61°303:**

- A prototypical **γ-ray binary system** (Be star+compact object that is likely a pulsar), with orbital period ~26.5 days, d ~2 kpc.
- Variable VHE γ-ray emission (up to 10 TeV range) detected by MAGIC, VERITAS.




Phase-resolved emission of LS I +61°303 across different energy bands.




**UHE Emission:**

- Detection extends well into the UHE band, reaching $> 100$ TeV
- Identifies this $\gamma$-ray binary as a viable Galactic PeVatron candidate

**Orbital Modulation:**

- Significant orbital modulation detected between 25 **and** 100 TeV, with hints of energy-dependent behavior

**Implication:** The UHE emission is tightly coupled to the dynamic local environment of the binary system

LHAASO, PRL, 136, 181001 (2026) arXiv:2510.23345

# Binary Systems as Galactic PeVatrons

- **Microquasars (BH + Relativistic Jets):** Promising sites for extreme multi-PeV particle acceleration.
  - *Highlight:* UHE emission from the variable super-PeVatron Cygnus X-3.

- **Gamma-Ray Binaries:** Strong PeVatron candidates.
  - *Highlight:* Evidenced by recent UHE emission from LS I +61° 303.

# Summary and Outlook

Spanning tens of TeV to PeV energies with unprecedented sensitivity, LHAASO is reshaping our understanding of Galactic cosmic rays.

## Galactic Cosmic-Ray Landscape

- **CR Spectra at the Knee:** Fine structures in p+He spectra indicate multiple components and source populations.
- **Diffuse Emission Anomalies:** Spatial distribution deviates from conventional gas tracers; unexplained flux excesses and the nature of UHE extensions remain key open questions.
- **Diverse PeVatron Population:** LHAASO has uncovered a rich population of Galactic PeVatrons (and candidate super-PeVatrons), indicating our Galaxy hosts a rich population of PeVatrons/super-PeVatrons driven by varying channels (SNR shocks, PWNe, stellar winds, jets).

## Cosmic-Ray Anisotropy Highlights

- **Solar Modulation:** Discovery of solar-related phenomena driving significant modulation in TeV-scale cosmic-ray anisotropy.
- **Centroid Shifts:** Observation of pronounced energy-dependent shifts in the centroids of two prominent excess regions.
- **RigidityScaling:** First comprehensive measurement tracing anisotropy evolution across separated proton, $p$ + He, and all-particle samples.

# 谢谢！
# Muchas gracias!
# Thank you!

